Report 1830

DEPARTMENT OF THE NAVY

HYDROMECHANICS

o

AERODYNAMICS

o

STRUCTURAL MECHANICS

o

APPLIED MATHEMATICS

o

ACOUSTICS AND VIBRATION

PREDICTION OF THE AERODYNAMIC CHARACTERISTICS OF ANNULAR AIRFOILS

by

W. B. Morgan
and
E. B. Caster

HYDROMECHANICS LABORATORY
RESEARCH AND DEVELOPMENT REPORT

January 1965 Report 1830

DISCLAIMER NOTICE

THIS DOCUMENT IS BEST QUALITY PRACTICABLE. THE COPY FURNISHED TO DTIC CONTAINED A SIGNIFICANT NUMBER OF PAGES WHICH DO NOT REPRODUCE LEGIBLY.

PREDICTION OF THE AERODYNAMIC CHARACTERISTICS OF ANNULAR AIRFOILS

by

W. B. Morgan

and

E. B. Caster

January 1965

Report 1830

TABLE OF CONTENTS

LIST OF TABLES

LIST OF FIGURES

NOTATION

a	Duct chord
$C_1(Z)$	Mean line ordinate of the duct section measured from the nose-tail line
$E(k)$	Complete elliptic integral of the second kind
h	$(a/2\ R_d)$ chord-diameter ratio of the duct
$K(k)$	Complete elliptic integral of the first kind
k	Modulus of the elliptic integrals
q	Ring-source strength
R_d	Duct radius
(r, ϕ, Z)	Cylindrical coordinates
$S(Z)$	Half-thickness ordinate of the duct section
V	Free-stream velocity
W_a	Axial component of induced velocity
W_0	Component of free-stream velocity in direction of duct axis
W_r	Radial component of induced velocity
X	Radial coordinate nondimensionalized by the propeller radius
Z	Axial coordinate nondimensionalized by the duct chord
α	Angle of attack of a duct section
α_{id}	Ideal angle of attack of a duct section
α_r	Relative angle between free-stream velocity and duct
Γ	Ring-vortex strength
ρ	Mass density of fluid
ω_0	Angular velocity

Subscripts

d	Duct
q	Ring source
γ	Ring vortex
$\frac{\partial \gamma}{\partial \phi}$	Trailing vortex system of the vortex cylinder

Note: Many functions are defined in the text.

ABSTRACT

A computer program is presented which calculates the aerodynamic characteristics of annular airfoils on an IBM-7090 high-speed computer. A brief review of the theory is also presented. Experimental and computer results indicate that the theory gives reasonable prediction of the lift, induced-drag, and moment coefficients and also of the pressure distribution except when separation is present on the annular airfoil. The computer program can also be used for the design of ducted propellers if an infinite number of blades is assumed.

ADMINISTRATIVE INFORMATION

This work was covered by Subproject S-R011 01 01 of Task 0401 under the Bureau of Ships In-House Independent Research Program.

1. INTRODUCTION

Annular airfoils have found use in both aeronautics and naval architecture where their application has generally been as shroud rings around propellers. The aeronautical application has been to increase the thrust of propellers for hovering flight such as applied to vertical take-off craft. In naval architecture Kort nozzles have been used for many years for increasing the efficiency of heavily loaded propellers, whereas pumpjets are a more recent innovation for delaying cavitation.

In most applications the annular airfoil is used as an integral part of the propulsor, and a theoretical treatment must consider the interaction between the propeller and airfoil. The present theories, however, use an interative procedure between propeller and annular airfoil theory so that the usefulness of the complete theory depends on the verification of each part. One purpose of this report is to present a comparison of theoretical and experimental results for a number of annular airfoils.

The first theoretical development of annular airfoils is that due to Dickmann[1] who represented the annular airfoil by a distribution of ring vortices. This approach implies that the airfoil has no thickness. Other contributors have been Stewart,[2] Kuchemann,[3,4] Pivko,[5] Malavard,[6] and Hacques.[7] A more complete review of each of these contributions can be found in References 8 and 9. The most complete theoretical approach to date has, however, been that by Weissinger[10,11] who extended the work of Dickmann and has considered ducts with thickness, of arbitrary shape and at an angle of attack. His mathematical model of the annular airfoil was a distribution of ring vortices and ring sources lying on a cylinder of

---

[1]References are listed on page 82.

diameter representative of the duct and of length equal to the duct. This means that the boundary conditions are linearized and are satisfied on a representative duct cylinder and not on the duct surface.

A number of investigators have used the Dickmann-Weissinger mathematical model a have developed numerical methods for computing the pressure distribution on annular airfoi Bagley, Kirby, and Marcer[12] have presented a simplified method where the boundary conditions are satisfied at only a few points along the chord. A more complete method is that given in References 13 and 14, which has presented quite an extensive set of tables for a limited number of airfoil configurations.

In addition to the comparison of theoretical and experimental results mentioned previously, this report presents a computer program for the IBM-7090 which enables not only t pressure distribution of the annular airfoil to be obtained but also other aerodynamic characteristics. Specifically, the program calculates the pressure distribution, both linear and nc linear[15] for an annular airfoil of arbitrary section, the ideal angle of attack, the velocity di tribution, both on and in the flow field, and the various aerodynamic forces which arise. T annular airfoil is assumed to be axisymmetric but may have an angle of attack and be in an axisymmetric flow field. Consideration of such a flow field allows the inclusion of an infinitely bladed propeller or a central body within the duct. The mathematical model used for these calculations is the Dickmann-Weissinger model and the approach is that of Reference 9 and 15.

The following discussion is divided into four main sections. The development of th theory is reviewed briefly, then the computer program is described, and finally, the results of the calculations and comparison with the experimental results are presented.

2. LINEARIZED THEORY OF THE ANNULAR AIRFOIL

The linearized theory of the annular airfoil has been developed adequately in the ref erences cited, but a brief development will be repeated here for completeness. Details of t mathematical manipulations which have been omitted will be found in References 9 and 15.

As indicated in the Introduction, the method of singularities is used for representati of the flow field about the annular airfoil. The mathematical model used will be a distribution of ring vortices and ring sources lying on a cylinder of a diameter representative of th duct diameter and of length equal to the duct length (the Dickmann-Weissinger model). In t use of this approach a number of assumptions are implied. Briefly these are:

a. The fluid is inviscid and incompressible and no separation occurs on the duct.

b. Body forces such as gravity are neglected.

c. The free-stream flow is, in general, axisymmetric but may have a small cross-flow component.

d. The annular airfoil is axisymmetric and of finite length.

e. The annular airfoil can be represented mathematically by a distribution of ring vortices and ring sources along a cylinder of constant diameter. This implies that the boundary conditions are linearized.

f. The trailing vortex system of the annular airfoil has the constant diameter of the annular airfoil and extends from the annular airfoil to infinity.

2.1 BOUNDARY CONDITIONS

The coordinate system used is a cylindrical system (r, ϕ, Z) with the axis located at the trailing edge and on the centerline of the duct. For convenience, the axial coordinate will be nondimensionalized by the chord c and the radial coordinate by the reference radius of the duct R_d. Figure 1 shows the annular airfoil coordinate system and Figure 2 is a delineation of the system.

The cross section of the annular airfoil is assumed known and will be delineated by a thickness distribution, a camber distribution, and an angle of attack.

In terms of the thickness, camber, and angle of attack, the slope of the outer surface of the duct is given by

$$a'(Z) = C_1'(Z) + \tan \alpha + S'(Z)$$

and the slope of the inner surface by

$$b'(Z) = C_1'(Z) + \tan \alpha - S'(Z)$$

The boundary conditions to be satisfied on the surface of an annular airfoil are that the normal velocity must be zero and that the Kutta condition must be satisfied at the trailing edge. In linearized theory, Reference 9, this means that the radial velocity at the reference cylinder must be equal to the slope of the section, or

$$\frac{W_r}{V}(X_d \pm 0, \phi, Z) = -[C_1'(Z) + \tan \alpha \pm S'(Z)] \qquad (0 \leq Z \leq 1) \qquad [2.1.1]$$

And at the trailing edge the radial velocity is zero, or

$$\frac{W_r}{V}(X_d \pm 0, \phi, 0) = 0 \qquad [2.1.2]$$

2.2 DERIVATION OF THE RING VORTEX AND SOURCE DISTRIBUTIONS TO REPRESENT THE ANNULAR AIRFOIL

In order to calculate the pressure distribution on the annular airfoil, the flow field around the foil, and the aerodynamic forces, it is necessary to obtain the strength of the ring vortices and ring sources. The ring-vortex strength and ring-source strength must be of such magnitude that they induce radial velocities which satisfy the boundary conditions given by Equation [2.1.1]. By substituting the equations for the radial velocity induced by the ring vortices and sources into Equation [2.1.1], a singular integral equation is obtained which can be solved for the various singularity distributions as shown in the following discussion.

The nondimensional elementary circulation of the ring vortices will be taken to be $\gamma(\phi, Z)$ and the strength of the ring sources to be $q(\phi, Z)$. If the ring-vortex strength is a function of the angular coordinate, then from vortex theory a trailing-vortex system exists behind the duct. The strength of the elementary vortex is $\frac{1}{X_d}\frac{\partial \gamma}{\partial \phi}$, and this vortex system induces radial velocities at the duct. Since the velocities are linear, they are additive, and the radial velocities by the duct are found to be

$$\frac{W_r}{V}(X_d \pm 0, \phi, Z) = \left[\frac{W_r}{V}(X_d, \phi, Z)\right]_\gamma + \left[\frac{W_r}{V}(X_d \pm 0, \phi, Z)\right]_q + \left[\frac{W_r}{V}(X_d, \phi, Z)\right]_{\frac{\partial \gamma}{\partial \phi}} + \left[\frac{W_r}{V}(X_d, Z)\right] + \alpha_r \cos \phi$$

$$(0 \leq Z \leq 1) \qquad [2.2.1]$$

And the various terms are defined as follows:

$[W_r(X_d, \phi, Z)]_\gamma$	The radial velocity induced on the duct by the ring-vortex system.
$[W_r(X_d \pm 0, \phi, Z)]_q$	The radial velocity induced on the duct by the ring source system.
$[W_r(X_d, \phi, Z)]_{\frac{\partial \gamma}{\partial \phi}}$	The radial velocity induced on the duct by the trailing-vortex system.

$[W_r(X_d, Z)]$	An arbitrary axisymmetric velocity at the duct such as induced by an infinitely bladed propeller or a center body.
$\alpha_r \cos\phi$	The radial component of the free-stream velocity when the duct is at an angle of attack.

The radial velocity components induced by the various singularity distributions at the reference cylinder have been derived in Reference 9 and are

For the ring vortices:

$$\left[\frac{W_r}{V}(X_d, \phi, Z)\right]_\gamma = \frac{h}{2\pi}\int_0^1\int_0^{2\pi} \frac{2h(Z-Z')\cos(\phi-\phi')\,\gamma(\phi', Z')}{\left[4h^2(Z-Z')^2 + 4\sin^2\frac{1}{2}(\phi-\phi')\right]^{3/2}}\,d\phi'\,dZ' \qquad [2.2.2]$$

For the ring sources:

$$\left[\frac{W_r}{V}(X_d \pm 0, \phi, Z)\right]_q = \frac{h}{2\pi}\int_0^1\int_0^{2\pi} \frac{[1-\cos(\phi-\phi')]\,q(\phi', Z')}{\left[4h^2(Z-Z')^2 + 4\sin^2\frac{1}{2}(\phi-\phi')\right]^{3/2}}\,d\phi'\,dZ' \pm \frac{1}{2}q(\phi, Z) \qquad [2.2.3]$$

For the trailing-vortex cylinder:

$$\left[\frac{W_r}{V}(X_d, \phi, Z)\right]_{\frac{\partial\gamma}{\partial\phi}} = \frac{h}{2\pi}\int_0^1\int_0^{2\pi} \cot\frac{1}{2}(\phi-\phi')\left[\frac{2h(Z-Z')}{\sqrt{4h^2(Z-Z')^2 + 4\sin^2\frac{1}{2}(\phi-\phi')}} + 1\right] \frac{\partial\gamma}{\partial\phi}(\phi', Z')\,d\phi'\,dZ' \qquad [2.2.4]$$

where $h = \frac{c}{2R_d}$.

These radial velocities are substituted into the boundary condition [2.1.1] which leads immediately to

$$q(\phi, Z) = -2S'(Z) \qquad [2.2.5]$$

From this equation it is seen that the strength of the source rings is a function only of the thickness slope and, for an axisymmetric duct, is independent of angle. In linearized airfoil

theory the same equation is obtained. Substituting the slope for the source strength into Equation [2.2.3], the radial velocity induced by the ring sources at the cylinder becomes

$$\left[\frac{W_r}{V}(X_d = 0, Z)\right]_q = -\frac{h}{\pi}\int_0^1 S'(Z')\,k[K(k)-E(k)]\,dZ' \mp S'(Z) \qquad [2.2.6]$$

where $k^2 = \dfrac{1}{h^2(Z-Z')^2+1}$ and $K(k)$ and $E(k)$ are complete elliptic integrals of the first and second kind, respectively.

Substitution of the various radial velocities into the boundary condition, Equation [2.2.1], led to the ring-source strength given by Equation [2.2.5]. This same substitution also led to the following integral equation for the ring-vortex circulation:

$$\frac{h}{2\pi}\int_0^1\int_0^{2\pi} \frac{2h(Z-Z')\cos(\phi-\phi')\,\gamma(\phi',Z')}{\left[4h^2(Z-Z')^2+4\sin^2\frac{1}{2}(\phi-\phi')\right]^{3/2}}\,d\phi'\,dZ'$$

$$+\frac{h}{2\pi}\int_0^1\int_0^{2\pi} \cot\frac{1}{2}(\phi-\phi')\left[\frac{2h(Z-Z')}{\sqrt{4h^2(Z-Z')^2+4\sin^2\frac{1}{2}(\phi-\phi')}}+1\right]\frac{\partial\gamma}{\partial\phi}(\phi',Z')\,d\phi'\,dZ'$$

$$= -\left\{[C_1'(Z)+\tan\alpha+\omega_r\cos\phi]-\frac{h}{\pi}\int_C^1 S'(Z')\,k[K(k)-E(k)]\,dZ'-\frac{W_r}{V}(X_d,Z)\right\}$$

$$= U(\phi, Z) \qquad [2.2.7]$$

This equation is a singular-integral equation for the ring-vortex circulation $\gamma(\phi, Z)$. In order to solve this equation, an assumption is made that $\gamma(\phi', Z')$ can be expanded in a Fourier series in ϕ, i.e.,

$$\gamma(\phi', Z') = \sum_{n=0}^{\infty} g_n(Z')\cos n\phi + \sum_{n=1}^{\infty} h_n(Z')\sin n\phi' \qquad [2.2.8]$$

The function $U(\phi, Z)$ is also expanded in a Fourier series in ϕ, but it is immediately obvious because of the form of $U(\phi, Z)$ that only two terms of the series exist, i.e.,

$$U(\phi, Z) = u_0 + u_1 \cos \phi \qquad [2.2.9]$$

where

$$u_0 = -\left\{[C_1'(Z) + \tan\alpha] - \frac{h}{\pi}\int_0^1 S'(Z')\, k[K(k) - E(k)]\, dZ' + \frac{W_r}{V}(X_d, Z)\right\}$$

$$u_1 = -\alpha_r$$

If Equations [2.2.8] and [2.2.9] are substituted into Equation [2.2.7] and the necessary mathematical manipulations are performed, a singular integral equation is obtained for the Euler coefficients $g_0(Z)$ and $g_1(Z)$. All other Euler coefficients are zero since a Fourier series is unique and, hence, the coefficients can be equated. Only u_0 and u_1 exist on the right-hand side of Equation [2.2.7]. The two integral equations obtained are

$$\oint_0^1 \mathcal{A}(Z - Z')\frac{g_0(Z')}{(Z - Z')}\, dZ' = H(Z) \qquad [2.2.10]$$

$$\oint_0^1 \frac{g_1(Z')}{(Z - Z')} W_1(Z - Z')\, dZ' + \pi h \int_0^1 g_1(Z')\, dZ' = -2\pi\alpha_r \qquad [2.2.11]$$

where

$$\mathcal{A}(Z - Z') = k\left\{4h^2(Z - Z')^2\,[K(k) - E(k)] - 2E(k)\right\} \qquad [2.2.12]$$

$$H(Z) = 4\pi[C_1'(Z) + \tan\alpha] - 4\pi\frac{W_r}{V}(X_d, Z) - 4h\int_0^1 S'(Z')\, k[K(k) - E(k)]\, dZ' \qquad [2.2.13]$$

$$k^2 = \frac{1}{h^2(Z - Z')^2 + 1}$$

$$W_1(Z-Z') = \frac{1}{k^3}[(2-k^2)^2 E(k) - 4(1-k^2)^2 K(k)]$$

Solution of these two integral equations gives the circulation distribution for an axisymmetric annular airfoil at an angle of attack, i.e.,

$$\gamma(\phi, Z) = g_0(Z) + g_1(Z)\cos\phi \qquad [2.2.14]$$

Actually, solution of Equation [2.2.10] gives the circulation distribution for an axisymmetric annular airfoil at zero angle of attack. It should be noted that the thickness distribution and the arbitrary axisymmetric radial velocity each contribute to the strength of the ring vortex. Solution of Equation [2.2.11] gives the circulation distribution on a right circular cylinder at an angle of attack with length equal to the duct chord and diameter equal to the representative diameter of the duct. This circulation distribution is independent of the shape of the duct.

The equations for the circulation distributions have been derived in terms of elliptic integrals. They can also be derived in terms of the half-order Legendre function of the second kind.[8] If the annular airfoil is not axisymmetric and the propeller has a finite number of blades, the use of the Legendre functions is preferred.

In the next few sections the two singular integral equations just derived are reduced to Fredholm equations of the second kind and the solution of these equations is discussed.

2.3 REDUCTION OF THE INTEGRAL EQUATION FOR THE AXISYMMETRIC CASE

Following Muskhelishvili,[16] as shown in Reference 9, Equation [2.2.10] can be reduced to a Fredholm equation of the second kind by adding and subtracting the term $g(Z-Z')$ from the kernel. Since at $Z = Z'$ the kernel is equal to -2, i.e., $g(Z-Z') = g(0) = -2$, Equation [2.2.10] becomes

$$\int_0^1 \frac{g_0(Z')}{(Z-Z')}\,dZ' = \frac{1}{2}\int_0^1 [2 + g(Z-Z')]\frac{g_0(Z')}{(Z-Z')}\,dZ' - \frac{1}{2}H(Z) = f_0(Z) \qquad [2.3.1]$$

The integrand of the integral on the right is not singular at the point $(Z = Z')$ and has the value of zero. This equation is in the form of the well-known Cauchy-type, singular-integral equation and has a unique inverse given by

$$g_0(Z) = \frac{1}{\pi\sqrt{Z(1-Z)}}\left[\frac{1}{\pi}\int_0^1 \frac{\sqrt{Z'(1-Z')}}{(Z'-Z)} f_0(Z')\,dZ' + 2\int_0^1 g_0(Z')\,dZ'\right] \qquad [2.3.2]$$

To this equation the second boundary condition, Equation [2.1.2], is applied. This boundary condition implies that the circulation at the trailing edge must be zero, and the constant term $\int_0^1 g_0(Z')\,dZ'$ is chosen so that $g_0(0) = 0$. If $f_0(Z')$ is substituted into this equation for $f_0(Z')$ and the constant chosen as just described, a Fredholm equation of the second kind is obtained for the circulation distribution:

$$g_0^*(Z) = \sqrt{1-Z}\; g_0(Z) = f(Z) + \int_0^1 K_1(Z, Z')\,\frac{g_0^*(Z')}{\sqrt{1-Z'}}\,dZ' \qquad [2.3.3]$$

where

$$f(Z) = -\frac{1}{2\pi^2}\sqrt{Z}\oint_0^1 \frac{1}{(Z-Z')}\sqrt{\frac{1-Z'}{Z'}}\,H(Z')\,dZ'$$

$$K_1(Z, Z') = \frac{1}{2\pi^2}\sqrt{Z}\oint_C \sqrt{\frac{1-Z''}{Z''}}\,\frac{[2+g(Z''-Z')]}{(Z''-Z)\,(Z''-Z')}\,dZ''$$

A new dependent variable is defined by this equation from which the circulation distribution can easily be obtained. This redefining is necessary since the circulation distribution $g_0(Z)$ is generally infinite at the leading edge. The case where $g_0(Z)$ is not infinite at the lead. edge will be discussed later.

Both functions $f(Z)$ and $K_1(Z, Z')$ are Cauchy Principal-value integrals and to evaluate, part of the integrand will be expanded in a Fourier series. For convenience, a change of variable of the form $Z = \frac{1}{2}(1 + \cos\theta)$ is made in Equation [2.3.3]. Then

$$g_0^*(\theta) = g_0(\theta)\sin\frac{1}{2}\theta = f(\theta) + \int_0^{\pi} K(\theta, \theta')\; g_0^*(\theta')\,d\theta' \qquad [2.3.4]$$

where

$$f(\theta) = -\frac{1}{2\pi^2}\cos\frac{1}{2}\theta \int_0^{\pi} \frac{(1-\cos\theta')}{(\cos\theta'-\cos\theta)} H(\theta')\,d\theta' \qquad [2.3.5]$$

$$K(\theta, \theta') = \frac{1}{\pi^2}\cos\frac{1}{2}\theta\cos\frac{1}{2}\theta' \int_0^{\pi} \frac{(1-\cos\theta'')}{(\cos\theta''-\cos\theta)} \left[\frac{2+g(\cos\theta''-\cos\theta')}{\cos\theta''-\cos\theta'}\right] d\theta'' \qquad [2.3.6]$$

To evaluate the function, $f(\theta)$, $H(\theta')$ is obtained in series form. This function is given by Equation [2.2.13] with the proper change in variable. The following half-range Fourier series expansions are made for the slope of the thickness distribution and the section mean line:

$$C_1'(Z) - \frac{W_r}{V}(X_d, Z) = C_1'(\theta) - \frac{W_r}{V}(X_d, \theta) = C_0 + \sum_{m=1}^{\infty} C_m \cos m\theta \qquad [2.3.7]$$

where

$$C_0 = \frac{1}{\pi}\int_0^{\pi} \left[C_1'(\theta) - \frac{W_r}{V}(X_d, \theta)\right] d\theta$$

$$C_m(\theta) = \frac{2}{\pi}\int_0^{\pi} \left[C_1'(\theta) - \frac{W_r}{V}(X_d, \theta)\right] \cos m\theta\, d\theta$$

and

$$S(Z) = S[\theta(Z)] = \sum_{m=1}^{\infty} S_m \sin m\theta \qquad [2.3.8]$$

where

$$S_m = \frac{2}{\pi}\int_0^{\pi} S(\theta) \sin m\theta\, d\theta$$

The slope of the thickness distribution is then given by

$$S'(Z) = \frac{\partial S}{\partial Z}[\theta(Z)] = -\frac{2}{\sin\theta}\sum_{m=1}^{\infty} S_m \cos m\theta$$

Use of the Fourier series expansion causes no restrictions on the thickness distribution; however, Equation [2.3.7] requires that the camber line slope be finite everywhere. Introducing the expansions into Equation [2.2.13] yields the following:

$$H(\theta') = \left\{4\pi\left[\tan\alpha + C_0 + \sum_{m=1}^{\infty} C_m \cos m\theta'\right] + 4h\sum_{m=1}^{\infty} S_m G(\theta', m)\right] \qquad [2.3.9]$$

where

$$G(\theta', m) = \frac{1}{3}\int_0^{\pi} k[K(k) - E(k)] \cos m\theta'' \, d\theta''$$

$$= \int_{\sqrt[3]{\pi-\theta'}}^{\sqrt[3]{\theta'}} t^2 k[K(k) - E(k)] \cos m(\theta' - t^3)\, dt \qquad [2.3.10]$$

$$k^2 = \frac{4}{h^2[\cos\theta' - \cos(\theta' - t^3)]^2 + 4}$$

The elliptic integral of the first kind $K(k)$ has a logarithmic singularity at $k = 1$, which results in the integrand of the left-hand integral of Equation [2.3.9] having a logarithmic singularity at this point. This is a singularity which can be removed by making the change in variable of $\theta' - \theta'' = t^3$. This has been done in the right-hand integral.

To complete the solution, the function $G(\theta', m)$ is expanded in a Fourier cosine series in θ', i.e.,

$$G(\theta', m) = a_0(m) + \sum_{p=1}^{\infty} a_p(m) \cos p\theta' \qquad [2.3.11]$$

where

$$a_0(m) = \frac{1}{\pi}\int_0^{\pi} G(\theta', m)\, d\theta'$$

$$a_p(m) = \frac{2}{\pi}\int_0^{\pi} G(\theta', m) \cos p\theta'\, d\theta'$$

With this expression for $G(\theta', m)$, Equation [2.3.9] is substituted into Equation [2.3.5] and the integral for $f(\theta)$ can now be evaluated. After the order of integration and summation are interchanged, the resulting integrals are of the Glauert type and $f(\theta)$ then becomes

$$f(\theta) = \left[2(\tan\alpha + C_0) + \sum_{m=1}^{\infty} S_m F_m\right] \cos\frac{1}{2}\theta$$

$$+ \left[-2\sum_{m=1}^{\infty} C_m \sin m\theta + \sum_{m=1}^{\infty} S_m B_m(\theta)\right] \sin\frac{1}{2}\theta \qquad [2.3.12]$$

where

$$F_m = \frac{6\lambda}{\pi} m a_0(m)$$

$$B_m(\theta) = -\frac{6\lambda}{\pi} m\left[\sum_{p=1}^{\infty} a_p(m) \sin p\theta\right]$$

To obtain the kernel $K(\theta, \theta')$ also involves the evaluation of a Cauchy principal-value integral. The method used to evaluate this integral is to expand the part of the integrand

$$\left[\frac{2 + g(\cos\theta'' - \cos\theta')}{\cos\theta'' - \cos\theta'}\right]$$

in a half-range Fourier cosine series in θ'. This term is continuous everywhere for $0 \le \theta'' \le \pi$ and has the value zero for $\theta'' = \theta'$.

$$\left[\frac{2+g(\cos\theta''-\cos\theta')}{\cos\theta''-\cos\theta'}\right] = b_0(\theta') + \sum_{n=1}^{\infty} b_n(\theta')\cos n\theta'' \qquad [2.3.13]$$

where

$$b_0(\theta') = \frac{1}{\pi}\int_0^{\pi}\left[\frac{2+g(\cos\theta''-\cos\theta')}{\cos\theta''-\cos\theta'}\right]d\theta''$$

$$b_n(\theta') = \frac{2}{\pi}\int_0^{\pi}\left[\frac{2+g(\cos\theta''-\cos\theta')}{\cos\theta''-\cos\theta'}\right]\cos n\theta''\,d\theta''$$

Substituting this equation into Equation [2.3.6] and evaluating the integrals gives the following for the kernel $K(\theta, \theta')$:

$$K(\theta, \theta') = \frac{1}{\pi}\cos\frac{1}{2}\theta'\left[-b_0(\theta')\cos\frac{1}{2}\theta + \sin\frac{1}{2}\theta\sum_{n=1}^{\infty} b_n(\theta')\sin n\theta\right] \qquad [2.3.14]$$

Both $f(\theta)$ and $K(\theta, \theta')$ are now in a form which can be handled numerically so that the Fredholm equation of the second kind, Equation [2.3.3], can be solved for the circulation distribution. Several methods exist for the solution of this type of integral equation;[17] however, the kernel $K(\theta, \theta')$ is of the degenerate (or product) type and the method applicable to this type of kernel will be used here. Details of this method are given in Reference 17 and only resulting equations are given here. Following this procedure, the equation for the circulation distribution becomes[9]

$$g_0^*(\theta) = f(\theta) + C(\theta)D_0(\theta)A_0 + C(\theta)A_1\sin\theta + \ldots + C(\theta)A_n\sin n\theta \qquad [2.3.15]$$

where $f(\theta)$ is given by Equation [2.3.12]

$$C(\theta) = \frac{1}{\pi}\sin\frac{1}{2}\theta$$

$$D_0(\theta) = -\cot\frac{1}{2}\theta$$

and A_n is given by the following set of simultaneous equations:

$$\begin{aligned}
&A_0(1-C_{00}) - A_1C_{01} - A_2C_{02} - \ldots - A_nC_{0n} = d_0 \\
&-A_0C_{10} + A_1(1-C_{11}) - A_2C_{12} - \ldots - A_nC_{1n} = d_1 \\
&\qquad\qquad \ldots\ldots\ldots\ldots\ldots\ldots \qquad\qquad [2.3.16] \\
&\qquad\qquad \ldots\ldots\ldots\ldots\ldots\ldots \\
&-A_0C_{n0} - A_1C_{n1} - A_2C_{n2} - \ldots + A_n(1-C_{nn}) = d_n
\end{aligned}$$

where

$$C_{ij} = \frac{1}{2\pi}\int_0^{\pi} b_i(\theta')\, D_j(\theta') \sin\theta'\, d\theta'; \qquad (i, j = 0, 1, 2, \ldots n)$$

$$D_0(\theta') = -\cot\frac{1}{2}\theta'$$

$$D_j(\theta') = \sin j\theta'$$

and

$$d_i = \left[2(\tan\alpha + C_0) + \sum_{m=1}^{\infty} S_m F_m\right] f_i - 2\sum_{m=1}^{\infty} C_m d_{im} + \sum_{m=1}^{\infty} S_m f_{im}; \qquad (i = 0, 1, 2 \ldots n)$$

$$f_i = \int_0^{\pi} b_i(\theta') \cos^2\frac{1}{2}\theta'\, d\theta'$$

$$d_{im} = \int_0^{\pi} b_i(\theta') \sin\theta' \sin m\theta'\, d\theta'$$

$$f_{im} = \int_0^{\pi} b_i(\theta')\, B_m(\theta') \sin\theta'\, d\theta'$$

2.4 THE IDEAL ANGLE OF ATTACK

In discussing Equation [2.3.2] of the previous section, the statement was made that the circulation distribution of the annular airfoil was generally infinite at the leading edge. This is not the case, however, if the annular-airfoil section is at its ideal angle of attack α_{id}, i.e., if the stagnation point occurs at the leading edge. This angle can be obtained from Equation [2.3.2] by not only making $g_0(0) = 0$ but also by taking the circulation at the leading edge to be zero, $g_0(1) = 0$, and solving for the angle α:

$$\tan\alpha_{id} \cong \alpha_{id} = \frac{1}{2\pi^2}\int_0^1 \frac{f_1(Z')}{\sqrt{(1-Z')Z'}}\,dZ' \qquad [2.4.1]$$

where

$$f_1(Z') = f_0(Z') + 2\tan\alpha$$

If this value of the ideal angle is substituted in place of the section angle α, an equation is obtained for the ideal circulation distribution:

$$\gamma_{id} = f_{id}(Z) + \int_0^1 K_{id}(Z, Z')\,\gamma_{id}(Z')\,dZ'$$

where

$$f_{id}(Z) = \frac{1}{2\pi^2}\sqrt{Z(1-Z)}\int_0^1 \frac{[H(Z') - 4\pi\tan\alpha]}{(Z'-Z)\sqrt{Z'(1-Z')}}\,dZ'$$

$$K_{id}(Z, Z') = \frac{1}{2\pi^2}\sqrt{Z(1-Z)}\int_0^1 \frac{2 + g(Z''-Z')}{(Z''-Z')(Z''-Z)\sqrt{Z'(1-Z'')}}\,dZ''$$

In this equation it is not necessary to solve for a pseudo-circulation since $\gamma_{id}(0)$ is not singular at the leading edge. By the following the procedure of the previous section, the coefficients $f_{id}(Z)$ and $K_{id}(Z, Z')$ are obtained as follows:

$$f_{id}(\theta) = \left[-2\sum_{m=1}^{\infty} C_m \sin m\theta + \sum_{m=1}^{\infty} S_m B_m(\theta) \right]$$

and

$$K_{id}(\theta, \theta') = \frac{1}{2\pi} \sin \theta' \sum_{n=1}^{\infty} b_n(\theta') \sin n\theta$$

The coefficients C_m, S_m, $B_m(\theta)$, and $b_n(\theta')$ are given in the previous section. The ideal circulation distribution $[g_0(0)]_{id}$ is given by Equation [2.3.15] with

$$C(\theta) = \frac{1}{2\pi}$$

$$D_0(\theta) = 0$$

and d_n is given by

$$\begin{aligned}
A_1(1-C_{11}) - A_2C_{12} - \ldots\ldots - A_nC_{1n} &= d_1 \\
-A_1C_{21} + A_2(1-C_{22}) - \ldots\ldots - A_nC_{2n} &= d_2 \\
\cdot \quad \cdot \quad \cdot \quad \cdot \quad \cdot \quad \cdot \quad \cdot \quad \cdot \quad \cdot \quad \cdot \quad \cdot & \qquad [2.4.2] \\
\cdot \quad \cdot \quad \cdot \quad \cdot \quad \cdot \quad \cdot \quad \cdot \quad \cdot \quad \cdot \quad \cdot \quad \cdot & \\
-A_1C_{n1} - A_2C_{n2} - \ldots\ldots + A_n(1-C_{nn}) &= d_n
\end{aligned}$$

All the coefficients are the same as given in the previous section except for d_i, which is given by

$$d_i = -2\sum_{m=1}^{\infty} C_m d_{im} + \sum_{m=1}^{\infty} S_m f_{im}; \qquad (i = 1, 2, 3 \ldots n)$$

Once the ideal circulation distribution is obtained, the ideal angle of attack at which the section must operate for the stagnation point to be at the leading edge is given by Equation [2.4.1]. Substituting for $f_1(Z')$ into this equation yields the following for α_{id}:

$$\alpha_{id} = \frac{1}{4\pi}\int_0^{\pi} b_0(\theta')\,[g_0(\theta')]_{id}\,\sin\theta'\,d\theta' - \left(\gamma_0 + \frac{1}{2}\sum_{m=1}^{\infty} F_m\right) \qquad [2.4.3]$$

2.5 REDUCTION OF THE INTEGRAL EQUATION FOR THE ANNULAR AIRFOIL AT AN ANGLE OF ATTACK

In Section 2.2 an integral equation was derived for the circulation distribution of an annular airfoil at an angle of attack. This equation showed for the linearized theory that the section shape had no effect on the circulation distribution, which was dependent only on the chord-diameter ratio h and the angle of attack α_r.

The reduction of this Equation [2.2.11] to a Fredholm equation of the second kind follows the procedure outlined in Section 2.3 and is more fully described in Reference 9. The resulting equation is

$$g_1^*(\theta) = \left(\sin\frac{1}{2}\theta\right) g_1(\theta)$$

$$= 2\alpha_r \cos\frac{1}{2}\theta - \frac{2}{\pi}\int_0^{\pi}\left\{\cos\frac{1}{2}\theta'\left[-b_0(\theta')\cos\frac{1}{2}\theta\right.\right.$$

$$\left.\left. + \left\{\sin\frac{1}{2}\theta\right)\sum_{m=1}^{\infty} b_m(\theta')\sin m\theta\right]\right\} g_1^*(\theta')\,d\theta' \qquad [2.5.1]$$

where

$$b_0(\theta') = \frac{\pi}{2}h + \frac{1}{\pi}\int_0^{\pi}\left[\frac{W_1(\cos\theta''-\cos\theta')-1}{(\cos\theta''-\cos\theta')}\right]d\theta'$$

$$b_m(\theta') = \frac{2}{\pi}\int_0^{\pi}\left[\frac{W_1(\cos\theta''-\cos\theta')-1}{(\cos\theta''-\cos\theta')}\right]\cos m\theta''\,d\theta''$$

Here, as in Section 2.3, it is necessary to solve for a pseudo-circulation. From Reference 17 the solution of this equation for the pseudo-circulation is obtained in the following form:

$$g_1^*(\theta) = 2\omega_r \cos\frac{1}{2}\theta - \frac{2}{\pi}A_0\cos\frac{1}{2}\theta - \frac{2}{\pi}[A_1 \sin\theta + {}_2\sin 2\theta + \ldots + A_n \sin n\theta] \qquad [2.5.2]$$

The coefficients A_n are obtained from the set of simultaneous equations given by Equation [2.3.1], except that the coefficients C_{nn} and d_n are

$$C_{ij} = -\frac{1}{\pi}\int_0^{\pi} b_i(\theta')\, D_j(\theta')\sin\theta'\, d\theta'; \qquad (i, j = 0, 1, 2 \ldots n)$$

$$d_i = 2\omega_r \int_0^{\pi} \cos^2\frac{1}{2}\theta'\, b_i(\theta')\, d\theta'; \qquad (i = 1, 2, 3 \ldots n)$$

with

$$D_0(\theta') = -\cot\frac{1}{2}\theta'$$

$$D_j(\theta') = \sin j\theta'; \qquad (j = 1, 2, 3 \ldots n)$$

3. VELOCITY, PRESSURE, AND FORCES

3.1 VELOCITY DISTRIBUTION

In linearized theory the flow field is given by summing the free-stream velocity and the velocities induced by singularities in the flow field. For the annular airfoil at zero angle of attack, this means that to the free-stream velocity must be added the velocity induced by the ring sources and ring vortices. For the zero-incidence case, only axial and radial velocities are induced by the duct and these are[9]

Axial-induced velocity:

$$\left[\frac{W_a}{V}(X, Z)\right]_{\gamma} = -\frac{3h}{\pi\left(\frac{X}{X_d}\right)^{1/2}}\int_{-\sqrt[3]{\theta}}^{\sqrt[3]{\pi-\theta}} g_0^*(\theta')\, k_2\left[K(k_2) - E(k_2)\right.$$

$$\left. - \frac{2\left(\frac{X}{X_d}-1\right)E(k_2)}{k^2(\cos\theta - \cos\theta')^2 + \left(\frac{X}{X_d}-1\right)^2}\right]\cos\frac{1}{2}\cdot(\bar{\theta}^3 + \bar{\theta})\,\bar{\theta}^3\, d\bar{\theta} \qquad [3.1.1]$$

$$\left[\frac{W_a}{V}(X,Z)\right]_q = -\frac{h}{\pi\left(\frac{X}{X_d}\right)^{1/2}}\int_0^{\pi} S'(\theta')\,k_2\left[\frac{2h(\cos\theta-\cos\bar{\theta}')\,E(k_1)}{h^2(\cos\theta-\cos\bar{\theta}')^2+\left(\frac{X}{X_d}-1\right)^2}\right]d\theta' \quad [3.1.2]$$

Radial-irduced velocity:

$$\left[\frac{W_r}{V}(X,Z)\right]_\gamma = \frac{h}{2\pi\left(\frac{X}{X_d}\right)^{3/2}}\int_0^{\pi} g_0^*(\theta')\,k_1[2h(\cos\theta-\cos\theta')]\left[K(k_1)-E(k_1)\right.$$

$$\left.-\frac{2\left(\frac{X}{X_d}\right)E(k_1)}{h^2(\cos\theta-\cos\theta')^2+\left(\frac{X}{X_d}-1\right)^2}\right]\cos\frac{1}{2}\theta'\,d\theta' \quad [3.1.3]$$

$$\left[\frac{W_r}{V}(X,Z)\right]_q = -\frac{3h}{\pi\left(\frac{X}{X_d}\right)^{3/2}}\int_{-\sqrt[3]{\theta}}^{\sqrt[3]{\pi-\theta}} S'(\theta')\,k_2\left[K(k_2)-E(k_2)\right.$$

$$\left.+\frac{2\left(\frac{X}{X_d}\right)\left(\frac{X}{X_d}-1\right)E(k_2)}{h^2(\cos\bar{\theta}-\cos\theta')^2+\left(\frac{X}{X_d}-1\right)^2}\right]\bar{\eta}^2\,d\bar{\theta} \quad [3.1.4]$$

where

$$k_1^2 = \frac{4\left(\frac{X}{X_d}\right)}{h^2(\cos\theta-\cos\theta')^2+\left(\frac{X}{X_d}+1\right)^2}$$

$$k_2^2 = \frac{4\left(\frac{X}{X_d}\right)}{h^2[\cos\theta-\cos(\bar{\theta}^3+\theta)]^2+\left(\frac{X}{X_d}+1\right)^2}$$

and

$$Z = \frac{1}{2}(1 + \cos\theta)$$

$$\theta' - \theta = \bar{\theta}^3 \qquad [3.1.5]$$

The foregoing equations for the induced velocities have been derived in a form for ease in making numerical calculations. Changes in variables have been made in order to remove singularities from the integrand.

On the annular airfoil itself, these equations are considerably simplified since $X = X_d$. However, across a singular vortex sheet there is a discontinuity in the tangential velocity while across a singular source sheet there is a discontinuity in the normal velocity. On the duct itself then; i.e., $X = X_d$ and $0 \leq Z \leq 1$,

Axial-induced velocity:

$$\left[\frac{W_a}{V}(X_d, \omega)\right]_\gamma = \frac{h}{2\pi}\int_{-\sqrt[3]{\theta}}^{\sqrt[3]{\pi-\theta}} g_0^*(\theta')\,\bar{k}\,[K(\bar{k}) - E(\bar{k})]\cos\frac{1}{2}(\bar{\theta}^3 - \theta)\,3\bar{\theta}^2\,d\bar{\theta} = \frac{1}{2}g_0(\theta) \qquad [3.1.6]$$

$$\left[\frac{W_a}{V}(X_d, Z)\right]_q = \frac{2}{\pi}\int_0^\pi \frac{S'(\theta')\,kE(k)}{(\cos\theta - \cos\theta')}\,d\theta' = -\frac{2}{\sin\theta}\sum_{n=1}^{\infty} a_n \sin n\theta \qquad [3.1.7]$$

and

$$a_n = \frac{2}{\pi}\int_0^\pi S'(\theta')\,kE(k)\cos n\theta'\,d\theta'$$

Radial-induced velocity:

$$\left[\frac{W_r}{V}(X_d, Z)\right]_\gamma = \frac{1}{\pi}\int_0^\pi \frac{g_0^*(\theta')\,\bar{k}}{(\cos\theta - \cos\theta')}\left\{k^2(\cos\theta - \cos\theta')^2\,[K(k) - E(k)] - E(k)\right\}\cos\frac{1}{2}\theta'\,d\theta'$$

$$= \frac{1}{\sin\theta}\sum_{n=1}^{\infty} \bar{a}_n \sin n\theta \qquad [3.1.8]$$

and

$$\bar{a}_n = \frac{2}{\pi}\int_0^{\pi} g_0^*(\theta')\cos\frac{1}{2}\theta'\cos n\theta'\,d\theta'$$

$$\left[\frac{W_r}{V}(X_d, Z)\right]_q = -\frac{3h}{\pi}\int_{-\sqrt[3]{\theta}}^{\sqrt[3]{\pi-\theta}} S'(\theta')\,k[K(k)-E(k)]\,\bar{\theta}^2\,d\bar{\theta} \mp 2S'(\theta) \qquad [3.1.9]$$

where

$$k^2 = \frac{4}{h^2(\cos\theta-\cos\theta')^2+4}$$

$$\bar{k}^2 = \frac{4}{h^2[\cos\theta-\cos(\bar{\theta}^3+\theta)]^2+4} \qquad [3.1.10]$$

If the annular airfoil is at angle of attack, then to these induced velocities must be added those induced by the trailing-vortex system and the circulation distribution $g_1(Z)$. The free-vortex system from the duct, when it is at an angle of attack, is straight-line vortices trailing from the duct to infinity and parallel to the z-axis. Consequently, they do not induce any axial velocity but only radial and tangential velocities. These induced velocities are given in Reference 15. On the duct itself, the contribution to the axial-induced velocity due to angle of attack arises only from the vortex distribution on the duct and is

$$\left[\frac{W_a}{V}(X_d, \phi, Z)\right]_{g_1} = \left[-\frac{h}{2\pi}\int_0^1 \frac{g_1(Z')}{k}\left\{(1-k^2)\,[E(k)-3K(k)]\right.\right.$$

$$\left.\left. + 3E(k)-K(k)\right\} dZ' \mp g_1(Z)\right]\cos\phi \qquad [3.1.11]$$

It should be noted that at the duct leading edge, the linearized theory gives rise to infinite velocities unless the duct section is operating at its ideal angle of attack; i.e., unless $g_0(1) \neq \infty$.

3.2 PRESSURE DISTRIBUTION ON THE ANNULAR AIRFOIL

Since the flow field is assumed to be irrotational, steady, and incompressible and body forces are neglected, on the duct itself the pressure distribution is obtained from Bernoulli's equation as

$$C_p = \frac{p(X_d, \phi, Z) - p_0}{\frac{1}{2}\rho V^2} = 2\frac{W_a}{V}(X_d, \phi, Z) - \left(\left[\frac{W_a}{V}(X_d, \phi, Z) \right]^2 + \left[\frac{W_r}{V}(X_d, \phi, Z) \right]^2 + \left[\frac{W_t}{V}(X_d, \phi, Z) \right]^2 \right) \qquad [3.2.1]$$

The velocities W_a, W_r, and W_t are the total velocities induced by the various singularities in the flow. The pressur p_0 is the pressure infinitely far ahead of the duct while $p(X_d, \phi, Z)$ is the local pressure on the duct surface. If the perturbation velocities are small, then the squared terms in this equation can be neglected. This gives the linearized Bernoulli equation, which on the duct itself is

$$C_p = 2\frac{W_a}{V}(X_d, \phi, Z) \qquad [3.2.2]$$

Since, as discussed in the previous section, in the linearized theory the axial velocity induced by the ring vortices has a singularity at the duct leading edge, so does the pressure. An approximate nonlinear correction to the theory which removes this singularity can be made using the argument given in Reference 15. The result of this argument is to multiply the axial velocity by the coefficient

$$\frac{1}{\sqrt{1 + [f'(Z)]^2}} \qquad [3.2.3]$$

As normal airfoil shapes have infinite slopes at their leading edges, this coefficient will suppress the singularity arising in the velocity.

3.3 FORCES ON THE ANNULAR AIRFOIL

The forces on the annular airfoil follow directly from the Kutta-Joukowski law,[18] which for each section is

$$F = \rho V \Gamma \qquad [3.3.1]$$

The velocity V is the velocity perpendicular to the direction of the force F and does not include the self-induced velocity. The function Γ is the circulation and ρ is the mass density. To obtain the total force in any one direction, the force on each section is integrated around the duct.

The total lift L is defined in some arbitrary direction which here will be taken to be positive radially outward, perpendicular to the axial coordinate z, and at $\phi = 0$. For the axisymmetric case, the lift on each section is radially outward but, since it is equal at each angular position, the total lift is zero. By the same reasoning, the lift in an arbitrary axisymmetric velocity is also zero. The only net lift occurs when the duct is at an angle of attack, and this is given by[9]

$$C_L = \frac{L}{\rho_{\frac{1}{2}} V^2 a R_d} = 2\pi \int_0^1 g_1(Z')\,dZ' = 2\pi \int_0^\pi g_1^*(\theta) \cos\frac{1}{2}\theta\, d\theta \qquad [3.3.2]$$

The induced drag also follows directly from Equation [3.3.1]. As for the lift, the induced drag of the duct at zero incidence is also zero. However, an arbitrary axisymmetric-radial velocity by the duct, such as induced by a propeller, does induce a drag. The induced drag then follows[9] as

$$C_{D_i} = \frac{D_i}{\rho_{\frac{1}{2}} V^2 a R_d} = -2 \int_0^1 \int_0^{2\pi} \gamma(\phi, Z') \left(\left[\frac{W_r}{V} \right]_{\frac{\partial \gamma}{\partial \phi}} + \left[\frac{W_r}{V} \right] \right) d\phi\, dZ \qquad [3.3.3]$$

For the duct at zero incidence, this equation reduces to

$$C_{D_i} = -4\pi \int_0^1 g_0(Z') \left[\frac{W_r}{V}(X_d, Z') \right] dZ' = 4\pi \int_0^\pi g_0^*(\theta) \frac{W_r}{V}(\theta) \cos\frac{1}{2}\theta\, d\theta \qquad [3.3.4]$$

where the velocity W_r is the arbitrary axisymmetric-radial velocity by the duct. Obviously, for the duct at zero incidence and purely axisymmetric flow, the induced drag is zero. If the duct is at an angle of incidence in otherwise purely axisymmetric flow, Equation [3.3.3] becomes, after some manipulation,

$$C_{D_i} = \frac{\dot{n}}{4\pi} C_L^2 \qquad [3.3.5]$$

which is the result obtained by Ribner.[19] To find the total drag, the viscous drag must be added to the induced drag.

The total moment on the axisymmetric duct at zero incidence and, also, in the presence of an arbitrary axisymmetrical flow is zero. Consequently, the only moment arises when the duct is at an angle of attack. This moment arises from two sources, one being from the vertical forces (lift) and the other from the horizontal forces (drag). This differs somewhat from two-dimensional airfoil theory where only the lift force contributes. The moment M follows also from Equation [3.3.1] as

$$C_M = \frac{M}{\rho_\infty V^2 a^2 R_d} = C_{M_V} + C_{M_H} \qquad [3.3.6]$$

where, about the leading edge

$$\left(C_{M_V}\right)_{\ell.e.} = -\pi \int_0^\pi g_1^*(\theta) \sin\theta \sin\frac{1}{2}\theta \, d\theta \qquad [3.3.7]$$

and

$$C_{M_H} = \frac{C_L}{4} \int_0^\pi g_0^*(\theta) \cos\frac{1}{2}\theta \, d\theta$$

$$+ \int_0^\pi g_0^* \cos\frac{1}{2}\theta \left\{ \int_0^\pi g_1^*(\theta') \cos\frac{1}{2}\theta' \left[\frac{h(\cos\theta - \cos\theta')}{k} K(k) - E(k) \right] d\theta' \right\} d\theta \qquad [3.3.8]$$

The moment from the drag force is normally small compared to that from the lift force, but it should not be neglected.

To obtain the moment about any point on the duct, the contribution due to the vertical forces is shifted from the leading edge by the following relation:

$$C_{M_V} = \left(C_{M_V}\right)_{l.e.} + C_L(1-Z) \qquad [3.3.8]$$

4. COMPUTER PROGRAM

The calculations based on the theory for the annular airfoil operating at a given angle of attack have been programmed for the IBM-7090 high-speed computer. Input consists of the section camber and thickness ordinates, the section angle of attack, and the chord-diameter ratio of the annular airfoil. An arbitrary axisymmetric velocity can also be included.

The standard output consists of the lift, drag, and moment coefficients as well as the circulation and pressure distribution on the duct. There are options also for obtaining the ideal angle of attack of the duct section and the velocity field inside the duct.

It takes approximately 10 minutes on the IBM-7090 high-speed computer to calculate the duct forces, pressure distribution, and the velocity field inside the duct. The input-output format and the FORTRAN listing of the computer program are discussed in the following sections.

4.1 INPUT FORMAT

The duct identification is key punched on the first IBM input card using Format 12A6 where Columns 1 through 72 can be used. The remainder of the input data is punched on IBM cards using Format F8.6 where up to nine field point parameters, each having a field width of eight columns, can be punched on a card. These particular formats are described in Reference 20.

Seven parameters are punched on the second input card with the first four quantities being the number of camber ordinates, the number of section thickness ordinates, the chord-diameter ratio of the duct, and the section angle of attack α in degrees, respectively. If the camber is zero, the number of camber ordinates input is zero and if the ideal angle of attack is desired, the section angle input is zero. The number of camber and thickness ordinates which can be input is a minimum of 17 and a maximum of 39.

The fifth quantity on the second input card is an option for calculating the ideal angle of attack of the duct section. If the ideal angle of attack is not to be calculated, the fifth input quantity is zero; if this angle is to be calculated, 1.0 is used. The sixth and seventh quantities on the second input card are input options concerning the induced radial and axial velocities, respectively. If these velocities are taken as zero, the input values are zero; if either or both of these velocities are zero, 1.0 is used.

The stations along the section chord and the corresponding camber ordinates, nondimensionalized on the section-chord length, are punched on the first and second sets of input data cards, respectively. These cards are omitted, however, if the section camber is zero.

The stations along the section chord and the corresponding half thickness ordinates, nondimensionalized on the section chord length, are punched on the third and fourth sets of input data cards, respectively. If the section ideal angle of attack is to be computed, no other input data is required for the computer program.

The number of points (a minimum of 17 and a maximum of 39) along the section chord where the radial velocity is given as input should be punched on the next input data card. Following this card, the stations along the section chord and the corresponding radial velocity, nondimensionalized by the ship speed, are punched on the fifth and sixth sets of input data cards, respectively. If the input radial velocity is zero, these data cards are omitted.

The number of points (a minimum of 17 and a maximum of 39) along the section chord where the axial velocity is given as input should be punched on the next input data card. Following this card, the stations along the section chord and the corresponding axial velocit nondimensionalized on the ship speed, are punched on the seventh and eighth sets of input data cards, respectively. If the input axial velocity is zero, these data cards are omitted.

The number of different geometric angles of attack for computing the duct pressure distribution (which must be less than 41) is punched on the next input data card. Geometric angles of attack in degrees and the corresponding angular positions of the duct section in degrees at which the calculations are to be made are punched on the ninth and tenth sets of input data cards, respectively. The program always makes calculations for $\phi = 0$; thus it is not necessary to input this value.

The next card is an option card for calculating the velocity field inside the duct. If this velocity is not to be calculated, the input quantity is zero; if the velocity is to be calculated, 1.0 is used. If the input is zero, no additional data are required for the computer program.

Two input quantities should be punched on the next card if the above input data are 1.0. The first quantity gives the number of different radial positions (which should be less than or equal to 11). The duct radii and the stations along the duct chord are punched on the eleventh and twelfth sets of input data cards, respectively. An example showing the input data for a duct where the radial and axial-induced velocities are zero and the pressure distribution and velocity field inside the duct are desired is shown in Appendix A.

Option 10, which allows the program to overload the operating system,[20] must also be added to this program. The binary common reassignment card must have a minus sign, 7, and 9 punched in Column 1, a plus sign punched in Column 2, and a plus sign and zero punched in Column 6.

4.2 OUTPUT FORMAT

The input is printed on the first page of output and the duct forces, including the lift, drag, and moment coefficients, are given on the second page. The third page of output gives the duct circulation distribution, nonlinear corrections, and the nonlinear pressure distribution inside and outside the duct for a given geometric angle of attack. It should be noted that the pressure distribution includes the effect of adding the axial-induced velocity given as input to that induced on the annular airfoil. If more than one geometric angle of attack is given as input, the parameters presented on the third page of output will be printed on a new page for each additional geometric angle of attack. The axial and radial velocities along the duct chord at a given radius inside the duct are printed on the next page of output if desired. If more than one duct radius is given as input, these velocities are printed on a new page for each additional duct radius given as input.

Note that if only the section ideal angle of attack is desired, this computed value, rather than the duct forces, will be printed on the second page of output. The output obtained from the input data of the annular airfoil given in Section 4.1 is also shown in Appendix A.

4.3 FORTRAN LISTING

The FORTRAN listing of the computer program is given in Appendix B. In addition to the subroutines furnished automatically by the Bell Monitor System on the IBM-7090, the binary coding for the BE-ELIP, E2-AMGMHA, B4-LACBRT, DI-GLGAU2, AMMAT1, AM-SIUF, VG-AS+C, and D1-AQAKK1 subroutines must be added to the FORTRAN listing of this program.

5. EXPERIMENTAL AND THEORETICAL RESULTS

5.1 EXPERIMENTAL RESULTS

Two ducts, 20 inches in diameter, were manufactured and tested in the Subsonic Wind Tunnel of the Aerodynamics Laboratory. The tests were run at a Reynolds number of 2.06×10^6 Both ducts had chord-diameter ratios of 0.8 and the section shapes were as shown in Figure 3. The cross section of Duct I is an NACA 0010 thickness distribution with an NACA 250 mean line of maximum camber-chord ratio of -0.0375. Each section operates at an angle of attack of 6 degrees. Such an annular airfoil typifies the shape used for Kort nozzles. Duct II has a cross section made up of an NACA 66 Mod. thickness distribution of maximum thickness-chord ratio of 0.10 with an NACA $a = 0.8$ mean line of a maximum camber-chord ratio of 0.04. The angle of attack of the section is zero.

Also shown in Figure 3 is a duct shape tested by the Bureau Technique Zborowski in France.[21] This duct has a chord-diameter ratio of 0.96. The section is an NACA 66-006 with no camber, and the angle of attack of each section is zero.

Force data in coefficient form, i.e., lift (C_L), drag (C_D), and moment (C_M), are plotted in Figure 4 for Duct I. These tests were carried out for geometric angles of attack covering a range of ± 10 degrees. Pressure distributions were made on both the inside and outside of the duct at geometric angles of attack from 0 to 10 degrees in steps of 2 degrees. Flow separation occurred on this duct even for zero angle of attack thus only the results for 0 and 6 degrees are shown here. Figure 5 shows the pressure distribution plotted against the chordwise location of the pressure tap for the zero angle of attack case. The results for the 6 degree angle of attack are plotted in Figures 6 and 7. Figure 6 is the pressure distribution for the duct section which is in the upward position as shown in Figure 1; i.e., $\phi = 0$ degrees. Figure 7 shows the pressure distribution at the lower section; i.e., $\phi = 180$ degrees.

The force data for Duct II are plotted in Figure 8 and again, the range of tests was ± 10 degrees. Pressure distributions for this duct are plotted in Figures 9 through 15. Figure 9 gives the pressure distribution of the inside and outside of the duct for zero angle of attack. Figures 10 and 11 give the pressure distribution for 4-degree angle of attack for the position $\phi = 0$ degrees and $\phi = 180$ degrees, respectively. Figures 12 and 13 are the pressure distributions for 8 degrees and $\phi = 0$ degrees and $\phi = 180$ degrees, respectively; Figures 14 and 15 are for 10 degrees for $\phi = 0$ degrees and $\phi = 180$ degrees, respectively.

The force data for the BTZ duct are shown in Figure 16, and the pressure distributions are given in Figure 17 through 19. Figure 17 gives the pressure distribution for the zero angle of attack case; Figures 18 and 19 are for the 9-degree angle of attack with $\phi = 0$ degrees and $\phi = 180$ degrees, respectively.

5.2 THEORETICAL RESULTS

5.2.1 Axisymmetric Duct

In this section, results of theoretical calculations are compared to the test results just presented. The theoretical calculations were made on an IBM-7090 computer by the Applied Mathematics Laboratory with the FORTRAN program presented in Section 4.

In making theoretical predictions of the aerodynamic characteristics of the annular airfoil, the first step involves the calculation of the section circulation distribution as given by Equations [2.3.4] and [2.3.15]. The circulation distributions for the three ducts are described in the previous section are shown in Figure 20 for a zero angle of attack. Since the BTZ duct has zero camber, the circulation distribution is solely a function of the thickness distribution. For Duct I the effect of local angle of attack is dominant near the leading edge, which no doubt gives an indication of the separation which occurred on the duct. For Duct II it must be concluded that camber is the dominant effect since the thickness distribution leads to a negative circulation distribution. It should be noted that these circulation distributions must be divided by $\sqrt{1-z}$ in order to obtain the actual circulation.

The actual circulation distribution is singular at the leading edge except when each section is operating at its ideal angle of attack. This ideal angle of attack is obtained from Equation [2.4.3]. For these three ducts, this equation gives the ideal angle of attack as:

	α_{id} degrees	α_{Design} degrees
Duct I	−1.67	6
Duct II	0.78	0
BTZ	0.020	0

The theoretical pressure distribution on the ducts is given by Equation [3.2.2]. Results of evaluation of this equation, using the nonlinear correction given by Equation [3.2.3] for the axisymmetric case, are shown as solid lines on Figures 5, 9, and 17 for Ducts I, II, and BTZ, respectively. The prediction is poor for the outside of Duct I where separation occurred near the leading edge. Inside the duct, however, the prediction is good. For both Duct II and the BTZ duct, the agreement between theory and experiment is quite good. Also shown in Figure 9 is the pressure distribution for Duct II, calculated from the linearized theory and by the method of Chaplin.[22] This last method is a nonlinear theory; therefore, this plot gives the comparison between the linear theory, nonlinear theory, and experiment. It is clear that the linear theory does not give quite as good a prediction as either the nonlinear correction or the nonlinear theory. However, the theoretical pressure distribution by any of the methods is quite reasonable except when separation occurs on the duct.

The separation occurring near the leading edge on Duct I is undoubtedly a laminar separation. With this type of separation, usually called leading edge bubble, the flow reattaches itself near the transition region. At high angles of attack, turbulent separation, of course, does occur and the annular foil stalls. These various flow regimes have been mapped on an annular airfoil by Eichelbrenner.[23]

In addition to knowing the pressure distribution on the duct (or velocity distribution), it is desirable to know the velocities induced anywhere in the flow field by the presence of the duct. These velocities, for the axisymmetric duct at zero angle of attack, are calculated by the computer program from Equations [3.1.1] to [3.1.4]. Figure 21 shows the radial variation of the velocity at the 1/2 chord point of Duct II as calculated from these equations. No experimental results are available for comparison.

5.2.2 Duct at an Angle of Attack

For the duct at an angle of attack, the forces and the effect on the pressure distribution are independent of the section shape except for the moment which arises from the horizontal forces C_{M_H}. The forces and pressure distribution are, of course, dependent on the chord-diameter ratio h.

Figure 22 shows the theoretical lift coefficient versus the chord-diameter ratio. Also plotted on this curve are the test spots from Ducts I, II, and BTZ along with test results by Fletcher.[24] The ducts tested by Fletcher had Clark-Y sections with thickness-chord ratios of 0.117. The theory gives a surprisingly good prediction, even for Duct I which had separation. The theoretical lift is also plotted on Figures 4, 8, and 16 as a solid line. These plots show that the theory gives good prediction of the lift through 10 degrees.

The induced drag is a function of the lift squared as shown by Equation [3.3.5]. The theoretical values, calculated from this equation, are shown on Figures 4, 8, and 16. Here the drag at zero angle of attack was taken as the profile drag and no attempt was made to calculate this drag.* It can be seen that the theoretical drag gives a good prediction; however, at the higher angles of attack, more deviation occurs than for the lift. For Ducts I and II the theory underpredicts the drag at the high angles of attack, which no doubt is due to separation. It should be noted that the much higher profile drag of Duct I is a consequence of a high pressure drag.

The theoretical moment, as given by Equation [3.3.6], consists of two parts, one due to vertical forces C_{M_V} and the other due to horizontal forces C_{M_H}. The moment C_{M_V}, as given by Equation [3.3.7], is plotted in Figure 23. Figures 4, 8, and 16 show the total theoretical moment as a solid line compared to the experimental values. Also shown on Figures 4 and 8 as a dashed line is the moment C_{M_V}. The effect of the horizontal term is small but its use does give a better prediction, especially for Duct II. It would be expected that the moment of Duct I would deviate somewhat from the theoretical value since the leading edge considerably alters the pressure distribution.

The theoretical pressure distribution contributed by the angle of attack as calculated using Equations [3.1.11] and [3.3.2] is shown in Figure 24 and is further tabulated in Tables 1 through 10. It can be seen that the chord-diameter ratio has a considerable effect on the pressure distribution and that the shorter the chord, the greater the effect. To obtain the total pressure distribution on a duct at an angle of attack, these values are added to those obtained for the axisymmetric case. For Duct I, the pressure distribution is shown at a 6-degree angle of attack in Figure 6 for the angular position $\phi = 0$ degrees, and in Figure 7

*The method of predicting drag of axisymmetric bodies as discussed by Granville[25] should give a reasonable estimate of the profile drag.

for the angular position ϕ = 180 degrees. Because of the flow separation occurring on the outside of the duct, the prediction is poor at ϕ = 0 degrees; however, for ϕ = 180 degrees, the predicted pressure distribution is quite reasonable. It is apparent that no separation is occurring in this part of the duct at the 6-degree angle of attack.

Theoretical pressure distributions are shown on Figures 10 through 15 for Duct II at various geometric angles of attack. All theoretical pressure distributions look reasonable up through 8 degrees. At 10 degrees, however, separation occurs on the inside of the duct at the angular position ϕ = 180 degrees (Figure 15). At 8 degrees there is some deviation from the experimental values as shown in Figure 13, which would indicate that flow is starting to separate at this angle. The predicted pressure distribution on the outside at ϕ = 0 degrees is quite reasonable even at 10 degrees (Figure 14).

For the BTZ duct, theoretical pressure distributions are plotted with the experimental points on Figures 18 and 19. The geometric angle of attack is 9 degrees, and for both the ϕ = 0-degree and ϕ = 180-degree angular positions, the comparison between theory and experiment is good. Some deviation does occur near the trailing edge inside the duct at ϕ = 0 degrees.

CONCLUSIONS

From the results of this investigation on the aerodynamic characteristics of annular airfoils, we can make the following conclusions:

1. The theory gives good predictions of the lift, induced-drag, and moment coefficients even when laminar separation occurs at the leading edge.

2. The theory gives good predictions of the pressure distribution except when separation is present.

3. The moment coefficient from the drag forces is normally small compared to that from the lift force but should not be neglected.

4. The nonlinear correction to the pressure distributions is normally small but should not be neglected.

5. The computer program, as compared to other methods, is efficient and quite versatile.

6. The computer program can be used for ducted propeller designs with the restriction of the assumption of infinite number of blades since an arbitrary axisymmetric velocity can be given as input.

7. The computer program can be used to obtain the ideal angle of attack of the duct section which is important for design purposes.

Pressure Distribution per Degree for
Chord-Diameter Ratio of 0.2

θ	X	Outside	Inside
0	-0.		
5	0.190265E-02	-0.597813E 00	0.603511E 00
10	0.759613E-02	-0.296685E-00	0.302493E-00
15	0.170371E-01	-0.195903E-00	0.201903E-00
20	0.301537E-01	-0.145178E-00	0.151452E-00
25	0.468461E-01	-0.114460E-00	0.121077E-00
30	0.669873E-01	-0.937352E-01	0.100754E-00
35	0.904240E-01	-0.787129E-01	0.861874E-01
40	0.116978E-00	-0.672667E-01	0.752097E-01
45	0.146447E-00	-0.582051E-01	0.666278E-01
50	0.178606E-00	-0.508019E-01	0.597374E-01
55	0.213212E-00	-0.446243E-01	0.540609E-01
60	0.250000E-00	-0.393695E-01	0.492941E-01
65	0.288691E-00	-0.348103E-01	0.452440E-01
70	0.328990E-00	-0.308363E-01	0.417203E-01
75	0.370590E-00	-0.273835E-01	0.385667E-01
80	0.413176E-00	-0.242706E-01	0.357984E-01
85	0.456422E-00	-0.215105E-01	0.332755E-01
90	0.500000E-00	-0.190641E-01	0.309376E-01
95	0.543578E 00	-0.167943E-01	0.288428E-01
100	0.586824E 00	-0.147792E-01	0.268493E-01
105	0.629410E 00	-0.129961E-01	0.249279E-01
110	0.671010E 00	-0.113317E-01	0.231486E-01
115	0.711309E 00	-0.985843E-02	0.214032E-01
120	0.750000E 00	-0.850522E-02	0.197319E-01
125	0.786788E 00	-0.723594E-02	0.181448E-01
130	0.821394E 00	-0.609190E-02	0.165778E-01
135	0.853553E 00	-0.505925E-02	0.150246E-01
140	0.883022E 00	-0.407189E-02	0.135356E-01
145	0.909576E 00	-0.311972E-02	0.120990E-01
150	0.933013E 00	-0.220399E-02	0.107052E-01
155	0.953154E 00	-0.129947E-02	0.936430E-02
160	0.969846E 00	-0.405717E-03	0.806464E-02
165	0.982963E 00	0.493535E-03	0.681127E-02
170	0.992404E 00	0.142657E-02	0.562183E-02
175	0.998097E 00	0.239725E-02	0.448994E-02
180	0.100000E 01		

Pressure Distribution per Degree for
Chord-Diameter Ratio of 0.4

θ	X	Outside	Inside
0	-0.		
5	0.190265E-02	-0.478596E-00	0.482088E-00
10	0.759613E-02	-0.237525E-00	0.241077E-00
15	0.170371E-01	-0.156527E-00	0.160441E-00
20	0.301537E-01	-0.115667E-00	0.119941E-00
25	0.468461E-01	-0.908030E-01	0.955290E-01
30	0.669873E-01	-0.739287E-01	0.791837E-01
35	0.904240E-01	-0.616271E-01	0.674558E-01
40	0.116978E-00	-0.521841E-01	0.586283E-01
45	0.146447E-00	-0.446671E-01	0.517292E-01
50	0 178606E-00	-0.385068E-01	0.461857E-01
55	0.213212E-00	-0.333298E-01	0.416455E-01
60	0.250000E-00	-0.289144E-01	0.378466E-01
65	0.288691E-00	-0.251252E-01	0.345897E-01
70	0.328990E-00	-0.218206E-01	0.317771E-01
75	0.370590E-00	-0.189202E-01	0.293131E-01
80	0.413176E-00	-0.164183E-01	0.270710E-01
85	0.456422E-00	-0.141901E-01	0.250731E-01
90	0.500000E-00	-0.121947E-01	0.232796E-01
95	0.543578E 00	-0.104876E-01	0.215702E-01
100	0.586824E 00	-0.896488E-02	0.199958E-01
105	0.629410E 00	-0.760698E-02	0.185316E-01
110	0.671010E 00	-0.646671E-02	0.170876E-01
115	0.711309E 00	-0.545243E-02	0.157239E-01
120	0.750000E 00	-0.454435E-02	0.144326E-01
125	0.786788E 00	-0.377189E-02	0.131608E-01
130	0.821394E 00	-0.310557E-02	0.119171E-01
135	0.853553E 00	-0.250621E-02	0.107221E-01
140	0.883022E 00	-0.196778E-02	0.956522E-02
145	0.909576E 00	-0.147467E-02	0.844713E-02
150	0.933013E 00	-0.100175E-02	0.737950E-02
155	0.953154E 00	-0.544656E-03	0.635450E-02
160	0.969846E 00	-0.821119E-04	0.538224E-02
165	0.982963E 00	0.404963E-03	0.447151E-02
170	0.992404E 00	0.930062E-03	0.362610E-02
175	0.998097E 00	0.150580E-02	0.284934E-02
180	0.100000E 01		

TABLE 3

Pressure Distribution per Degree for
Chord-Diameter Ratio of 0.6

θ	X	Outside	Inside
0	-0.		
5	0.190265E-02	-0.403608E-00	0.405472E-00
10	0.759613E-02	-0.200118E-00	0.202153E-00
15	0.170371E-01	-0.131682E-00	0.133997E-00
20	0.301537E-01	-0.969868E-01	0.996759E-01
25	0.468461E-01	-0.757777E-01	0.789250E-01
30	0.669873E-01	-0.613080E-01	0.649889E-01
35	0.904240E-01	-0.507058E-01	0.549581E-01
40	0.116978E-00	-0.425450E-01	0.473713E-01
45	0.146447E-00	-0.360058E-01	0.414477E-01
50	0.178606E-00	-0.306666E-01	0.366505E-01
55	0.213212E-00	-0.261740E-01	0.327240E-01
60	0.250000E-00	-0.223623E-01	0.294294E-01
65	0.288691E-00	-0.191183E-01	0.265993E-01
70	0.328990E-00	-0.163105E-01	0.241641E-01
75	0.370590E-00	-0.138699E-01	0.220439E-01
80	0.413176E-00	-0.117819E-01	0.201401E-01
85	0.456422E-00	-0.997413E-02	0.184363E-01
90	0.500000E-00	-0.840606E-02	0.169017E-01
95	0.543578E 00	-0.706241E-02	0.154933E-01
100	0.586824E 00	-0.590905E-02	0.141965E-01
105	0.629410E 00	-0.492522E-02	0.129906E-01
110	0.671010E 00	-0.411254E-02	0.118387E-01
115	0.711309E 00	-0.341087E-02	0.107699E-01
120	0.750000E 00	-0.280739E-02	0.977012E-02
125	0.786788E 00	-0.232387E-02	0.879401E-02
130	0.821394E 00	-0.192615E-02	0.785486E-02
135	0.853553E 00	-0.156449E-02	0.698402E-02
140	0.883022E 00	-0.128231E-02	0.612185E-02
145	0.909576E 00	-0.101655E-02	0.531725E-02
150	0.933013E 00	-0.785911E-03	0.453879E-02
155	0.953154E 00	-0.564170E-03	0.380156E-02
160	0.969846E 00	-0.330018E-03	0.311683E-02
165	0.982963E 00	-0.730192E-04	0.248593E-02
170	0.992404E 00	0.214832E-03	0.190850E-02
175	0.998097E 00	0.554444E-03	0.139763E-02
180	0.100000E 01		

TABLE 4

Pressure Distribution per Degree for
Chord-Diameter Ratio of 0.8

θ	X	Outside	Inside
0	-0.		
5	0.190265E-02	-0.353092E-00	0.354118E-00
10	0.759613E-02	-0.174861E-00	0.176064E-00
15	0.170371E-01	-0.114760E-00	0.116241E-00
20	0.301537E-01	-0.841747E-01	0.860249E-01
25	0.468461E-01	-0.654025E-01	0.676815E-01
30	0.669873E-01	-0.525384E-01	0.553118E-01
35	0.904240E-01	-0.430774E-01	0.463692E-01
40	0.116978E-00	-0.357698E-01	0.395837E-01
45	0.146447E-00	-0.299230E-01	0.342522E-01
50	0.178606E-00	-0.251301E-01	0.299478E-01
55	0.213212E-00	-0.211597E-01	0.263725E-01
60	0.250000E-00	-0.178090E-01	0.233767E-01
65	0.288691E-00	-0.149663E-01	0.208271E-01
70	0.328990E-00	-0.125600E-01	0.186182E-01
75	0.370590E-00	-0.105076E-01	0.166998E-01
80	0.413176E-00	-0.877502E-02	0.150033E-01
85	0.456422E-00	-0.730667E-02	0.135023E-01
90	0.500000E-00	-0.606232E-02	0.121696E-01
95	0.543578E 00	-0.502288E-02	0.109678E-01
100	0.586824E 00	-0.415279E-02	0.988435E-02
105	0.629410E 00	-0.342618E-02	0.890354E-02
110	0.671010E 00	-0.282963E-02	0.800272E-02
115	0.711309E 00	-0.233360E-02	0.718007E-02
120	0.750000E 00	-0.194454E-02	0.640177E-02
125	0.786788E 00	-0.163060E-02	0.567595E-02
130	0.821394E 00	-0.136728E-02	0.500651E-02
135	0.853553E 00	-0.116358E-02	0.436665E-02
140	0.883022E 00	-0.996742E-03	0.376377E-02
145	0.909576E 00	-0.858342E-03	0.319307E-02
150	0.933013E 00	-0.743332E-03	0.264825E-02
155	0.953154E 00	-0.633211E-03	0.213806E-02
160	0.969846E 00	-0.509822E-03	0.167227E-02
165	0.982963E 00	-0.373023E-03	0.124364E-02
170	0.992404E 00	-0.210835E-03	0.857634E-03
175	0.998097E 00	-0.909498E-05	0.522377E-03
180	0.100000E 01		

TABLE 5

Pressure Distribution per Degree for Chord-Diameter Ratio of 1.0

θ	X	Outside	Inside
0	-0.		
5	0.190265E-02	-0.316876E-00	0.317505E-00
10	0.759613E-02	-0.156667E-00	0.157479E-00
15	0.170371E-01	-0.102498E-00	0.103572E-00
20	0.301537E-01	-0.748307E-01	0.762609E-01
25	0.468461E-01	-0.577823E-01	0.596145E-01
30	0.669873E-01	-0.460556E-01	0.483412E-01
35	0.904240E-01	-0.374092E-01	0.401542E-01
40	0.116978E-00	-0.307245E-01	0.339160E-01
45	0.146447E-00	-0.253836E-01	0.289971E-01
50	0.178606E-00	-0.210236E-01	0.250157E-01
55	0.213212E-00	-0.174399E-01	0.217035E-01
60	0.250000E-00	-0.144479E-01	0.189294E-01
65	0.288691E-00	-0.119573E-01	0.165621E-01
70	0.328990E-00	-0.987592E-02	0.145315E-01
75	0.370590E-00	-0.813259E-02	0.127850E-01
80	0.413176E-00	-0.669183E-02	0.112599E-01
85	0.456422E-00	-0.549951E-02	0.993012E-02
90	0.500000E-00	-0.451283E-02	0.877122E-02
95	0.543578E 00	-0.371030E-02	0.774742E-02
100	0.586824E 00	-0.305329E-02	0.684802E-02
105	0.629410E 00	-0.251418E-02	0.605794E-02
110	0.671010E 00	-0.207860E-02	0.535467E-02
115	0.711309E 00	-0.172474E-02	0.472827E-02
120	0.750000E 00	-0.145257E-02	0.415165E-02
125	0.786788E 00	-0.124618E-02	0.361766E-02
130	0.821394E 00	-0.107272E-02	0.313963E-02
135	0.853553E 00	-0.939066E-03	0.269423E-02
140	0.883022E 00	-0.833559E-03	0.227945E-02
145	0.909576E 00	-0.752109E-03	0.188716E-02
150	0.933013E 00	-0.691044E-03	0.151197E-02
155	0.953154E 00	-0.633801E-03	0.116223E-02
160	0.969846E 00	-0.565946E-03	0.845768E-03
165	0.982963E 00	-0.487915E-03	0.556608E-03
170	0.992404E 00	-0.391925E-03	0.297749E-03
175	0.998097E 00	-0.265969E-03	0.768849E-04
180	0.100000E 01		

TABLE 6

Pressure Distribution per Degree for Chord-Diameter Ratio of 1.2

θ	X	Outside	Inside
0	-0.		
5	0.190265E-02	-0.289555E-00	0.289993E-00
10	0.759613E-02	-0.142886E-00	0.143497E-00
15	0.170371E-01	-0.931631E-01	0.940389E-01
20	0.301537E-01	-0.676771E-01	0.688954E-01
25	0.468461E-01	-0.519086E-01	0.535178E-01
30	0.669873E-01	-0.410401E-01	0.430497E-01
35	0.904240E-01	-0.330082E-01	0.354218E-01
40	0.116978E-00	-0.268010E-01	0.295897E-01
45	0.146447E-00	-0.218564E-01	0.249802E-01
50	0.178606E-00	-0.178440E-01	0.212461E-01
55	0.213212E-00	-0.145802E-01	0.181399E-01
60	0.250000E-00	-0.118907E-01	0.155455E-01
65	0.288691E-00	-0.968914E-02	0.133432E-01
70	0.328990E-00	-0.788199E-02	0.114723E-01
75	0.370590E-00	-0.639695E-02	0.988470E-02
80	0.413176E-00	-0.519696E-02	0.851984E-02
85	0.456422E-00	-0.422687E-02	0.735143E-02
90	0.500000E-00	-0.344394E-02	0.635319E-02
95	0.543578E 00	-0.282235E-02	0.549180E-02
100	0.586824E 00	-0.232401E-02	0.475463E-02
105	0.629410E 00	-0.191926E-02	0.412795E-02
110	0.671010E 00	-0.159530E-02	0.358765E-02
115	0.711309E 00	-0.133561E-02	0.311922E-02
120	0.750000E 00	-0.114164E-02	0.269530E-02
125	0.786788E 00	-0.997250E-03	0.231060E-02
130	0.821394E 00	-0.873475E-03	0.197644E-02
135	0.853553E 00	-0.776786E-03	0.167182E-02
140	0.883022E 00	-0.701805E-03	0.139021E-02
145	0.909576E 00	-0.647667E-03	0.112274E-02
150	0.933013E 00	-0.611354E-03	0.864556E-03
155	0.953154E 00	-0.575331E-03	0.626921E-03
160	0.969846E 00	-0.537518E-03	0.406926E-03
165	0.982963E 00	-0.489071E-03	0.209419E-03
170	0.992404E 00	-0.428520E-03	0.325264E-04
175	0.998097E 00	-0.345683E-03	-0.116533E-03
180	0.100000E 01		

TABLE 7

Pressure Distribution per Degree for
Chord-Diameter Ratio of 1.4

θ	X	Outside	Inside
0	-0.		
5	0.190265E-02	-0.268096E-00	0.268439E-00
10	0.759613E-02	-0.132028E-00	0.132540E-00
15	0.170371E-01	-0.857773E-01	0.865490E-01
20	0.301537E-01	-0.619910E-01	0.630933E-01
25	0.468461E-01	-0.472244E-01	0.496953E-01
30	0.669873E-01	-0.370195E-01	0.388590E-01
35	0.904240E-01	-0.294746E-01	0.316645E-01
40	0.116978E-00	-0.236437E-01	0.261594E-01
45	0.146447E-00	-0.190330E-01	0.217908E-01
50	0.178606E-00	-0.153137E-01	0.182615E-01
55	0.213212E-00	-0.123229E-01	0.153341E-01
60	0.250000E-00	-0.989410E-02	0.129028E-01
65	0.288691E-00	-0.794083E-02	0.108568E-01
70	0.328990E-00	-0.636780E-02	0.914038E-02
75	0.370590E-00	-0.510671E-02	0.770710E-02
80	0.413176E-00	-0.408935E-02	0.650732E-02
85	0.456422E-00	-0.329832E-02	0.549231E-02
90	0.500000E-00	-0.268399E-02	0.463429E-02
95	0.543578E 00	-0.219116E-02	0.392775E-02
100	0.586824E 00	-0.180986E-02	0.333137E-02
105	0.629410E 00	-0.150820E-02	0.283407E-02
110	0.671010E 00	-0.126114E-02	0.242522E-02
115	0.711309E 00	-0.106453E-02	0.207971E-02
120	0.750000E 00	-0.920742E-03	0.177143E-02
125	0.786788E 00	-0.813915E-03	0.149708E-02
130	0.821394E 00	-0.719491E-03	0.126588E-02
135	0.853553E 00	-0.643241E-03	0.105973E-02
140	0.883022E 00	-0.581799E-03	0.872107E-03
145	0.909576E 00	-0.543877E-03	0.686444E-03
150	0.933013E 00	-0.518784E-03	0.507227E-03
155	0.953154E 00	-0.495685E-03	0.340504E-03
160	0.969846E 00	-0.471045E-03	0.186156E-03
165	0.982963E 00	-0.438358E-03	0.478772E-04
170	0.992404E 00	-0.397558E-03	-0.765343E-04
175	0.998097E 00	-0.3[illegible]E-03	-0.180529E-03

TABLE 8

Pressure Distribution per Degree for
Chord-Diameter Ratio of 1.6

θ	X	Outside	Inside
0	-0.		
5	0.190265E-02	-0.250702E-00	0.250994E-00
10	0.759613E-02	-0.123203E-00	0.123660E-00
15	0.170371E-01	-0.797532E-01	0.804648E-01
20	0.301537E-01	-0.573351E-01	0.583663E-01
25	0.468461E-01	-0.433723E-01	0.447379E-01
30	0.669873E-01	-0.337093E-01	0.354247E-01
35	0.904240E-01	-0.265577E-01	0.285874E-01
40	0.116978E-00	-0.210525E-01	0.233411E-01
45	0.146447E-00	-0.167207E-01	0.191828E-01
50	0.178606E-00	-0.132567E-01	0.158336E-01
55	0.213212E-00	-0.105061E-01	0.130707E-01
60	0.250000E-00	-0.830683E-02	0.107950E-01
65	0.288691E-00	-0.657091E-02	0.890124E-02
70	0.328990E-00	-0.519987E-02	0.733639E-02
75	0.370590E-00	-0.411720E-02	0.605331E-02
80	0.413176E-00	-0.327047E-02	0.500111E-02
85	0.456422E-00	-0.262269E-02	0.412972E-02
90	0.500000E-00	-0.213069E-02	0.340905E-02
95	0.543578E 00	-0.174218E-02	0.283019E-02
100	0.586824E 00	-0.144554E-02	0.235419E-02
105	0.629410E 00	-0.121080E-02	0.196967E-02
110	0.671010E 00	-0.101731E-02	0.166382E-02
115	0.711309E 00	-0.863545E-03	0.141153E-02
120	0.750000E 00	-0.752582E-03	0.118862E-02
125	0.786788E 00	-0.669549E-03	0.993472E-03
130	0.821394E 00	-0.593629E-03	0.833902E-03
135	0.853553E 00	-0.529996E-03	0.694860E-03
140	0.883022E 00	-0.478792E-03	0.567996E-03
145	0.909576E 00	-0.446736E-03	0.440409E-03
150	0.933013E 00	-0.429288E-03	0.311796E-03
155	0.953154E 00	-0.411852E-03	0.193106E-03
160	0.969846E 00	-0.395353E-03	0.807532E-04
165	0.982963E 00	-0.371745E-03	-0.191505E-04
170	0.992404E 00	-0.342680E-03	-0.109748E-03
175	0.998097E 00	-0.300845E-03	-0.185021E-03

TABLE 9

Pressure Distribution per Degree for
Chord-Diameter Ratio of 1.8

θ	X	Outside	Inside
0	-0.		
5	0.190265E-02	-0.236240E-00	0.236508E-00
10	0.759613E-02	-0.115851E-00	0.114277E-00
15	0.170371E-01	-0.747192E-01	0.753922E-01
20	0.301537E-01	-0.534313E-01	0.544133E-01
25	0.468461E-01	-0.401356E-01	0.414533E-01
30	0.669873E-01	-0.309215E-01	0.325388E-01
35	0.904240E-01	-0.241362E-01	0.259968E-01
40	0.116978E-00	-0.188781E-01	0.209758E-01
45	0.146447E-00	-0.147924E-01	0.170031E-01
50	0.178606E-00	-0.115567E-01	0.138189E-01
55	0.213212E-00	-0.901301E-02	0.112206E-01
60	0.250000E-00	-0.702777E-02	0.908701E-02
65	0.288691E-00	-0.548529E-02	0.734267E-02
70	0.328990E-00	-0.427916E-02	0.593344E-02
75	0.370590E-00	-0.336099E-02	0.478589E-02
80	0.413176E-00	-0.264991E-02	0.387189E-02
85	0.456422E-00	-0.211661E-02	0.313129E-02
90	0.500000E-00	-0.171912E-02	0.253218E-02
95	0.543578E 00	-0.140916E-02	0.206246E-02
100	0.586824E 00	-0.117439E-02	0.168587E-02
105	0.629410E 00	-0.987638E-03	0.139090E-02
110	0.671010E 00	-0.828179E-03	0.116782E-02
115	0.711309E 00	-0.708317E-03	0.980632E-03
120	0.750000E 00	-0.619911E-03	0.819277E-03
125	0.786788E 00	-0.550350E-03	0.682773E-03
130	0.821394E 00	-0.489603E-03	0.569663E-03
135	0.853553E 00	-0.434823E-03	0.475546E-03
140	0.883022E 00	-0.390801E-03	0.388977E-03
145	0.909576E 00	-0.363594E-03	0.298941E-03
150	0.933013E 00	-0.349901E-03	0.204900E-03
155	0.953154E 00	-0.336550E-03	0.117333E-03
160	0.969846E 00	-0.324515E-03	0.332564E-04
165	0.982963E 00	-0.306620E-03	-0.414082E-04
170	0.992404E 00	-0.284776E-03	-0.109492E-03
175	0.998097E 00	-0.253669E-03	-0.166498E-03
180	0.100000E 01		

TABLE 10

Pressure Distribution per Degree for
Chord-Diameter Ratio of 2.0

θ	X	Outside	Inside
0	-0.		
5	0.190265E-02	-0.223994E-00	0.224233E-00
10	0.759613E-02	-0.109605E-00	0.110009E-00
15	0.170371E-01	-0.704500E-01	0.710751E-01
20	0.301537E-01	-0.500914E-01	0.510427E-01
25	0.468461E-01	-0.373631E-01	0.386250E-01
30	0.669873E-01	-0.285317E-01	0.330653E-01
35	0.904240E-01	-0.220377E-01	0.237771E-01
40	0.116978E-00	-0.170249E-01	0.189544E-01
45	0.146447E-00	-0.131607E-01	0.151509E-01
50	0.178606E-00	-0.101332E-01	0.121216E-01
55	0.213212E-00	-0.778614E-02	0.967312E-02
60	0.250000E-00	-0.598549E-02	0.769701E-02
65	0.288691E-00	-0.461079E-02	0.608804E-02
70	0.328990E-00	-0.355927E-02	0.481972E-02
75	0.370590E-00	-0.277272E-02	0.380791E-02
80	0.413176E-00	-0.217353E-02	0.302005E-02
85	0.456422E-00	-0.173146E-02	0.239583E-02
90	0.500000E-00	-0.140697E-02	0.193158E-02
95	0.543578E 00	-0.115641E-02	0.152280E-02
100	0.586824E 00	-0.967345E-03	0.122632E-02
105	0.629410E 00	-0.815445E-03	0.100112E-02
110	0.671010E 00	-0.684354E-03	0.836413E-03
115	0.711309E 00	-0.585700E-03	0.699954E-03
120	0.750000E 00	-0.513458E-03	0.582333E-03
125	0.786788E 00	-0.455465E-03	0.484254E-03
130	0.821394E 00	-0.404081E-03	0.404837E-03
135	0.853553E 00	-0.356165E-03	0.340758E-03
140	0.883022E 00	-0.317883E-03	0.280811E-03
145	0.909576E 00	-0.294347E-03	0.215905E-03
150	0.933013E 00	-0.283326E-03	0.145219E-03
155	0.953154E 00	-0.272834E-03	0.785421E-04
160	0.969846E 00	-0.263224E-03	0.141526E-04
165	0.982963E 00	-0.249886E-03	-0.441411E-04
170	0.992404E 00	-0.233208E-03	-0.972240E-04
175	0.998097E 00	-0.209266E-03	-0.141654E-03
180	0.100000E 01		

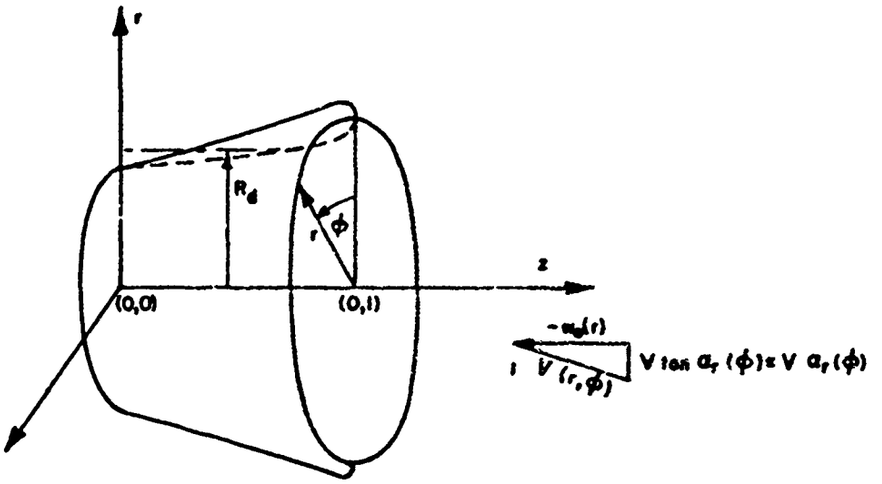

Figure 1 - The Annular Airfoil Coordinate System

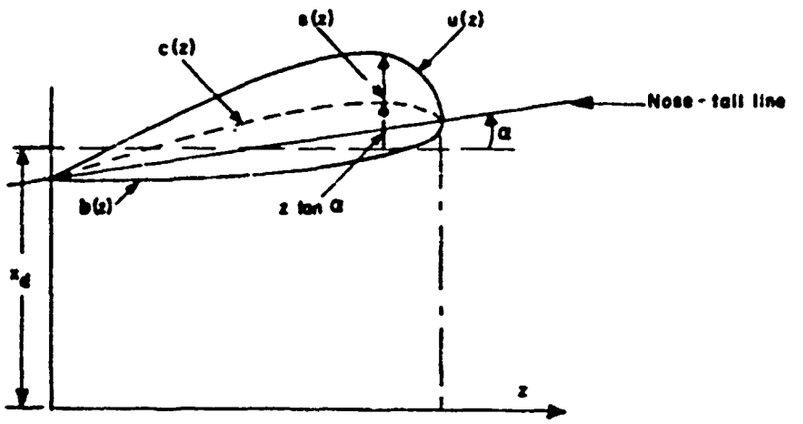

Figure 2 - Delineation of the Annular Airfoil Section

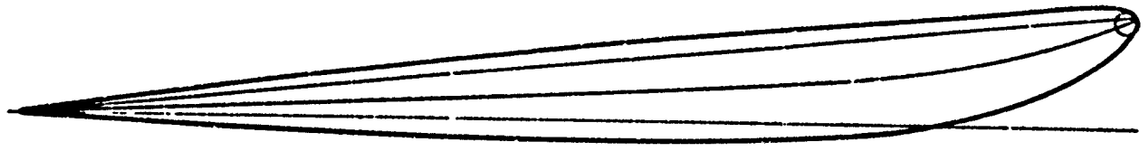

Duct Nº I

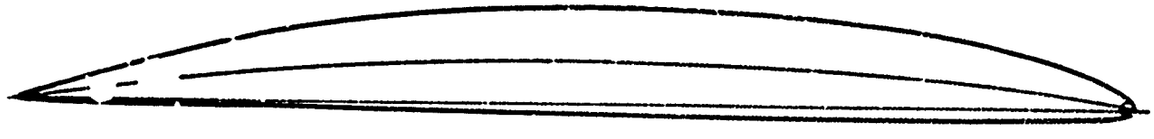

Duct Nº II

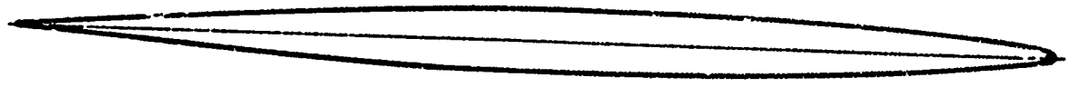

BTZ Duct

Figure 3 - Duct Profiles

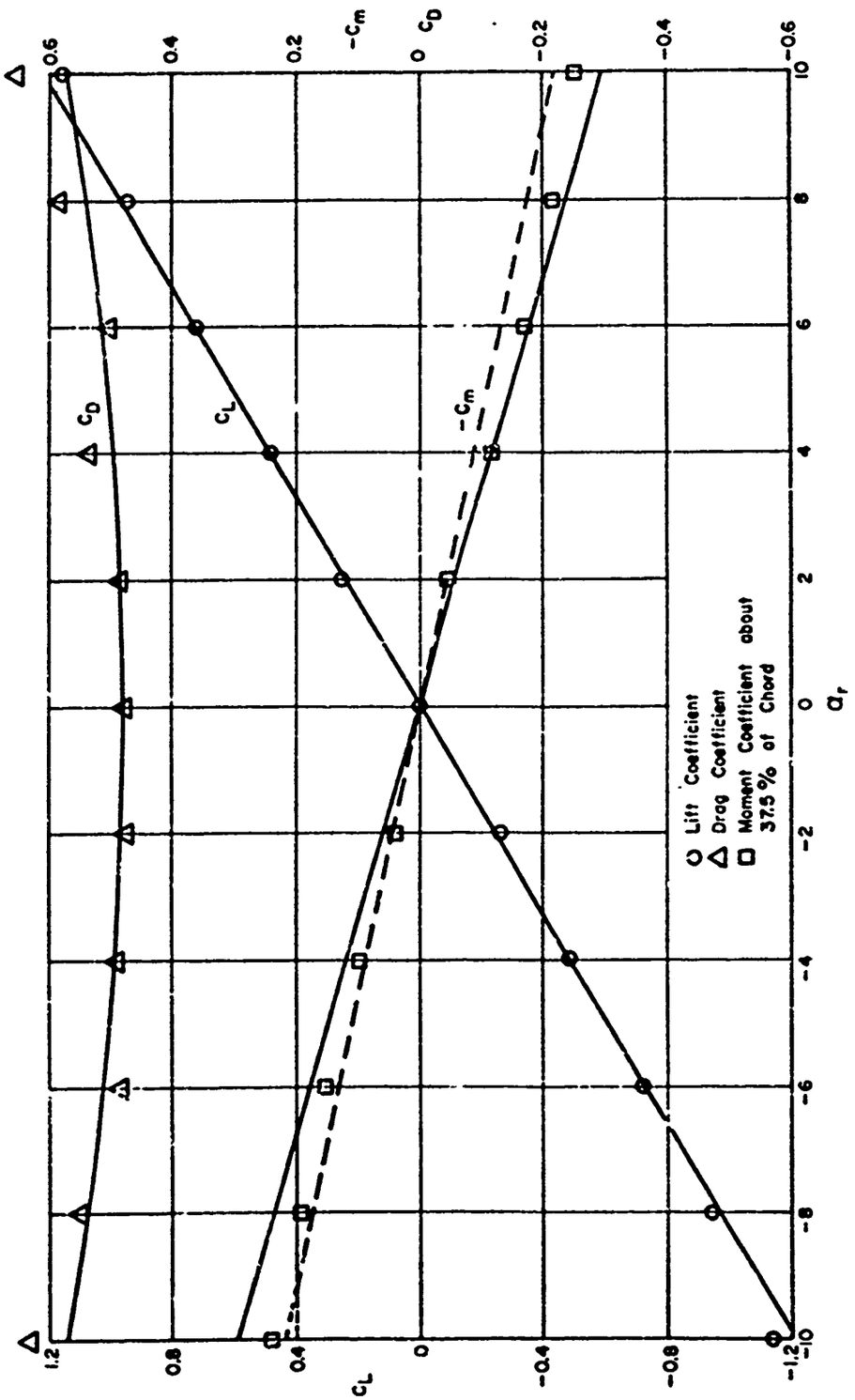

Figure 4 - Lift, Drag, and Moment Coefficients for Duct I

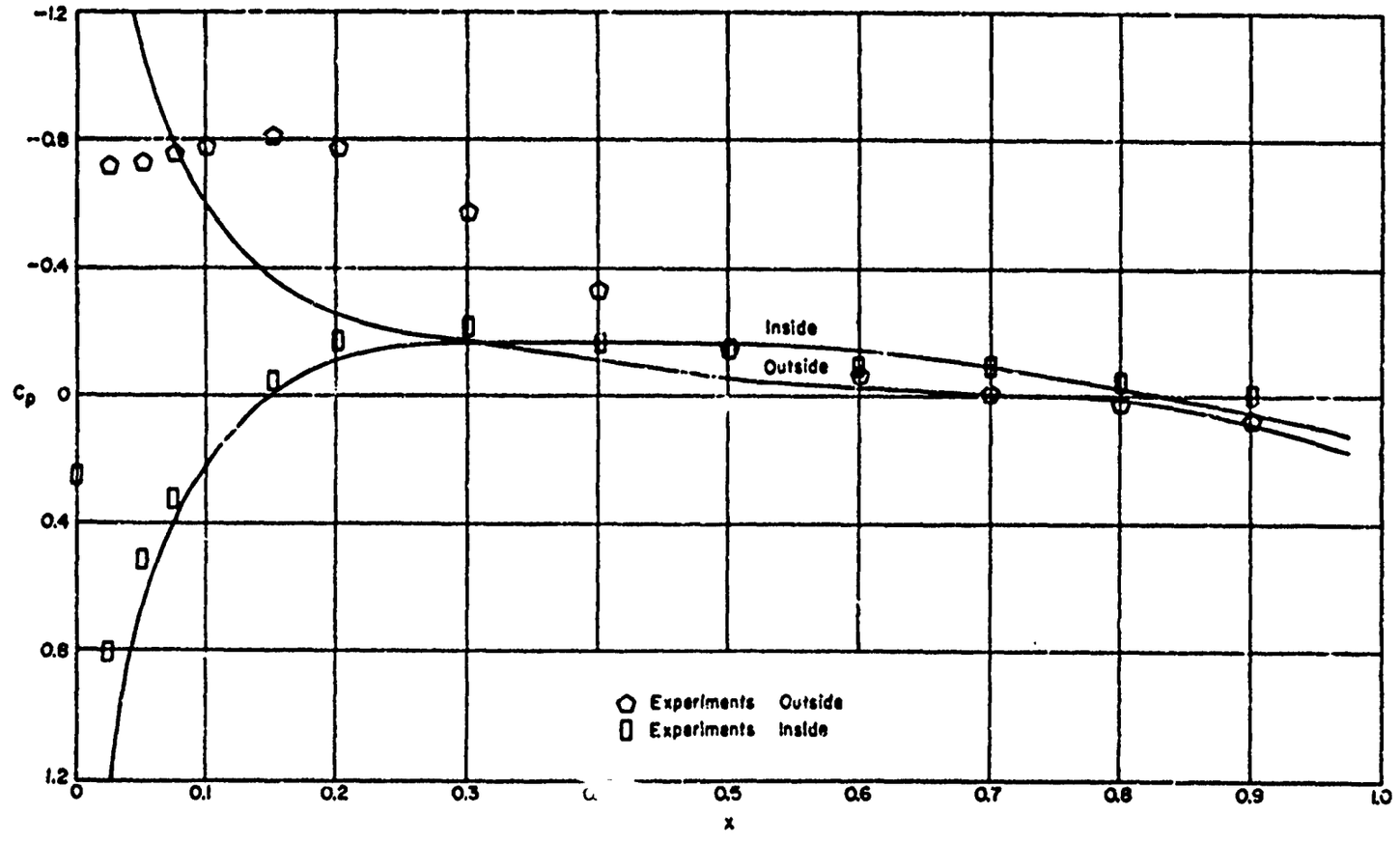

Figure 5 - Pressure Distribution for Duct I at Zero Angle of Attack ($\alpha_r = 0$)

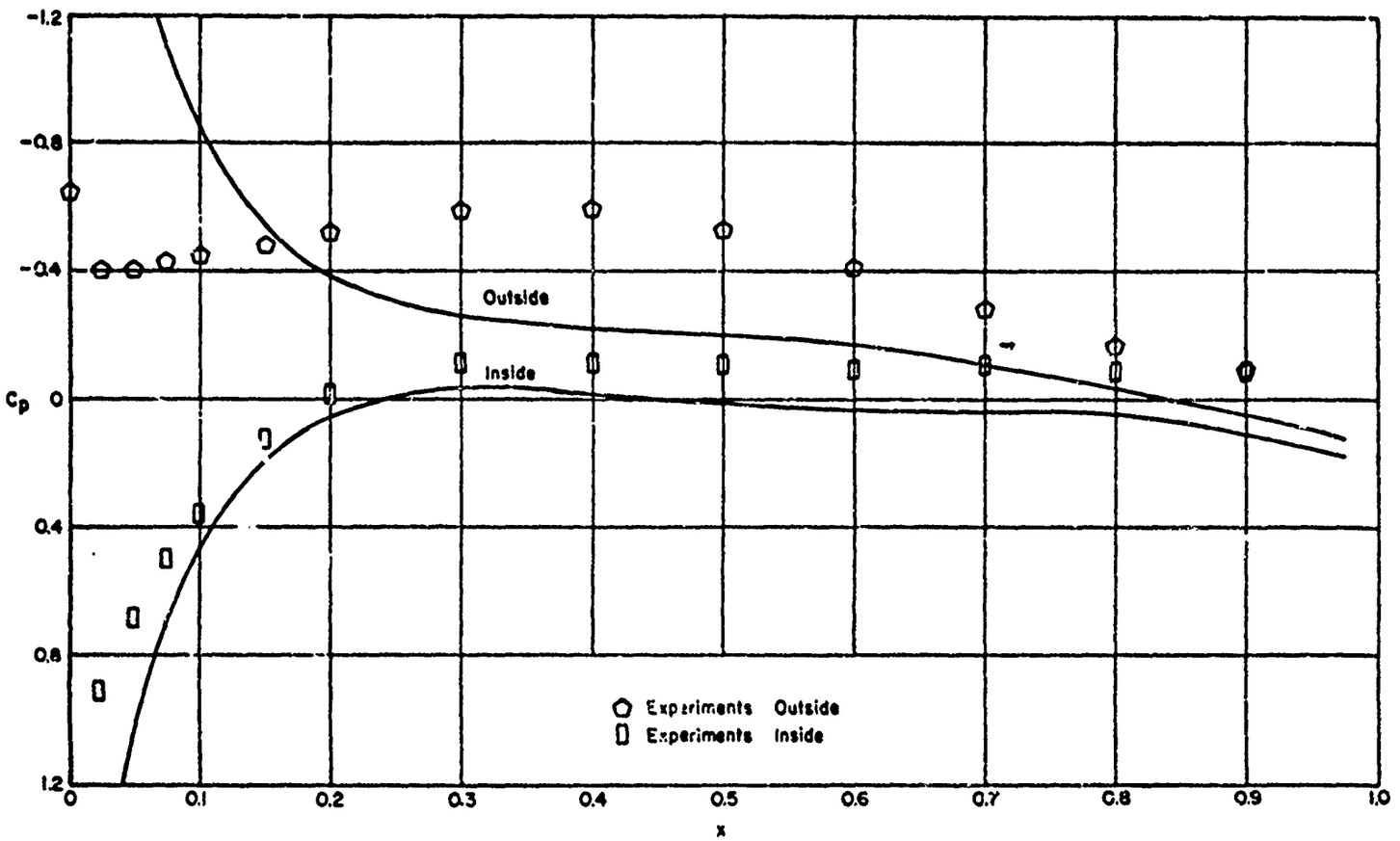

Figure 6 - Pressure Distribution for Duct I, α_r = 6 Degrees and ϕ = 0 Degrees

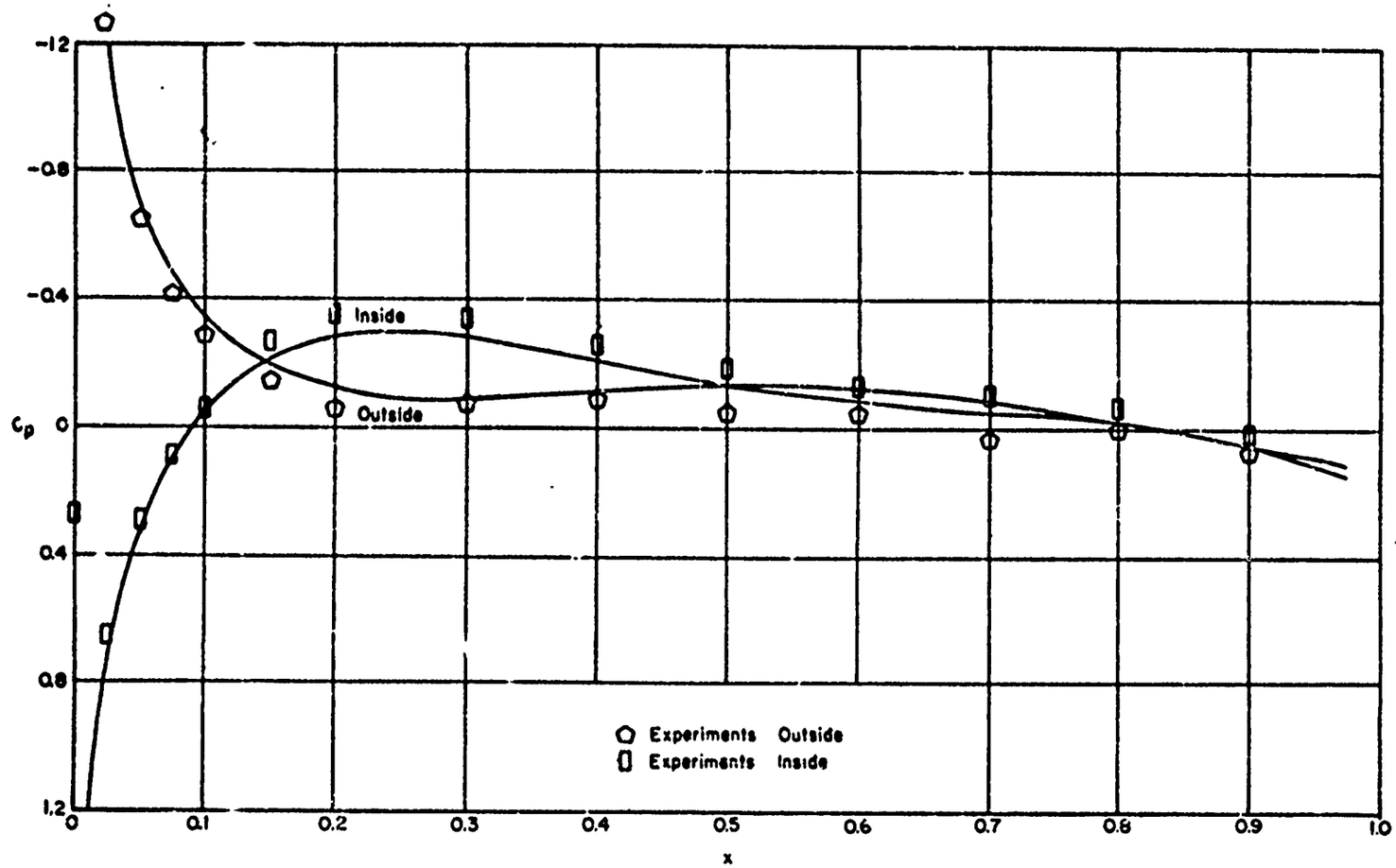

Figure 7 - Pressure Distribution for Duct I, α_r = 6 Degrees and ϕ = 180 Degrees

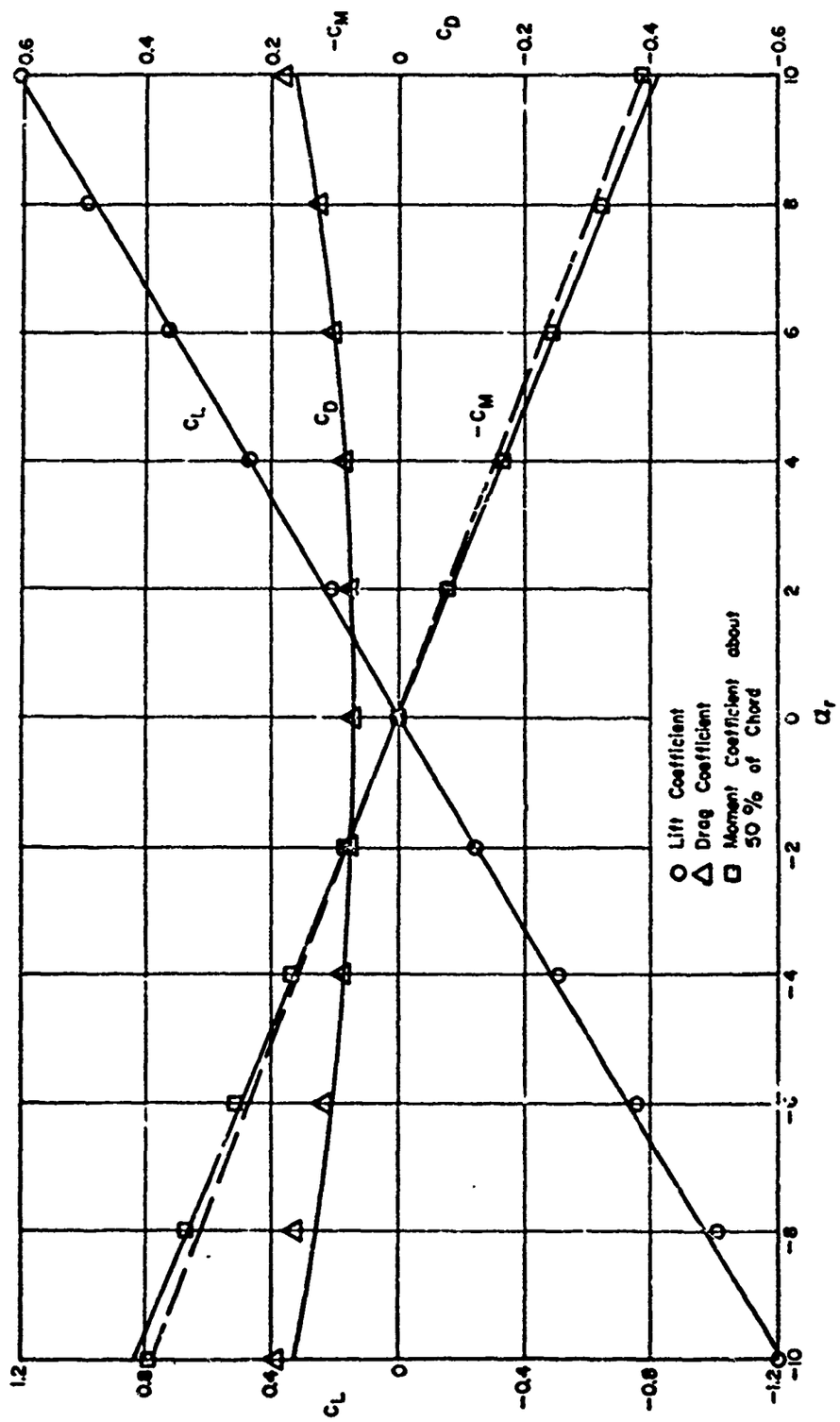

Figure 8 - Lift, Drag, and Moment Coefficients for Duct II

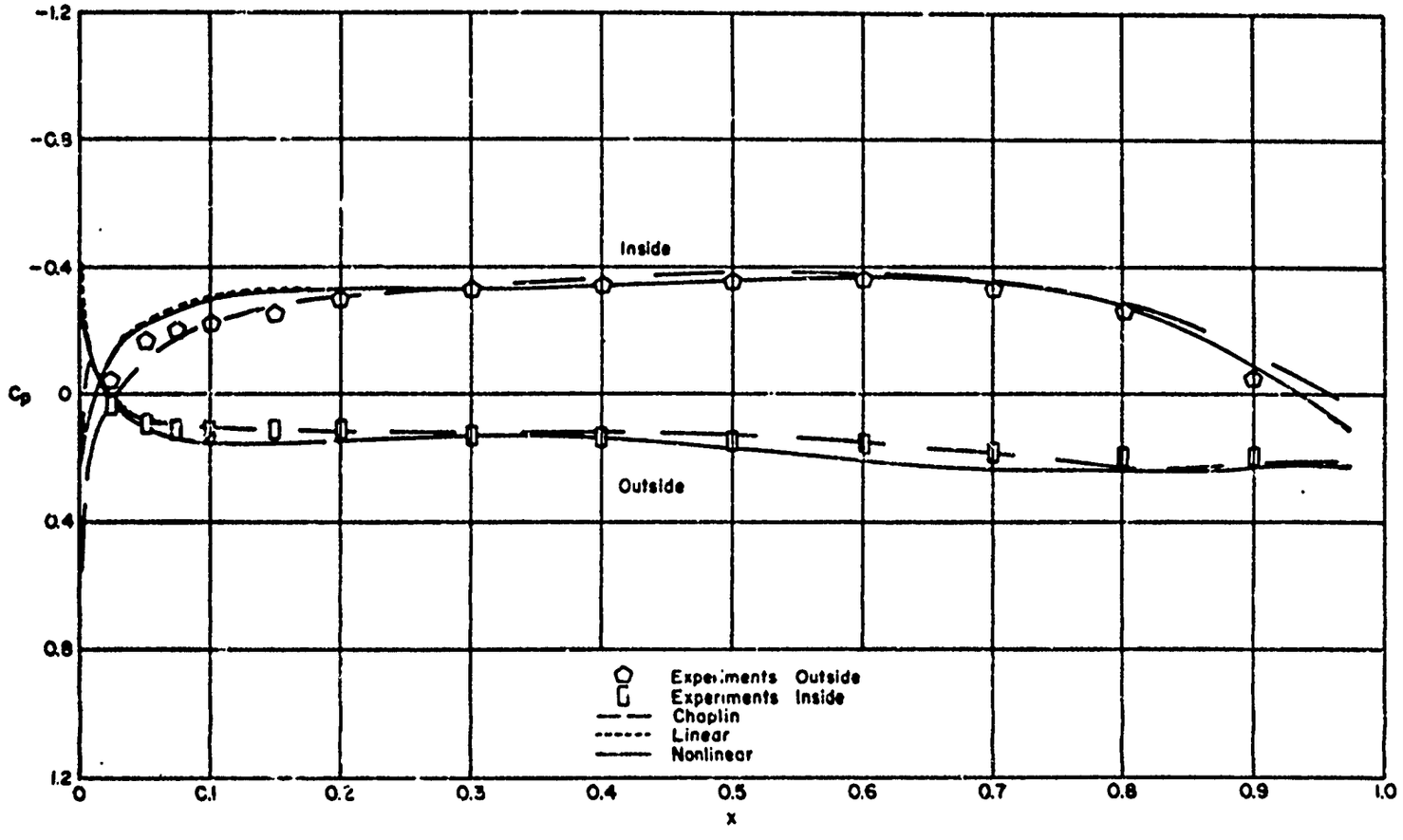

Figure 9 - Pressure Distribution for Duct II at Zero Angle of Attack ($\alpha_r = 0$)

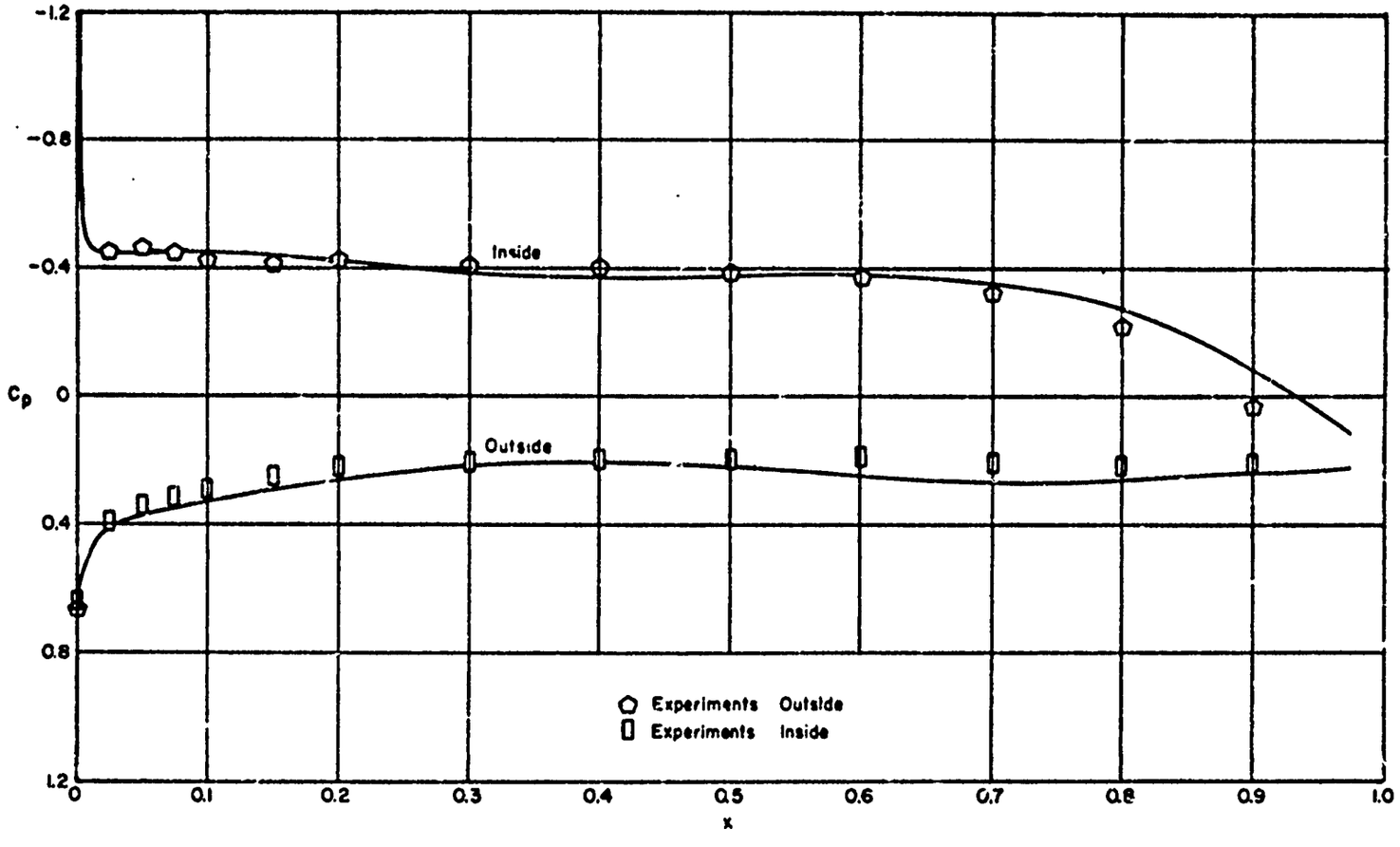

Figure 10 - Pressure Distribution for Duct II, α_r = 4 Degrees and ϕ = 0 Degrees

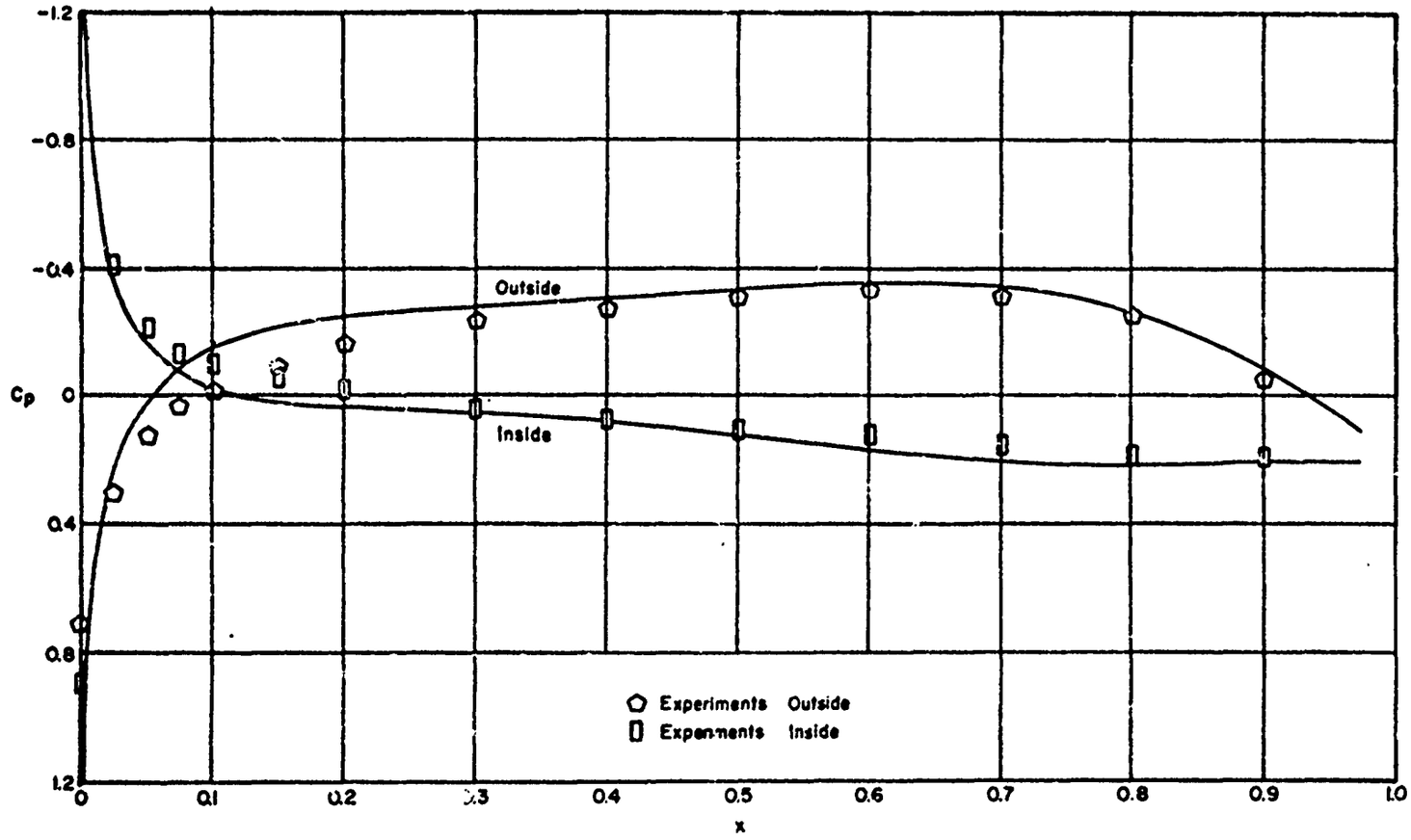

Figure 11 - Pressure Distribution for Duct II, α_r = 4 Degrees and ϕ = 180 Degrees

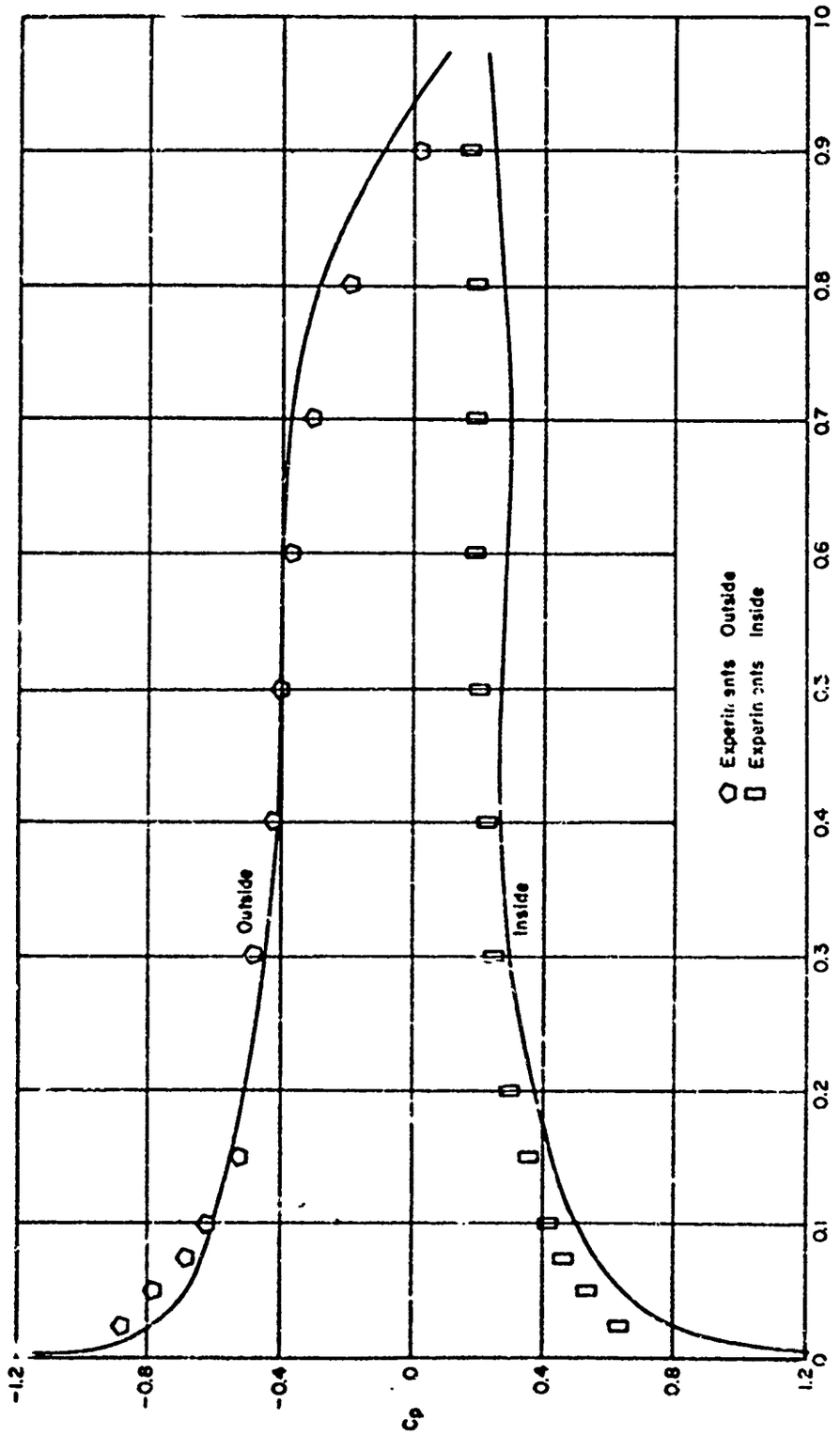

Figure 12 - Pressure Distribution for Duct II, α_r = 8 Degrees and ϕ = 0 Degrees

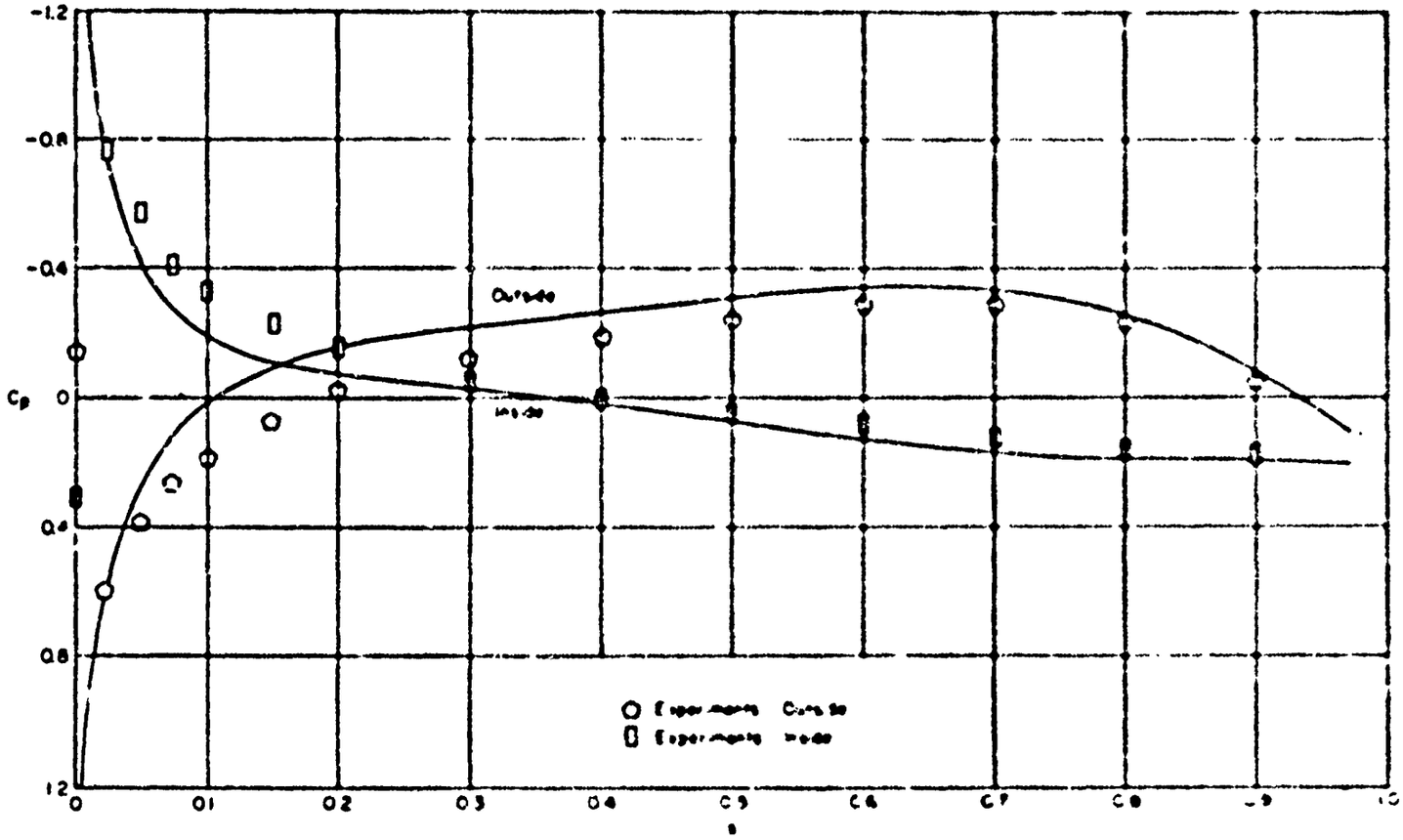

Figure 13 - Pressure Distribution for Duct II, α_p = 8 Degrees and ϵ = 180 Degrees

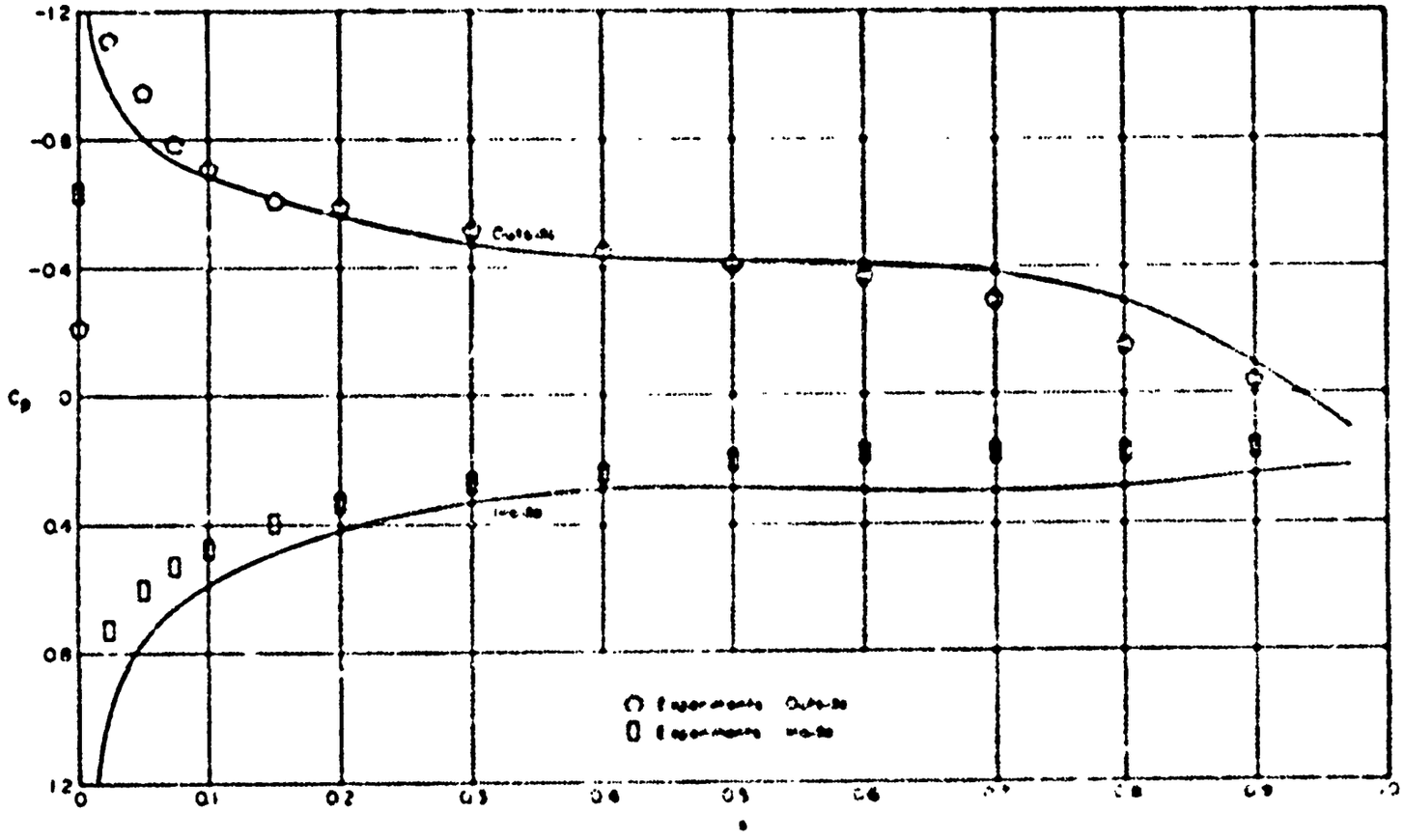

Figure 14 - Pressure Distribution for Duct II, α_p = 10 Degrees and β = 0 Degrees

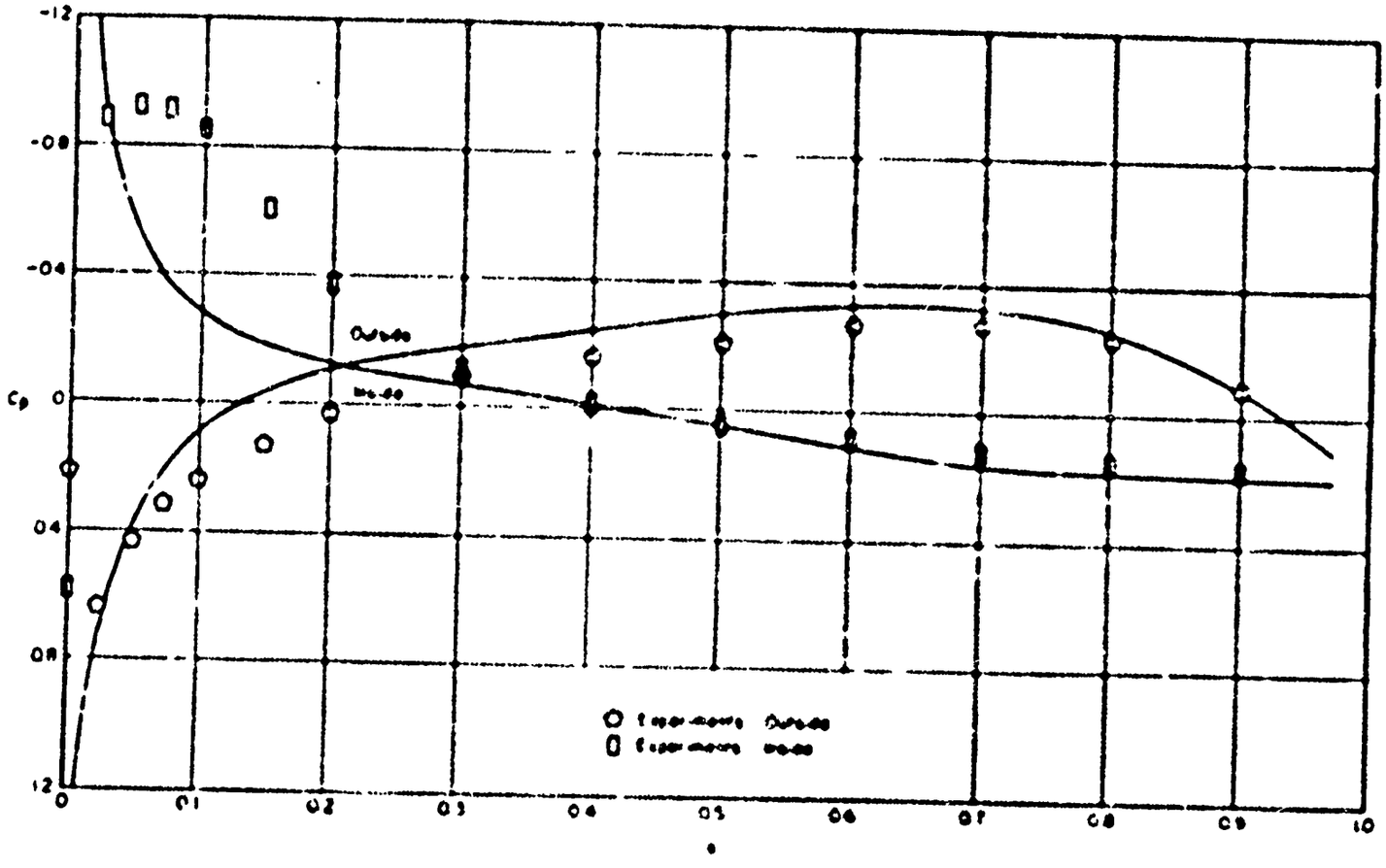

Figure 15 - Pressure Distribution for Duct II, α_g = 10 Degrees and ϕ = 180 Degrees

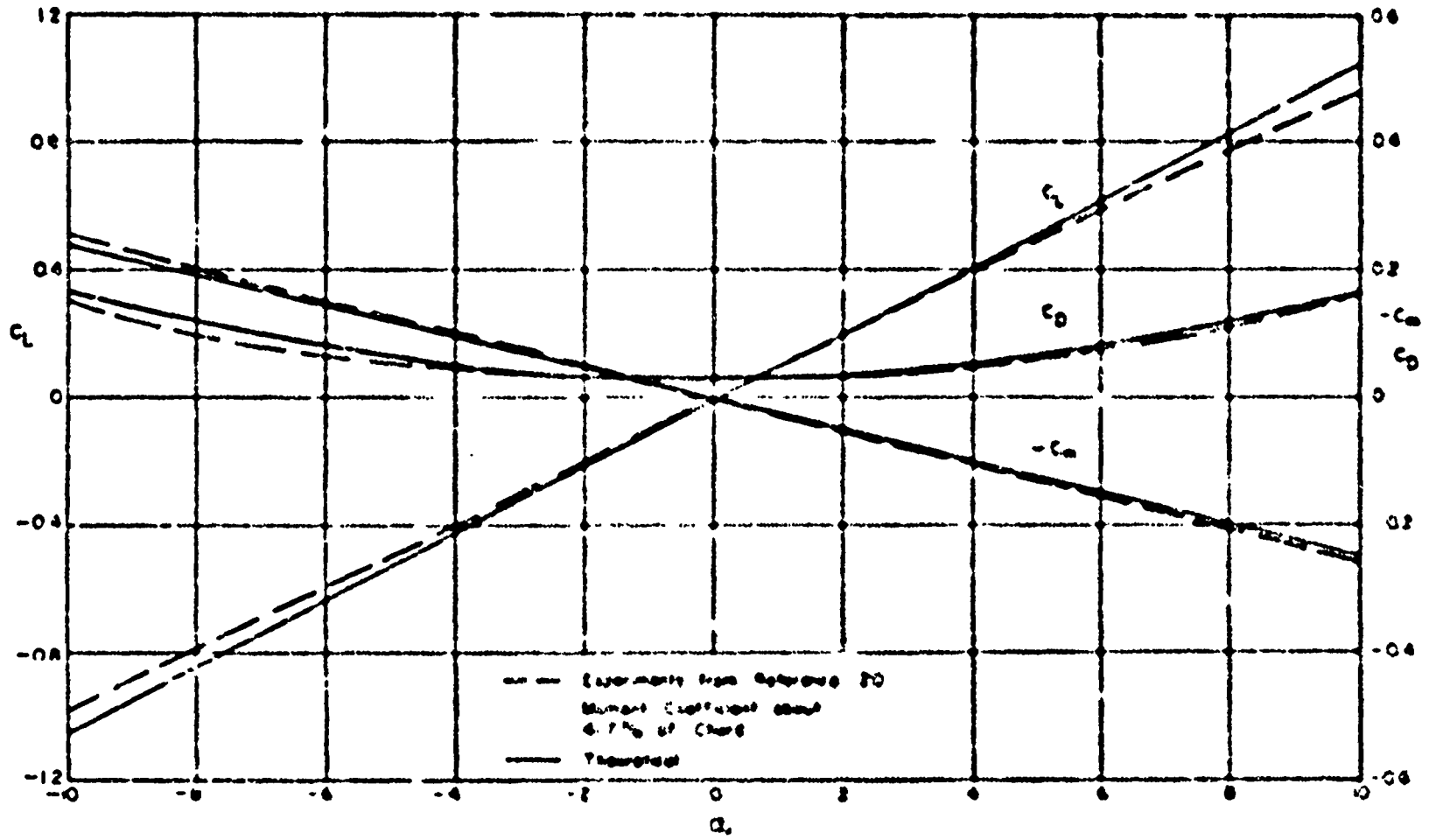
1.2
0.8
0.4
0
-0.4
-0.8
-1.2
c_L
0.8
0.4
0.2
$-c_m$
c_D
0
0.2
-0.4
-0.8
c_L
c_D
$-c_m$
Experiment from Reference 20
Moment Coefficient about
0.7 b_0 of Chord
Theoretical
-8
-6
-4
-2
0
2
4
6
8
10
α_o

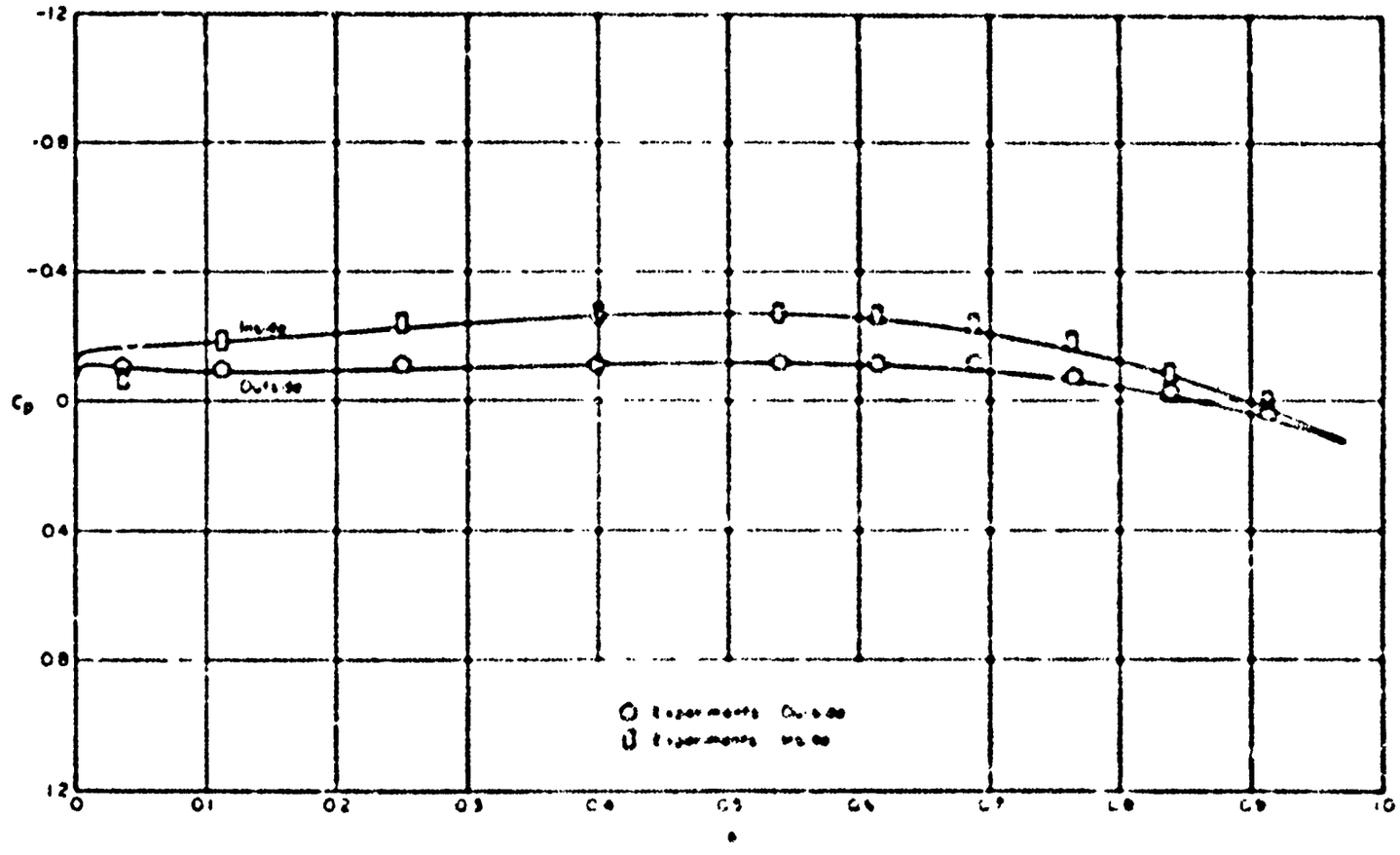

Figure 17 - Pressure Distribution for bTX Duct at Zero Angle of Attack ($\alpha_g = 0$)

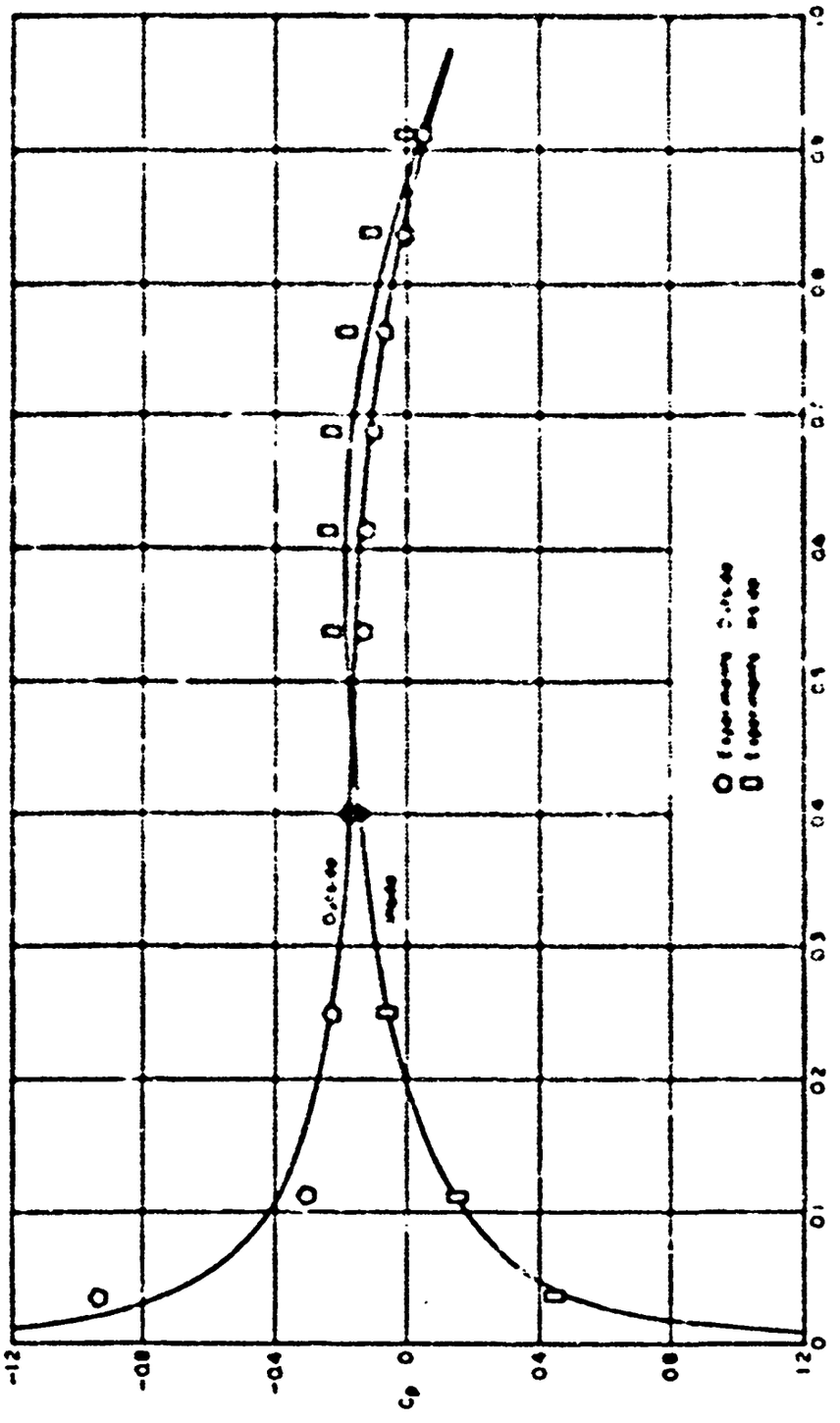

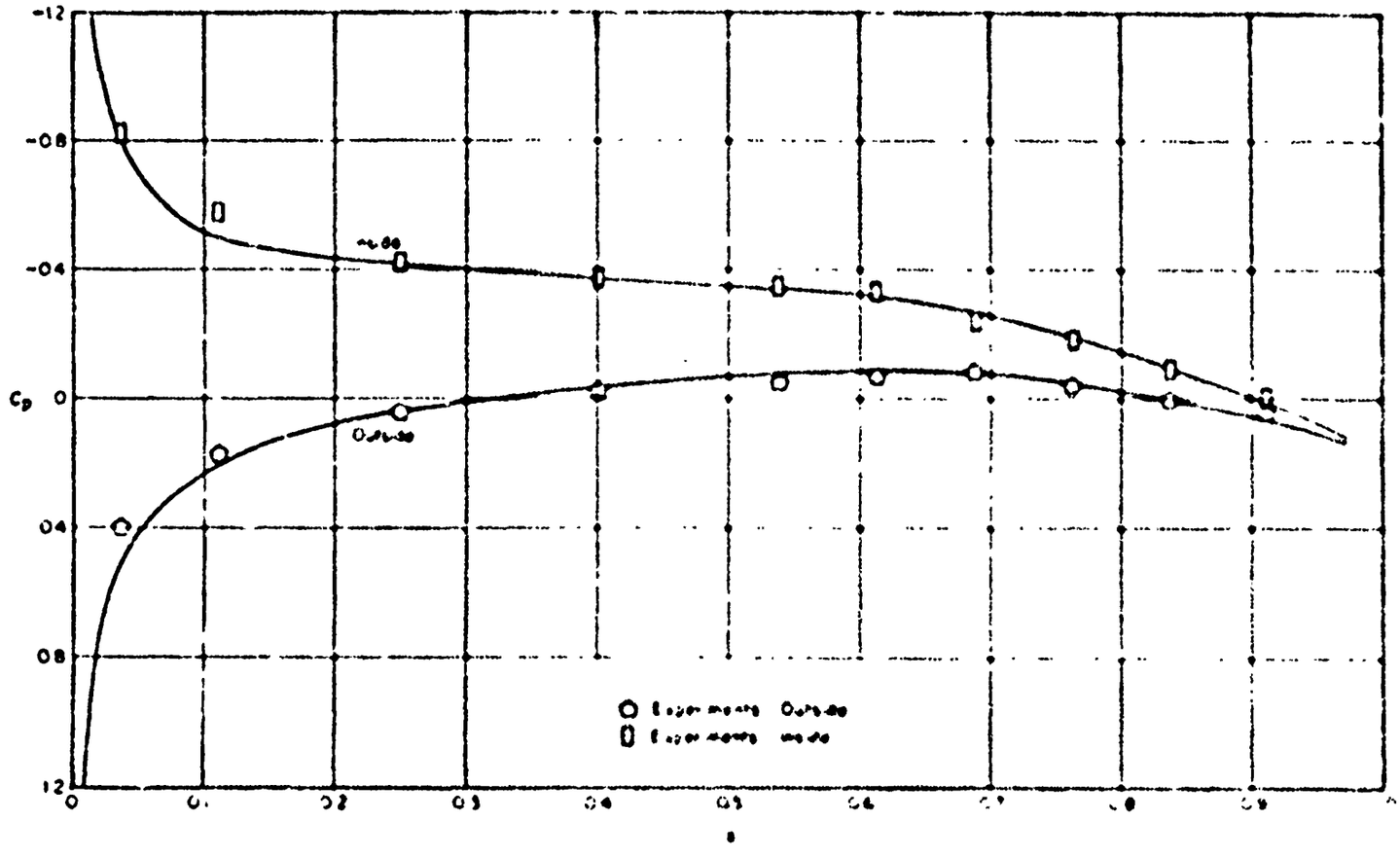

Figure 19 - Pressure Distribution for BTF Duct, α_p = 9 Degrees and ϕ = 180 Degrees

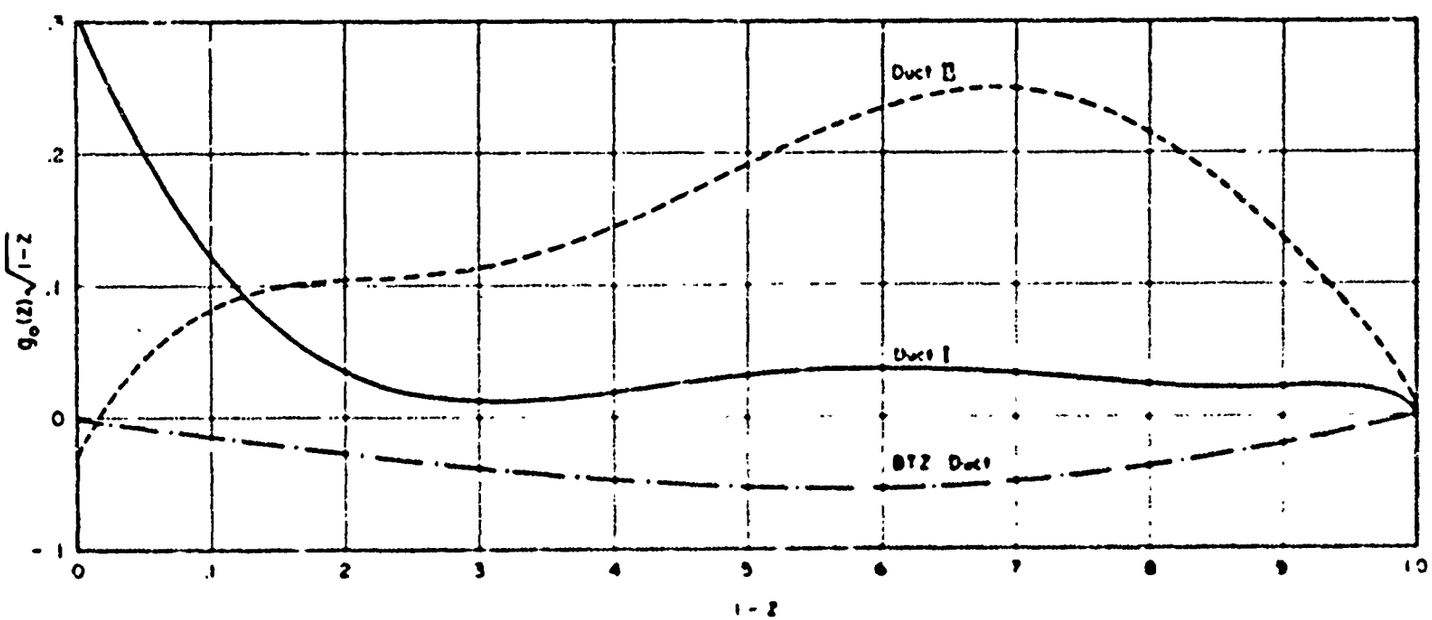

Figure 20 - Circulation Distribution for the Three Ducts

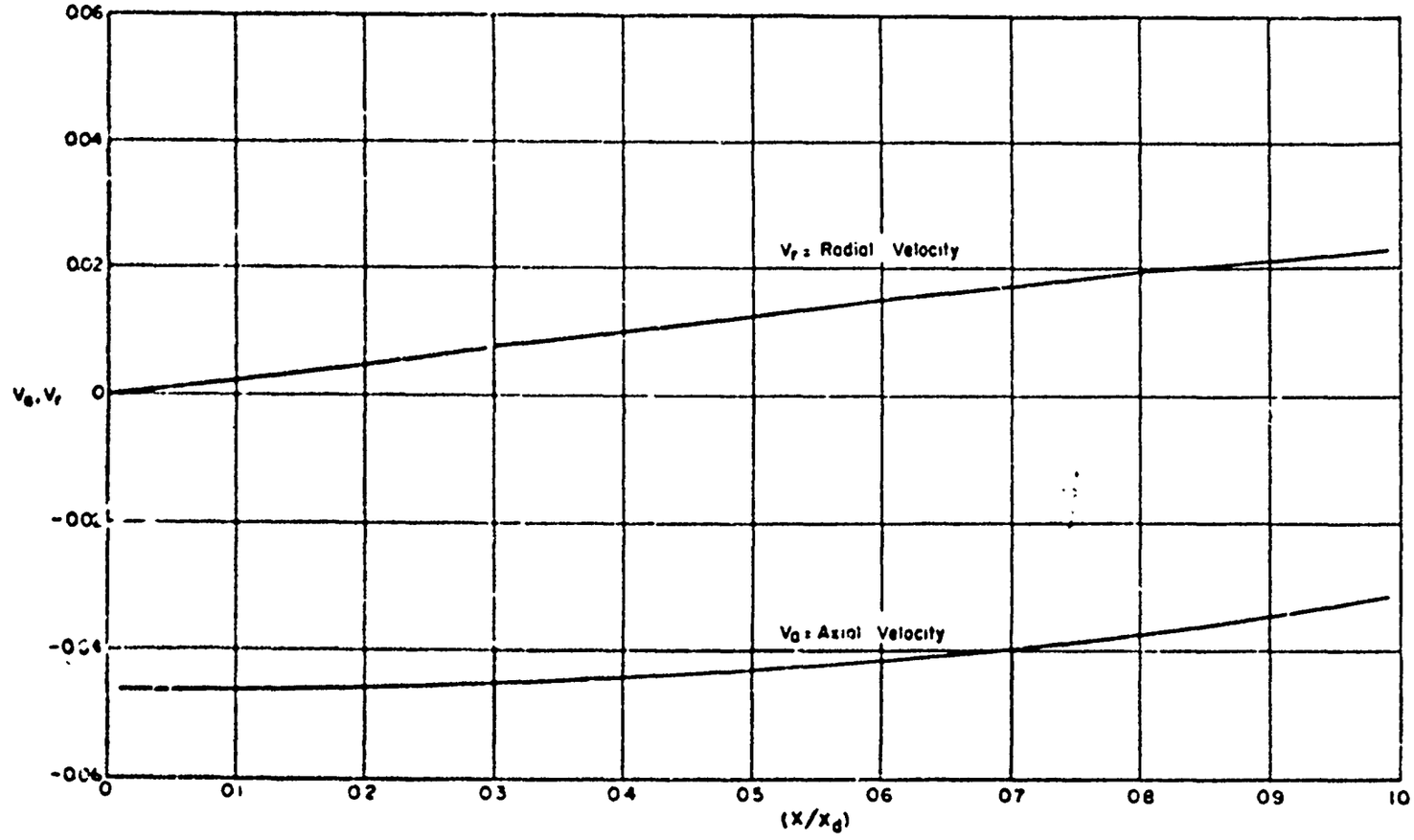

Figure 21 - Radial Variation of Velocity at ½ Chord Point for Duct II

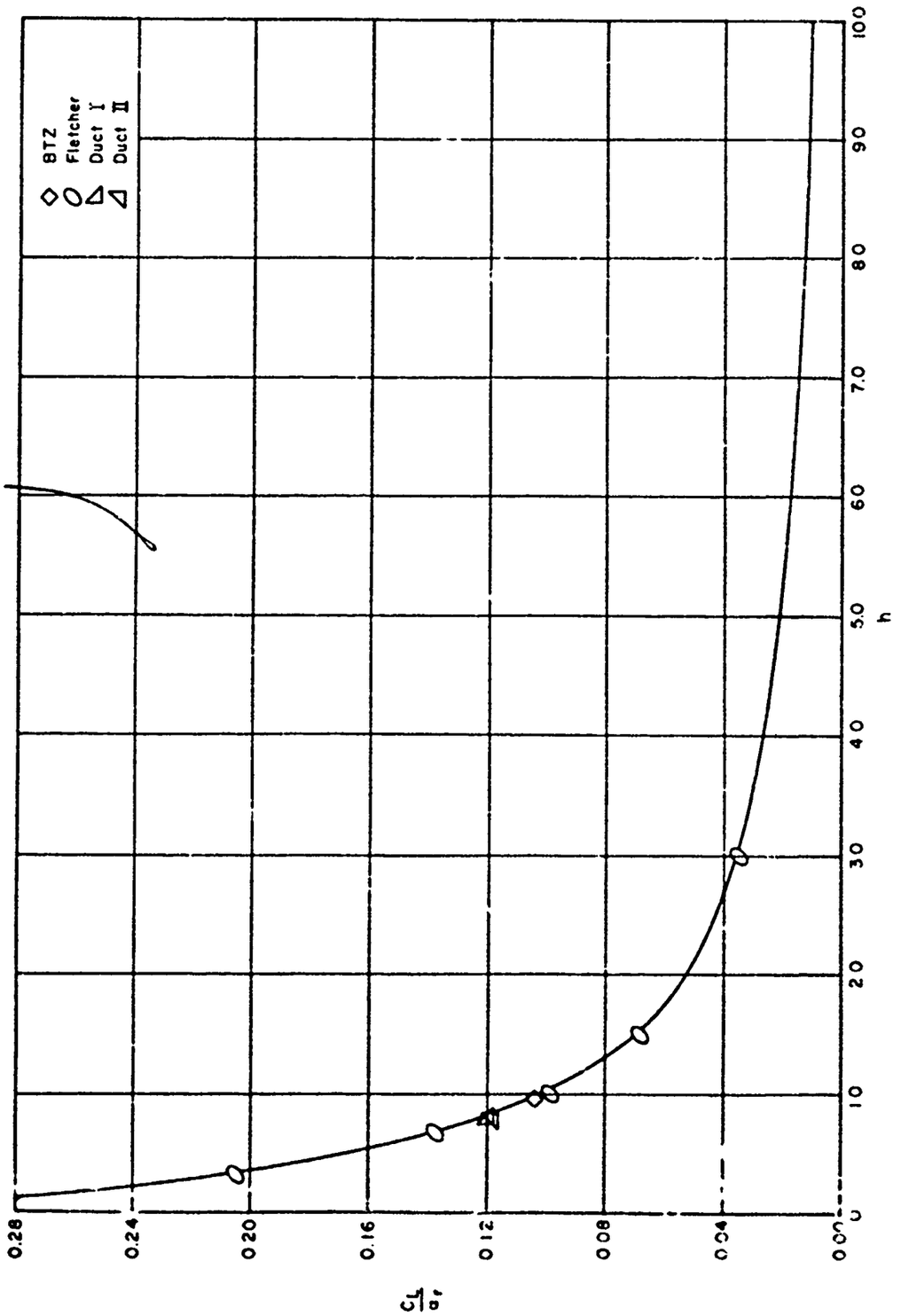
BTZ
Fletcher
Duct I
Duct II
0.28
0.24
0.20
0.16
0.12
0.08
0.04
0.00
0
10
20
30
40
50
60
70
80
90
100
h
$\frac{C_L}{\alpha_r}$

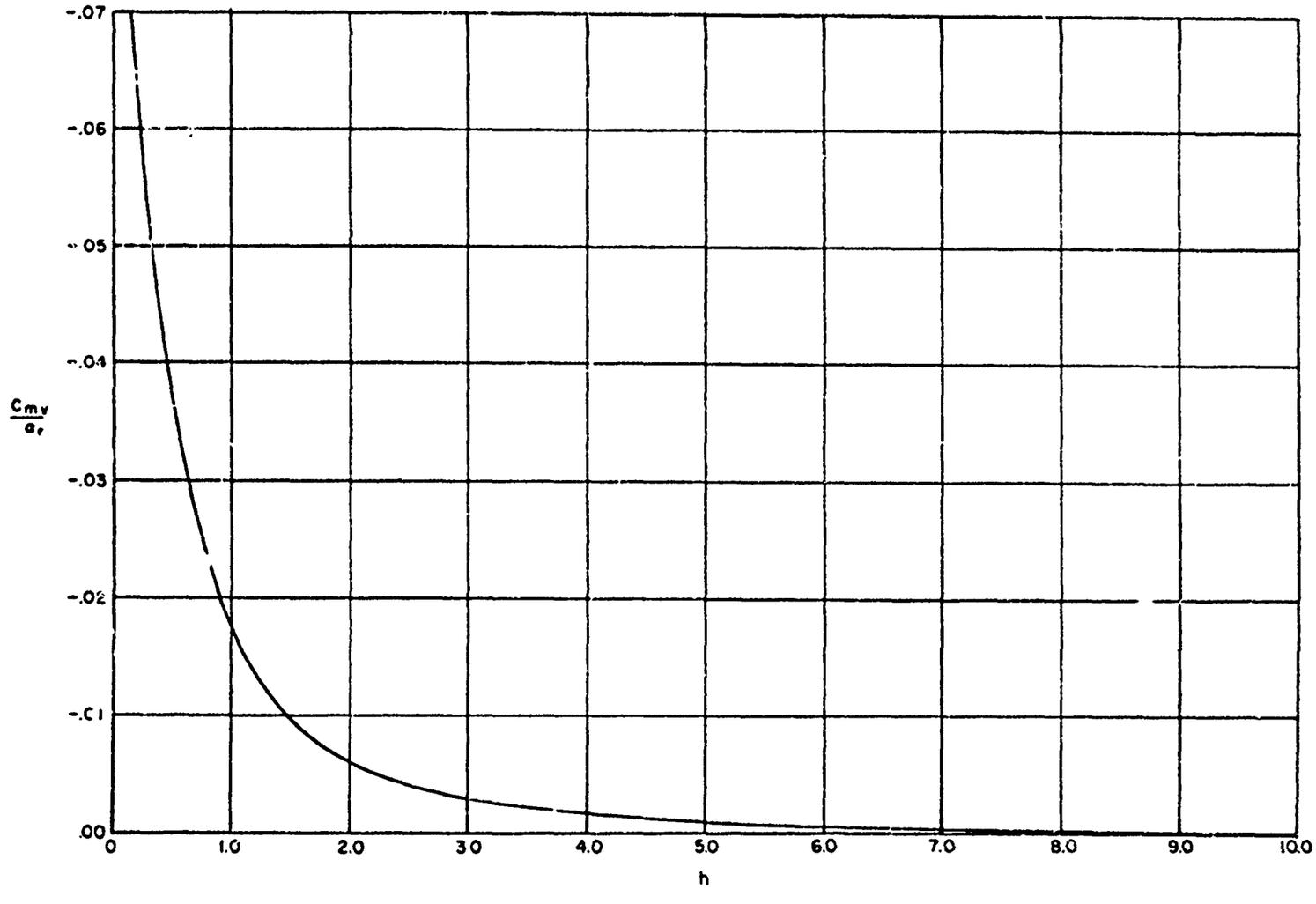

Figure 23 - Moment from Vertical Forces as Function of Duct Angle of Attack and Chord-Diameter Ratio

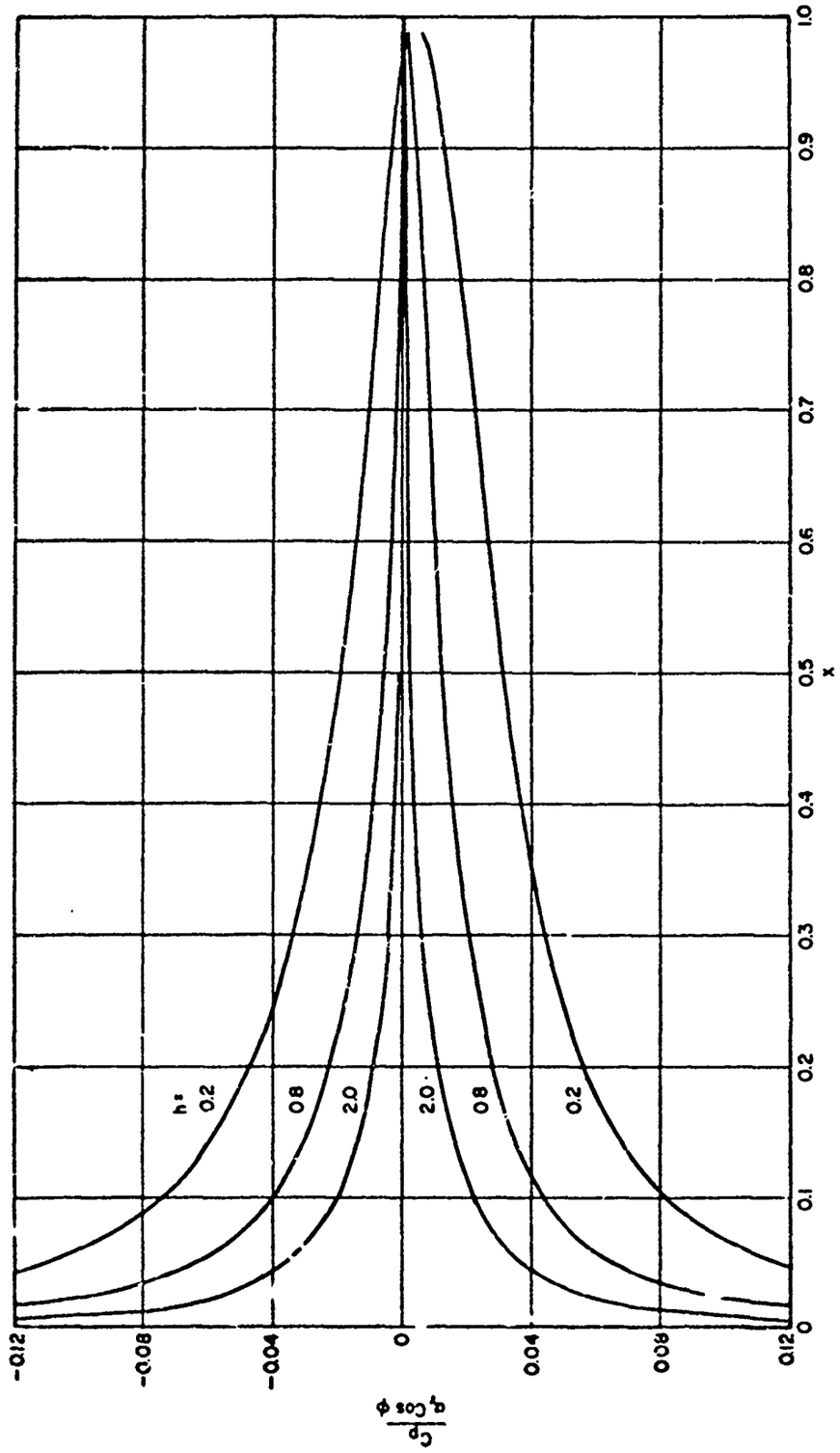

Figure 24 - Pressure Distribution as a Function of Duct Angle of Attack and Chord-Diameter Ratio

Figure 24 - Pressure Distribution as a Function of Duct Angle of Attack and Chord-Diameter Ratio

APPENDIX A – INPUT AND OUTPUT FOR AN ANNULAR AIRFOIL

```
DUCT II FORCES AND PRESSURE DISTRIBUTION, MAX CAMBER=.04, MAX THICKNESS=.1
25.    17.    .8     .0     .0     .0
.0     .005   .0075  .0125  .025   .05    .075   .1     .15
.2     .25    .3     .35    .4     .45    .5     .6     .65
.7     .75    .8     .85    .9     .95    1.0
.0     .001691 .002380 .003629 .006345 .010845 .014627 .017926 .023478
.027971 .031617 .034539 .036807 .038457 .039526 .04    .03914  .037732
.035564 .032483 .028106 .021697 .014345 .006851 .0
.0     .0125  .025   .05    .075   .1     .2     .3     .4
.45    .5     .6     .7     .8     .9     .95    1.0
.0     .01155 .0153  .02095 .0254  .0292  .040402 .046370 .049952
.05    .04962 .04653 .04035 .0311  .01877 .01143 .0
2.
.0     10.
180.   180.
1.
1.     11.
.5
.0     .1     .2     .3     .4     .5     6      .7     .8
.9     1.
```

OUTPUT

DUCT 11. MAXIMUM CAMBER=0.04. MAXIMUM THICKNESS=0.10

25.000000	17.000000	0.800000	-0.	-0.	-0.			
-0.	0.005000	0.007500	0.012500	0.025000	0.050000	0.075000	0.100000	0.150000
0.200000	0.250000	0.300000	0.350000	0.400000	0.450000	0.500000	0.600000	0.650000
0.700000	0.750000	0.800000	0.850000	0.900000	0.950000	1.000000		
-0.	0.001691	0.002380	0.003629	0.006345	0.010845	0.014627	0.017926	0.023478
0.027971	0.031617	0.034539	0.036807	0.038457	0.039523	0.040000	0.039140	0.037732
0.035564	0.032483	0.028106	0.021697	0.014345	0.006851	-0.		
-0.	0.012500	0.025000	0.050000	0.075000	0.100000	0.200000	0.300000	0.400000
0.450000	0.500000	0.600000	0.700000	0.800000	0.900000	0.950000	1.000000	
-0.	0.011550	0.015300	0.020950	0.025400	0.029200	0.040020	0.046370	0.049520
0.050000	0.049620	0.046530	0.040350	0.031100	0.018770	0.011430	-0.	

CHORD DIAMETER RATIO	0.8000
LIFT COEFFICIENT PER DEGREE (EQ3.3-2)	0.1215
INDUCED DRAG COEFFICIENT (EQ3.3-5)	0.0009
MOMENT COEFFICIENT FROM VERTICAL FORCES (EQ3.3-7)	-0.0236
MOMENT COEFFICIENT FROM HORIZONTAL FORCES (EQ3.3-8)	0.0038
TOTAL MOMENT COEFFICIENT ABOUT L. E. (EQ3.3-6)	-0.0197
[illegible]	0

GEOMETRIC ANGLE OF ATTACK IN DEGREES -0.

POSITION OF SECTION AT ANGLE (PA) IN DEGREES 0.1800E 03

T	X	GSTAR	NCO	NCI	PO	PI	POP	PIP
0	-0.	-0.3111E-01	0.	0.	-0.	-0.	0.	0.
5	0.1403E-02	-0.2721E-01	0.5711E 00	0.7803E 00	0.3241E-00	-0.5307E 00	0.3241E-00	-0.5307E 00
10	0.7596E-02	-0.1606E-01	0.6801E 00	0.8829E 00	0.8081E-01	-0.2205E-00	0.8081E-01	-0.2205E-00
15	0.1704E-01	0.7947E-03	0.8713E 00	0.9915E 00	-0.6569E-01	-0.6268E-01	-0.6569E-01	-0.6268E-01
20	0.3015E-01	0.2110E-01	0.9170E 00	0.9949E 00	-0.1777E-00	0.4916E-01	-0.1777E-00	0.4918E-01
25	0.4685E-01	0.4230E-01	0.9377E 00	0.9993E 00	-0.2540E-00	0.1199E-00	-0.2540E-00	0.1199E-00
30	0.6699E-01	0.6196E-01	0.9524E 00	0.9997E 00	-0.3029E-00	0.1606E-00	-0.3029E-00	0.1606E-00
35	0.9042E-01	0.7822E-01	0.9640E 00	0.9998E 00	-0.3300E-00	0.1779E-00	-0.3300E-00	0.1779E-00
40	0.1170E-00	0.9010E-01	0.9727E 00	1.0000E 00	-0.3400E-00	0.1774E-00	-0.3400E-00	0.1774E-00
45	0.1464E-00	0.9761E-01	0.9785E 00	1.0000E 00	-0.3376E-00	0.1651E-00	-0.3376E-00	0.1651E-00
50	0.1786E-00	0.1017E-00	0.9837E 00	1.0000E 00	-0.3287E-00	0.1471E-00	-0.3287E-00	0.1471E-00
55	0.2132E-00	0.1040E-00	0.9885E 00	1.0000E 00	-0.3186E-00	0.1283E-00	-0.3186E-00	0.1283E-00
60	0.2500E-00	0.1066E-00	0.9918E 00	1.0000E 00	-0.3103E-00	0.1137E-00	-0.3103E-00	0.1137E-00
65	0.2887E-00	0.1114E-00	0.9945E 00	1.0000E 00	-0.3069E-00	0.1062E-00	-0.3069E-00	0.1062E-00
70	0.3290E-00	0.1200E-00	0.9967E 00	1.0000E 00	-0.3100E-00	0.1073E-00	-0.3100E-00	0.1073E-00
75	0.3706E-00	0.1329E-00	0.9982E 00	1.0000E 00	-0.3192E-00	0.1169E-00	-0.3192E-00	0.1169E-00
80	0.4132E-00	0.1501E-00	0.9993E 00	0.9999E 00	-0.3335E-00	0.1333E-00	-0.3335E-00	0.1333E-00
85	0.4564E-00	0.1705E-00	0.9999E 00	0.9999E 00	-0.3505E-00	0.1542E-00	-0.3505E-00	0.1542E-00
90	0.5000E-00	0.1922E-00	0.9999E 00	0.9998E 00	-0.3671E-00	0.1766E-00	-0.3671E-00	0.1766E-00
95	0.5436E 00	0.2131E-00	0.9993E 00	0.9998E 00	-0.3805E-00	0.1974E-00	-0.3805E-00	0.1974E-00
100	0.5868E 00	0.2308E-00	0.9982E 00	0.9997E 00	-0.3874E-00	0.2144E-00	-0.3874E-00	0.2144E-00
105	0.6294E 00	0.2433E-00	0.9964E 00	0.9997E 00	-0.3856E-00	0.2262E-00	-0.3856E-00	0.2262E-00
110	0.6710E 00	0.2490E-00	0.9941E 00	0.9996E 00	-0.3736E-00	0.2321E-00	-0.3736E-00	0.2321E-00
115	0.7113E 00	0.2474E-00	0.9906E 00	0.9997E 00	-0.3503E-00	0.2330E-00	-0.3503E-00	0.2330E-00
120	0.7500E 00	0.2385E-00	0.9869E 00	0.9998E 00	-0.3169E-00	0.2297E-00	-0.3169E-00	0.2297E-00
125	0.7868E 00	0.2231E-00	0.9802E 00	1.0000E 00	-0.2735E-00	0.2240E-00	-0.2735E-00	0.2240E-00
130	0.8214E 00	0.2026E-00	0.9720E 00	0.9999E 00	-0.2228E-00	0.2179E-00	-0.2228E-00	0.2179E-00
135	0.8536E 00	0.1786E-00	0.9666E 00	0.9999E 00	-0.1685E-00	0.2124E-00	-0.1685E-00	0.2124E-00
140	0.8830E 00	0.1530E-00	0.9626E 00	0.9998E 00	-0.1121E-00	0.2091E-00	-0.1121E-00	0.2091E-00
145	0.9096E 00	0.1272E-00	0.9633E 00	0.9998E 00	-0.5597E-01	0.2086E-00	-0.5597E-01	0.2086E-00
150	0.9330E 00	0.1026E-00	0.9555E 00	1.0000E 00	-0.1507E-02	0.2109E-00	-0.1507E-02	0.2109E-00
155	0.9532E 00	0.8006E-01	0.9486E 00	0.9986E 00	0.4849E-01	0.2148E-00	0.4849E-01	0.2148E-00
160	0.9698E 00	0.5997E-01	0.9405E 00	0.9969E 00	0.9245E-01	0.2194E-00	0.9245E-01	0.2194E-00
165	0.9830E 00	0.4237E-01	0.9371E 00	0.9941E 00	0.1297E-00	0.2226E-00	0.1297E-00	0.2226E-00
170	0.9924E 00	0.2692E-01	0.9291E 00	0.9927E 00	0.1583E-00	0.2227E-00	0.1583E-00	0.2227E-00
175	0.9981E 00	0.1304E-01	0.9388E 00	0.9910E 00	0.1805E-00	0.2164E-00	0.1805E-00	0.2164E-00
180	0.1000E 01	0.3125E-08	0.	0.	-0.	-0.	-0.	-0.

T AND X=STATIONS ALONG CHORD WHERE X=.5(1-COS(T))

GSTAR =CIRCULATION DISTRIBUTION (EQ2.3-15)

NCO AND NCI=NONLINEAR CORRECTION OUTSIDE AND INSIDE DUCT RESPECTIVELY (EQ3.2-3)

PO AND PI=NONLINEAR PRESSURE DISTRIBUTION OUTSIDE AND INSIDE THE DUCT RESPECTIVELY FOR PA=0 DEGREES

POP AND PIP =NONLINEAR PRESSURE DISTRIBUTION OUTSIDE AND INSIDE THE DUCT RESPECTIVELY FOR PA=INPUT

GEOMETRIC ANGLE OF ATTACK IN DEGREES 0.1000E 02

POSITION OF SECTION AT ANGLE (PA) IN DEGREES 0.1800E 03

T	X	GSTAR	NCO	NCI	PO	PI	POP	PIP
0	-0.	-0.3111E-01	0.	0.	0.	0.	-0.	-0.
5	0.1903E-02	-0.2721E-01	0.5711E 00	0.7803E 00	-0.1692E 01	0.2232E 01	0.2341E 01	-0.3294E 01
10	0.7596E-02	-0.1606E-01	0.6801E 00	0.8829E 00	-0.1109E 01	0.1334E 01	0.1270E 01	-0.1775E 01
15	0.1704E-01	0.7947E-03	0.8713E 00	0.9915E 00	-0.1066E 01	0.1090E 01	0.9342E 00	-0.1215E 01
20	0.3015E-01	0.2110E-01	0.9170E 00	0.9989E 00	-0.9496E 00	0.9085E 00	0.5941E 00	-0.8101E 00
25	0.4685E-01	0.4230E-01	0.9377E 00	0.9993E 00	-0.8673E 00	0.7962E 00	0.3593E-00	-0.5564E 00
30	0.6699E-01	0.6196E-01	0.9524E 00	0.9997E 00	-0.8033E 00	0.7136E 00	0.1974E-00	-0.3923E-00
35	0.9042E-01	0.7822E-01	0.9640E 00	0.9998E 00	-0.7453E 00	0.6415E 00	0.8522E-01	-0.2858E-00
40	0.1170E-00	0.9610E-01	0.9727E 00	1.0000E 00	-0.6879E 00	0.5732E 00	0.7945E-02	-0.2185E-00
45	0.1464E-00	0.9761E-01	0.9785E 00	1.0000E 00	-0.6304E 00	0.5076E 00	-0.4479E-01	-0.1774E-00
50	0.1786E-00	0.1017E-00	0.9837E 00	1.0000E 00	-0.5759E 00	0.4466E-00	-0.8155E-01	-0.1524E-00
55	0.2132E-00	0.1040E-00	0.9885E 00	1.0000E 00	-0.5277E 00	0.3920E-00	-0.1094E-00	-0.1355E-00
60	0.2500E-00	0.1066E-00	0.9918E 00	1.0000E 00	-0.4869E-00	0.3474E-00	-0.1336E-00	-0.1201E-00
65	0.2887E-00	0.1114E-00	0.9945E 00	1.0000E 00	-0.4557E-00	0.3145E-00	-0.1580E-00	-0.1020E-00
70	0.3290E-00	0.1200E-00	0.9967E 00	1.0000E 00	-0.4351E-00	0.2934E-00	-0.1848E-00	-0.7893E-01
75	0.3706E-00	0.1329E-00	0.9982E 00	1.0000E 00	-0.4241E-00	0.2838E-00	-0.2143E-00	-0.5014E-01
80	0.4132E-00	0.1501E-00	0.9993E 00	0.9999E 00	-0.4212E-00	0.2833E-00	-0.2459E-00	-0.1673E-01
85	0.4564E-00	0.1705E-00	0.9999E 00	0.9999E 00	-0.4236E-00	0.2892E-00	-0.2775E-00	0.1918E-01
90	0.5000E-00	0.1922E-00	0.9999E 00	0.9998E 00	-0.4277E-00	0.2982E-00	-0.3065E-00	0.5489E-01
95	0.5436E 00	0.2131E-00	0.9993E 00	0.9998E 00	-0.4306E-00	0.3070E-00	-0.3303E-00	0.8770E-01
100	0.5868E 00	0.2308E-00	0.9982E 00	0.9997E 00	-0.4289E-00	0.3132E-00	-0.3460E-00	0.1156E-00
105	0.6294E 00	0.2433E-00	0.9964E 00	0.9997E 00	-0.4197E-00	0.3152E-00	-0.3514E-00	0.1372E-00
110	0.6710E 00	0.2490E-00	0.9941E 00	0.9996E 00	-0.4017E-00	0.3121E-00	-0.3455E-00	0.1521E-00
115	0.7113E 00	0.2474E-00	0.9906E 00	0.9997E 00	-0.3734E-00	0.3048E-00	-0.3272E-00	0.1613E-00
120	0.7500E 00	0.2385E-00	0.9869E 00	0.9998E 00	-0.3361E-00	0.2937E-00	-0.2977E-00	0.1657E-00
125	0.7868E 00	0.2231E-00	0.9802E 00	1.0000E 00	-0.2895E-00	0.2808E-00	-0.2575E-00	0.1673E-00
130	0.8214E 00	0.2026E-00	0.9720E 00	0.9999E 00	-0.2361E-00	0.2679E-00	-0.2095E-00	0.1678E-00
135	0.8536E 00	0.1786E-00	0.9666E 00	0.9999E 00	-0.1797E-00	0.2560E-00	-0.1572E-00	0.1687E-00
140	0.8830E 00	0.1530E-00	0.9626E 00	0.9998E 00	-0.1217E-00	0.2467E-00	-0.1025E-00	0.1714E-00
145	0.9096E 00	0.1272E-00	0.9633E 00	0.9998E 00	-0.6423E-01	0.2405E-00	-0.4770E-01	0.1767E-00
150	0.9330E 00	0.1026E-00	0.9555E 00	1.0000E 00	-0.8610E-02	0.2374E-00	0.5595E-02	0.1844E-00
155	0.9532E 00	0.8006E-01	0.9486E 00	0.9986E 00	0.4248E-01	0.2362E-00	0.5449E-01	0.1935E-00
160	0.9698E 00	0.5997E-01	0.9405E 00	0.9969E 00	0.8766E-01	0.2361E-00	0.9724E-01	0.2027E-00
165	0.9830E 00	0.4237E-01	0.9371E 00	0.9941E 00	0.1262E-00	0.2349E-00	0.1332E-00	0.2102E-00
170	0.9924E 00	0.2692E-01	0.9291E 00	0.9927E 00	0.1563E-00	0.2313E-00	0.1602E-00	0.2142E-00
175	0.9981E 00	0.1304E-01	0.9388E 00	0.9910E 00	0.1804E-00	0.2216E-00	0.1806E-00	0.2112E-00
180	0.1000E 01	0.3125E-08	0.	0.	-0.	-0.	-0.	-0.

T AND X=STATIONS ALONG CHORD WHERE X=.5(1-COS(T))

GSTAR =CIRCULATION DISTRIBUTION (EQ2.3-15)

NCO AND NCI=NONLINEAR CORRECTION OUTSIDE AND INSIDE DUCT RESPECTIVELY (EQ3.2-3)

INDUCED VELOCITY INSIDE THE DUCT AT A DUCT RADIUS OF .9000E 00

Z	VA	VR
-0.	-0.1031314E-01	0.4657122E-02
1.0000000E-01	-0.2119968E-01	0.9644072E-02
0.2000000E-00	-0.2497895E-01	0.8701752E-02
0.3000000E-00	-0.2[illegible]6518E-01	0.8402688E-02
0.4000000E-00	-0.[illegible]4783E-01	0.1017478E-01
0.5000000E 00	-0.4251123E-01	0.1210610E-01
0.6000000E 00	-0.5119535E-01	0.1616164E-01
0.7000000E 00	-0.6163258E-01	0.1570435E-01
0.8000000E 00	-0.7249818E-01	0.1596172E-01
0.9000000E 00	-0.8630277E-01	0.1397612E-01
0.1000000E 01	-0.9359118E-01	0.9773976E-02

APPENDIX B – FORTRAN LISTING OF COMPUTER PROGRAM

```
      DIMENSION SSM(181),SCM(181),CT(481),ST(181),CTM(181),STM(181),SJT(
     1 40,40),CJT(40,40),G(40,20),SM(1M2),AMM(20,20),P(20),CM(40,20),B(40
     2,20),C(20,20),PP(181),A(20),G1(181),W(181),SU(181),VU(20),VO(200)
     3, RVO(181),
     4P1(20),  D1MM(20),  P1MM(20),AR(100),MA(100),MV(200),GR(200)
      COMMON SSM,SCM,CT,ST,CTM,STM,SJT,CJT,GG,SM,APM,P,CM,M,C,PP,A,G1,B,S
     1U,VG,VO,RVO,P11,D1MM,P1MM,AA,GR,MV,GR,M,11,12,13,14,15,53,40,MM,NM
      DIMENSION V(181),S(181),TITLE(121),A(181),BB(181),EC(40,2),ET(40,2)
     1,ASC(40,2)
      COMMON V,S,TITLE,A,AR,EC,BB,ASC
      DIMENSION AR1(40),MR1(40),A2(40),UR2(40)
      COMMON MP,US,AR,A01,A02,ALFA,MP1
      DIMENSION GG(181),GP(181),SM2(20),R1(20),T1(181),T2(181),Z1(20),Z
     1Z1(20),BR2(20,40),BT2(20,40)
      COMMON GG,GP,SM2,R1,T1,Z1,Z2,T2,BR,,BT2  ,BR    ,AT
      DIMENSION BB1(20,40),BT1(20,40),BW1(20)
      COMMON BR1,BT1,BW1,CD1

      DIMENSION POL(181),PIL(181),PORL(141),PIWL(181),POO(181),PII(181)
      COMMON POL,PIL,PORL,PIWL,POO,PII,CJ1,CJ0,ALFAR,CL,CD,CM,CM1,CM2,PM
     1I
      I1=1
      I3=181
      I2=5
      MPP=5
      NN=36
      MP1=5
      ERASE IN
      IN1=0
      DO 9999 I=I1,I3,I2
      IN=IN+1
      IF(I-1) 9992,9993,9992
97    IN1=IN1+12
93    T=FLOATF(IN1)/57.29578
      TH=.367
      CTM(I)=COSF(TH)
      STM(I)=SINF(TH)
      DO 8888 J=1,36
      TJ=FLOATF(J)*T
      CJT(IN,J)=COSF(T J)
      SJT(IN,J)=SINF(TJ)
      CT(I)=CJT(IN,1)
88    ST(I)=SJT(IN,1)
99    CONTINUE
      PRINT 103
93    FORMAT(1H1)
      CALL SUB MA
      R1=0.0
      J=0
      ERASE IN
      DO 11=11,13,12
      IN=IN+1
      IF(I-1)92,93,92
92    J=J+12
93    T=FLOATF(J)/57.29578
      DO 90 K=1,MP1
      M=K
```

```
      MP=NMP+M
      SLT=-(CUBERTF(I)*1616-I)
      ULT=CUBERTF(I)
      PR=GAUSS(SLT,ULT,MP,DT)
      AR=SQRTF(4./(M**2)*(C(I)*I-COSF(I-DI**3))**2+4.)
      IF(AR-1.) 2,10,10
    2 IF(AR-.99) 8,9,9
    8 CALL ELLIPE(R,AR,R3,R4,MP,MS)
      GO TO 7
    9 AR2=AR**2
      CALL VSELLE(AR2,R5,MP)
      GO TO 7
   10 ERASE MP,M5
    7 PR=DI**2*AA*(BP-BS)*COSF(FLOATF(M)*(I-DI**3))
   99 G(IN,M)=PR
    1 NP=NMP
      ALFA=ATANF(ALFA)
      DR=FLOATF(I2)/171.99736
      DO 1001 I=2,13,2
      SM(I)=4.0
 1001 SM(I+1)=2.0
      SM(1)=1.0
      SM(13)=1.0
      DO 230 M=1,MP1
      ERASE AP,IN
      DO 300 I=11,13,12
      IN=IN+1
  300 AP=AP+G(IN,M)*SM(I)
      APM(1,M)=AP*DR/3.1416
  200 P(M)=-A.09*FLOATF(M)*APM(1,M)/3.1416
      DO 600 IP=2,MP1
      DO 600 M=1,MP1
      ERASE AP,IN
      DO 11500 I=11,13,12
      IN=IN+1
11500 AP=AP+G(IN,M)*SM(I)*SJ(IN,IP-1)
  600 APM(IP,M)=.0196*R**DA
      ERASE IN
      DO 900 I=11,13,12
      IN=IN+1
      DO 900 M=1,MP1
      ERASE SUM
      DO 901 IP=2,MP1
  901 SUM=SUM+APM(IP,M)*SJ(IN,IP-1)
  900 CB(IN,M)=-A.09*FLOATF(M)*SUM/3.1416
      ERASE IN
      DO 600 I=11,13,12
      IN=IN+1
      DO 611 K=1,MP1
      MP=NMP+M
      MM=1
      PR=GAUSS(0.0,3.1416,MP,DT)
      CMC=COSF(DI*I-C(I))
      IF(CMC) 699,610,699
  699 AR=SQRTF(4./(M**2*(CMC**2+4.0))
      IF(AR-1.) 602,610,610
  602 IF(AR-.99) 608,609,609
  608 CALL ELLIPE(R1,AR,R3,R4,MP,M5)
```

```
      GO TO 607
  606 AR2=AR**2
      CALL VSELL (AR2,BS,MP)
      GO TO 607
  610 PR=0.0
      GO TO 660
  607 PR=(1./CMC)*(2.*AR*(M**2*CMC**2*(BP-BS1-2.*BS))
  660 IF(M) 666,666,555
  555 PR=PR*COSP(FLOATF(M)*DT)
  666 PR=PR
      IF(M) 777,777,888
  777 B(IN,1)=.318309*PR
      GO TO 611
  888 B(IN,1)=.636618*PR
  611 CONTINUE
  600 MP=MP+1
      ERASE C11,C12,IN
      DO 910 I=11,13,12
           IN   =   IN+1
      C11=C11+B(IN
     *             ,1)*(1.+CT(I))*SM(I)
  910 C12=C12+B(IN
     *             ,1)*((ST(I))**2)*SM(I)
      C(1,1)=-.159154*C11*DR
      C(1,2)=.159154*C12*DR
      DO 911 J=3,MP1
      ERASE AC1,IN
      DO 912 I=11,13,12
      IN=IN+1
  912 AC1=AC1+B(IN,1)*SJT(IN,J-1)*ST(I)*SM(I)
  911 C(1,J)=.159154*AC1*DR
      DO 920 K=2,MP1
      ERASE ACR1,IN
      DO 913 I=11,13,12
      IN=IN+1
  913  ACR1 ACR1+B(IN,K)*(1.+CT(I))*SM(I)
  920 C(K,1)=-.159154*ACR1*DR
      DO 921 K=2,MP1
      DO 921 J=2,MP1
      ERASE AC,IN
      DO 922 I=11,13,12
      IN=IN+1
  922 AC=AC+B(IN,K)*SJT(IN,J-1)*ST(I)*SM(I)
  921 C(K,J)=.159154*AC*DR
      IF(AT) 1312,1313,1312
 1312 C(1,1)=1.0
      DO 1314 K=2,MP1
 1314 C(K,1)=0.0
 1313 DO 1100 K=1,MP1
      DO 1100 J=1,MP1
      IF(K-J) 1102,1101,1102
 1101 C(K,J)=1.-C(K,J)
      GO TO 1100
 1102 C(K,J)=-C(K,J)
 1100 CONTINUE
      ERASE IN
 8000 DO 1300 I=11,13,12
      IN=IN+1
```

```
      ERASE SUM1,SUM2,SUM3
      DO 1200 M=1,MP1
      SUM1=SUM1+SSM(M)*F(M)
      SUM2=SUM2+SCM(M+1)*SJT(IN,M)
1200  SUM3=SUM3+SSM(M)*CB(IN,M)
      IF(AT) 1316,1323,1316
1316  FF(I)=-2.*SUM2+SUM3
      GO TO 1300
1323  FF(I)=((2.*SINF(ALFA)/COSF(ALFA)+2.*SCM(1)*SUM1)*CTH(I)+STH(I)*(-2
     1.*SUM2+SUM3))
1300  CONTINUE
      DO 1301 K=1,MP1
      ERASE FI,IN
      DO 1201 I=I1,I3,I2
      IN=IN+                                          1
1201  FI=FI+B(IN,K)*CTH(I)**2*SM(I)*DX
1301  FII(K)=FI
      DO 1405 K=1,MP1
      DO 1500 M=1,MP1
      ERASE DIM,FIM,IN
      DO 1400 I=I1,I3,I2
      IN=IN+1
      DIM=DIM+B(IN,K)*ST(I)*SJT(IN,M)*SM(I)*DX
1400  FIM=FIM+B(IN,K)*CB(IN,M)*ST(I)*SM(I)*D..
      DIMM(M)=DIM
1500  FIMM(M)=FIM
      S4=2.*(SINF(ALFA)/COSF(ALFA)+SCM(1))*FII(K)
      ERASE S1,S2,S3
      DO 1404 M=1,MP1
      S1=S1+SSM(M)*F(M)*FII(K)
      S2=S2+SCM(M+1)*DIMM(M)
1404  S3=S3+SSM(M)*FIMM(M)
      IF(AT)1318,1333,1318
1318  A(K)=-2.*S2+S3
      A(1)=0.0
      GO TO 1405
1333  A(K)=S1-S2+.5*S3+S4
1405  CONTINUE
      IF(AT)2200,2000,2200
2200  MP1=MP1-1
      DO 3333 K=1,MP1
      DO 3333 J=1,MP1
      C(K,J)=C(K+1,J+1)
3333  A(K)=A(K+1)
2000  CALL MATINV(C,MP1,A,1,0,ID)
      IF(ID-1) 1601,1600,1601
1601  PRINT 88
  88  FORMAT(14H C IS SINGULAR)
      GO TO 1603
1600  IF(AT)1660,1670,1660
1670  G1(1)=FF(1)-.318309*A(1)
      IN=1
      I9=I1+I2
      DO 1700I=I9,I3,I2
      IN=IN+1
      ERASE SUM
      DO 1701 J=2,MP1
1701  SUM=SUM+.318309*STH(I)*A(J)*SJT(IN,J-1)
```

```
 1700 G1(I)=FF(I)-.318309*CTH(I)*A(I)+SUM
      CALL SUB AT
29993 NH=36
      ERASE NX
      DO 20001 I=11,13,12
      NX=NX+1
20001 GX(NX)=G1(I)
      NN=2*NX-2
      KX=NX-2
      DO 20002 KK=1,KX
      NX1=NX+KK
      NX2=NX-KK
20002 GX(NX1)=+GX(NX2)
      CALL GMHAS(NN,NH,GX,RY(200))
      AO=RY(200)
      DO 20003 J=1,NH
      JFIX=200-J*5
      AX(J)=RY(JFIX)
20003 BX(J)=RY(JFIX-1)
      BO=RY(199)
20004 FORMAT(I10,2E15.6)
      ERASE IN
      PRINT 103
      DO 20006 I=11,13,12
      IN=IN+1
      ERASE Y1,Y2
      DO 20005 K=1,NH
      Y1=Y1+AX(K)*CJT(IN,K)
20005 Y2=Y2+BX(K)*SJT(IN,K)
      Y3=AO+Y1+BO+Y2
      IF(I-1)27000,27001,27000
27001 GG(I)=Y3/SINF(1./57.29578)
      GO TO 27002
27000 GG(I)=Y3/STH(I)
27002 L=I-1
      XE=-(.5*(1.+CT(I)))+1.0
20006 CONTINUE
      ERASE Y1
      DO 28001 I=1,181,5
28001 Y1=Y1+12.5664*G1(I)*W(I)*CTH(I)*SM(I)*DX
      CDI=Y1
      CTD=2.*H*CDI/3.1416
28004 FORMAT(I10,2E15.6)
26000 FORMAT(9F8.6)
26009 FORMAT(7E15.6)
      PRINT 103
      ERASE IN,J
      DO 1900 I=11,13,12
      ERASE XU
      IN=IN+1
      DO 1901 M=1,MP1
 1901 XU=XU+FLOAT(M)*SSM(M)*CJT(IN,M)
 1900 SU(I)=XU
      ERASE IN
      DO 20007 IB=11,13,12
      IN=IN+1
      IF(IB-1)20009,20008,20009
20009 J=J+12
```

```
20008 T=FLOATF(J)/57.29578
      SLT=-CUBERTF(T)
      ULT=CUBERTF(3.1416-T)
      PR=GAUSS(SLT,ULT,NP,DT)
      AK=SQRTF(4./(H**2*(CT(IB)-COSF(DT**3+T))**2+4.))
      IF(AK-1.) 20011,20012,20012
20011 IF(AK-.99) 20014,20013,20013
20014 CALL ELLIP(X1,AK,X3,X4,BF,BS)
      GO TO 20015
20013 AK2=AK**2
      CALL YSELL(AK2,BS,BF)
      GO TO          2          0       015
20012 ERASE BS,BF
20015 ERASE Y1,Y2
      DO 20016 K=1,NH
      ZK=FLOATF(K)*(DT**3+T)
      Y1=Y1+AX(K)*COSF(ZK)
20016 Y2=Y2+BX(K)*SINF(ZK)
      Y3=A0+Y1+B0+Y2
      PR=Y3*AK*(BF-BS)*COSF(.5*(DT**3+T))*3.*DT**2
       VG(IB)=.159154*H*PR
      DO 1807 I=I1,I3,I2
      AK=SQRTF(4./(H**2*(CT(IB)-CT(I))**2+4.))
      IF(AK-1.)1802,1810,1810
 1802 IF(AK-.99)1808,1809,1809
 1808 CALL ELLIP(X1,AK,X3,X4,BF,BS)
      GO TO 1807
 1809 AK2=AK**2
      CALL YSELL(AK2,BS,BF)
      GO TO 1807
 1810 BS=1.0
 1807 BVQ(I)=SU(I)*AK*BS
      ERASE GX0
      DO 6666 I=I1,I3,I2
 6666 GX0=GX0+BVQ(I)
     X                *SM(I)*DX/3.1416
      DO 6662 M=1,MP1
      ERASE GXX,INN
      DO 6661 I=I1,I3,I2
      INN=INN+1
 6661 GXX=GXX+2.*BVQ(I)*SM(I)*CJT(INN,M)*DX/3.1416
 6662 GX(M)=GXX
      ERASE SUM10,SUM9,SUM8
      DO 11905 M=1,MP1
      SUM10=SUM10+GX(M)*SJT(IN,M)
      SUM9=SUM9-FLOATF(M)*GX(M)*2.
11905 SUM8=SUM8+2.*(-1.**M)*FLOATF(M)*GX(M)
      IF(IB-1) 11912,11908,11912
11912 IF(IB-181) 11907,11906,11907
11907 WQ=(-2./ST(IB))*(GX0+SUM10)
      GO TO 20007
11908 WQ=SUM9
      GO TO 20007
11906 WQ=SUM8
20007 VQ(IB)=WQ
      ERASE IN
20000 DO 20020 IB=I1,I3,I2
      IN=IN+1
```

```
      IF(IB-1)20021,20020,20021
    1 HV6=VG(IB)+T2(IB)
                                 GISTH=.5*G1(IB)/STH(IB)
      WGO=HV6-GISTH
      WG1=HV6+GISTH
    ' WOO=           VO(IB)
      WGG=VG(IB)
      PO=2.*(WGO+WOO)
      PI=2.*(WG1+WOO)
      POL(IB)=PO
      PIL(IB)=PI
      PON=S(IN)*PO
      PIN=Y(IN)*PI
      X(IN)=.5*PO
      XX(IN)=.5*PI
    ) CONTINUE
    3 FORMAT(I10,7E15.6)
      GO TO 1603
    ) ERASE IN
      A(1)=0.0
      DO 1669 I=I1,I3,I2
      IN=IN+1
      ERASE SUM
      DO 1661 J=2,MP1
    1 SUM=SUM+A(J)*SJT(IN,J-1)
      G1(I)=FF(I)+.15915**SUM
      GG(I)=G1(I)
      IX=I-1
    9 CONTINUE
      ERASE T,IN
      DO 1234 I=I1,I3,I2
      IN=IN+1
    4 T=T+B(IN,1)*G1(I)*ST(I)*SM(I)*DX
      ANT=ATANF(.079577*T-.5*SUM1-SCM(1))*57.29578
      ERASE AT
    3 FORMAT(55H1IDEAL ANGLE OF ATTACK IN DEGREES
     1F9.6)
      PRINT 1753,ANT
      DO 20024 I=I1,I3,I2
    4 G1(I)=G1(I)*STH(I)
      IF(AT) 1667,1668,1667
    7 CALL SUB AT
      GO TO 29993
    2 FORMAT(I10,5E15.6)
    1 FORMAT(8F9.6)
    0 FORMAT(5I4,4F10.6/1814)
    2 FORMAT(8F10.6)
    1 FORMAT(8E15.6)
    3 CALL SUBWR
    8 CALL END JOB
      END
```

```
        FOR
        SUBROUTINE SUB HA
        DIMENSION SSM(181),SCM(181),CT(181),ST(181),CTH(181),STH(181),SJT(
       140,40),CJT(40,40),G(40,20),SM(182),APM(20,20),F(20),CB(40,20),B(40
       2,20),C(20,20),FF(181),A(20),GI(181),W(181),SU(181),VG(200),VO(200)
       3, BVQ(181),
       4FII(20), DIMM(20), FIMM(20),AX(100),BX(100),RY(200),GX(200)
        COMMON SSM,SCM,CT,ST,CTH,STH,SJT,CJT,G,SM,APM,F,CB,B,C,FF,A,GI,W,S
       1U,VG,VO,BVO,FII,DIMM,FIMM,AX,BX,RY,GX,H,II,I2,I3,DX,X1,X3,X4,NP,NH
        DIMENSION Y(181),S(181),TITLE(12),X(181),XX(181),XC(40,2),XT(40,2)
       1,XSC(40,2)
        COMMON Y,S,TITLE,X,XX,XC,XT,XSC
        DIMENSION AX1(40),BX1(40),AX2(40),BX2(40)
        COMMON BF,BS,AK,AO1,AO2,ALFA,MP1
        DIMENSION GG(181),GP(181),SMZ(20),XI(20),T1(181),T2(181),ZI(20),Z
       12(20),WR2(20,40),WT2(20,40)
        COMMON GG,GP,SMZ,X1,T1,Z1,Z2,T2,WR2,WT2 ,WK     ,AT
        DIMENSION WR4(20,40),WT4(20,40),WR6(20)
        COMMON WR4,WT4,WR6,CDI
        DIMENSION POL(181),PIL(181),PORL(181),PIRL(181),POO(181),PII(181)
        COMMON POL,PIL,PORL,PIRL,POO,PII,CDI,CTD,ALFAR,CL,CD,CM,CM1,CM2,PH
       11
        ERASE IN,T1,T2
        DO 2901 I=1,181,5
        IN=IN+1
        XX(IN)=.5*(1.-CT(I))
 2901 X(IN)=FLOATF(I-1)
        PRINT 103
        ERASE XC,XT
        ERASE AX,BX
        READ 21993,TITLE
        PRINT 21990,TITLE
        READ 21998,CC,TT,H,ALFA,AT,WK,WW
        PRINT 1752,CC,TT,H,ALFA,AT,WK,WW
        NC=CC
        NT=TT
        M=NC/2
21993 FORMAT(12A6)
21990 FORMAT(1H1,12A6)
21998 FORMAT(9F8.6)
        ERASE XSC,SCM
        IF(CC)2601,2602,2601
 2601 READ 21998,(X(I),I=1,NC)
        READ 21998,(Y(I),I=1,NC)
        PRINT 1752,(X(I),I=1,NC)
        PRINT 1752,(Y(I),I=1,NC)
        DO 2599 I=1,37
        S1=XX(I)
        CALL DISCOT(S1,S1,X,Y,Y,-120,NC,0,S2)
 2599 T1(I)=S2
 2602 READ 21998,(X(I),I=1,NT)
        READ 21998,(Y(I),I=1,NT)
        PRINT 1752,(X(I),I=1,NT)
        PRINT 1752,(Y(I),I=1,NT)
        DO 2598 I=1,37
        S1=XX(I)
        CALL DISCOT(S1,S1,X,Y,Y,-120,NT,0,S2)
 2598 T2(I)=S2
 3000 FORMAT(3E13.4)
21005 FORMAT(I10,6E15.6)
```

```
000 FORMAT(I8,4F8.6)
    DO 21888 IC=1,2
    DO 2597 I=1,37
597 Y(I)=T1(I)
    Y(1)=.0
    Y(37)=.0
001 FORMAT(9E13.4)
498 FORMAT(3E15.6)
    DO 21001 KK=1,35
    NX1=37+KK
    NX2=37-KK
001 Y(NX1)=-Y(NX2)
    IF(IC-2) 2408,2409,2408
408 IG=2
    GO TO 2410
409 IG=1
410 DO 21002 IS=1,IG
    IF(T1(S)) 21977,21978,21977
978 ERASE RY
    GO TO 21976
977 CALL GMHAS(72,36,Y,RY(200))
976 AO=RY(200)
    XC(1,IS)=AO
    DO 21997 J=1,36
    JFIX=200-J*5
    AX(J)=RY(JFIX)
    XC(J+1,IS)=AX(J)
    BX(J)=RY(JFIX-1)
997 XT(J,IC)=BX(J)
    BO=RY(199)
    ERASE IH
996 FORMAT(I10,2E15.6)
    ERASE IN
    DO 29000 I=1,181,5
    IN=IN+1
    ERASE Y1,Y2,SS
    L=I-1
    DO 21995 K=1,36
    Y1=Y1+AX(K)*CJT(IN,K)
    Y2=Y2+BX(K)*SJT(IN,K)
    IF(IS-2)24000,23000,24000
3000 ERASE S
    GO TO 21984
4000 IF(I-1)21983,21982,21983
1983 IF(I-181)21981,21980,21981
1982 TOS=2./SINF(1./57.29578)
    GO TO 21995
1980 TOS=2./SINF(179./57.29578)
    GO TO 21995
1981 TOS=2./ST(I)
1995 SS=SS-FLOATF(K)*BX(K)*CJT(IN,K)*TOS
    Y(IN)=-SS
    XSC(IN,IC)=-SS
    S(I)=-SS
1984 Y3=AO+Y1+BO+Y2
3000 CONTINUE
    DO 21006 KK=1,35
    NX1=37+KK
```

```
      NX2=37-KK
21006 Y(NX1)=+Y(NX2)
      Y(37)=Y(36)
21002 Y(36)=Y(36)
      DO 2596 I=1,37
 2596 T1(I)=T2(I)
21888 CONTINUE
21994 FORMAT(I10,2E15.6,I10,3E15.6)
      ALFA=SINF(ALFA/57.29578)/COSF(ALFA/57.29578)
29001 DO 22001 I=1,37
      S(I)=1./SQRTF(1.+(XSC(I,1)+ALFA+XSC(I,2))**2)
22001 Y(I)=1./SQRTF(1.+(XSC(I,1)+ALFA-XSC(I,2))**2)
      DO 22889 J=1,36
      SCM(J)=-XC(J,2)
22889 SSM(J)=XT(J,2)
      S(1)=.0
      Y(1)=.0
      S(37)=.0
      Y(37)=.0
      ERASE IN,W
      DO 22222 I=1,181,5
      IN=IN+1
      X(IN)=FLOATF(I-1)
22222 XX(IN)=.5*(1.-CT(I))
      ERASE IN
      IF(WK)96,97,96
   97 ERASE  W
      GO TO 190
   96 READ 21998,ANR
      NR=ANR
      READ 21998,(T1(I),I=1,NR)
      READ 21998,(T2(I),I=1,NR)
       PRINT 1752,(T1(I),I=1,NR)
      PRINT 1752,(T2(I),I=1,NR)
      ERASE IN
      DO 2699 I=1,181,5
      IN=IN+1
      S1=XX(IN)
      CALL DISCOT(S1,S1,T1,T2,T2,-120,NR,0,S2)
2699 W(I)=S2
 190 IF(WW)196,197,196
 197 ERASE T2
      GO TO 95
 196 READ 21998,ANA
      NA=ANA
      READ 21998,(T1(I),I=1,NA)
      READ 21998,(T2(I),I=1,NA)
      PRINT 1752,(T1(I),I=1,NA)
      PRINT 1752,(T2(I),I=1,NA)
      ERASE IN
      DO 2698 I=1,181,5
      IN=IN+1
      S1=XX(IN)
      CALL DISCOT(S1,S1,T1,T2,T2,-120,NA,0,S2)
2698 T1(I)=S2
1752 FORMAT(9F10.6)
 103 FORMAT(1H1)
  95 RETURN
      END
```

```
      FOR
     SUBROUTINE SUB AT


     DIMENSION SSM(181),SCM(181),CT(181),ST(181),CTH(181),STH(181),SJT(
    140,40),CJT(40,40),G(40,20),SM(182),APM(20,20),F(20),CB(40,20),B(40
    2,20),C(20,20),FF(181),A(20),G1(181),W(181),SU(181),VG(200),VQ(200)
    3, BVQ(181),
    4FII(20), DIMM(20), FIMM(20),AX(100),BX(100),RY(200),GX(200)
     COMMON SSM,SCM,CT,ST,CTH,STH,SJT,CJT,G,SM,APM,F,CB,B,C,FF,A,G1,W,S
    1U,VG,VQ,BVQ,FII,DIMM,FIMM,AX,BX,RY,GX,H,I1,I2,I3,DX,X1,X3,X4,NP,NH
     DIMENSION Y(181),S(181),TITLE(12),X(181),XX(181),XC(40,2),XT(40,2)
    1,XSC(40,2)
     COMMON Y,S,TITLE,X,XX,XC,XT,XSC
     DIMENSION AX1(40),BX1(40),AX2(40),BX2(40)
     COMMON BF,BS,AK,A01,A02,ALFA,MP1
     DIMENSION GG(181),GP(181),SMZ(20),XI(20),T1(181),T2(181),Z1(20),Z
    22(20),WR2(20,40),WT2(20,40)
     COMMON GG,GP,SMZ,XI,T1,Z1,Z2,T2,WR2,WT2   ,WK    ,AT
     DIMENSION WR4(20,40),WT4(20,40),WR6(20)
     COMMON WR4,WT4,WR6,CDI

     DIMENSION POL(181),PIL(181),PORL(181),PIRL(181),P00(181),PII(181)
     COMMON POL,PIL,PORL,PIRL,P00,PII,CDI,CTD,ALFAR,CL,CD,CM,CM1,CM2,PH
    1I
     DIMENSION SCD(181),CXT(181),P(181)
     DIMENSION R(181)
     ERASE PII,P00,ALFAR,PHI,CL,CD,CM,CM1,CM2
     ALFA1=ALFA
     NM=10
     NPP=5
     K1=10
     J1=10
     NH=36
     ALFAR=1.
     PHI=.0
556  ALFA=ALFAR
394  FORMAT (8E15.6)
198  FORMAT(8F9.6)
     XI=0.
     ERASE IN
     DO 11 I=I1,I3,I2
     IN=IN+1
 97  DO 10 K=1,NM
     M=K-1
     NP=NPP+M
     P2=GAUSS(0.0,3.1416,NP,CT)
     CMC=COSF(CT) -CT(I)
     IF(CMC)99,2,99
 99  AK=SQRTF(4./(M
    1                **2+CMC**2+4.))
     IF(    AK -1.     )111 ,2
111  IF(AK-.99)108,109,109
108  CALL ELLIP(X1,AK,X3,X4,BF,BS)
     GOTO 107
109  AK2=AK**2
     CALL YELL(AK2,BS,BF)
     GOTO 107
  2  Z=0.
     GOTO 80
```

```
  107 Z=(((2.-AK**2)**2*BS-4.*(1.-AK**2)**2*BF)/(CMC*AK**3)-1./CMC)
   60 IF(M)6,6,5
    5 Z=Z*COSF(FLOATF(M)*DT)
    6 PR=Z
      IF (M)7,7,8
    7 B(IN,K)=-1.5708*M+.318309*PR
      GO TO 10
    8 B(IN,K)=.636618*PR
   10 CONTINUE
   11 NP=NPP
   20 FORMAT( 18I4)
   40 FORMAT(I4/(10F7.3))
      DX=FLOATF(I2  )/171.88734
      DO 501 I=3,I3,2
      SM(I)=4.0
  501 SM(I+1)=2.0
      SM(1)=1.0
      SM(I3)=1.0
 8000 ERASE C11,F1,C12,IN
       DO 1100 I = I1 , I3,I2
      IN=IN+1
      C11=C11+.636618*B(IN,1)*CTH(I)**2*SM(I)*DX
      F1=F1-2.*ALFA*B(IN,1)*CTH(I)**2*SM(I)*DX/57.29578
 1100 C12=C12+.318309*B(IN,1)*ST(I)**2*SM(I)*DX
      C(1,1)=C11
      C(1,2)=C12
      F(1)=F1
      DO 100 J=3,J1
      ERASE XC1,IN
       DO 1200 I = I1 , I3,I2
      IN=IN+1
 1200 XC1=XC1+.318309*ST(I)*SJT(IN,J-1)*SM(I)*DX*B(IN,1)
  100 C(1,J)=XC1
      DO 200 K=2,K1
       ERASEXCK1 ,XF
      ERASE IN
       DO 1300 I = I1 ,  I3 ,I2
      IN=IN+1
      XCK1=XCK1-.636618*B(IN,K)*CTH(I)**2*SM(I)*DX
 1300 XF=XF+2.*AL A*B(IN,K)*CTH(I)**2*SM(I)*DX/57.29578
      F(K)=XF
  200 C(K,1)=XCK1
       DO 1500 K = 2 , K1
       DO 1500 J = 2 , J1
      ERASE XC,IN
       DO 1600 I = I1 , I3,I2
      IN=IN+1
 1600 XC=XC-.318309*B(I  )*SJT(IN,J-1)*ST(I)*SM(I)*DX
 1500 C(K,J)=XC
      DO 700 K=1,K1
      DO 700 J=1,J1
      IF (K-J)702,701,702
  701 C(K,J)=1.-C(K,J)
      GO TO 700
  702 C(K,J)=-C(K,J)
  700 CONTINUE
      DO 799 K=1,K1
  799 A(K)=F(K)
```

```
  FORMAT (///////8E15.6)
  CALL MATINV(C,K1,A,1,X,ID)
  IF (ID-1)901,900,901
  PRINT 88
  FORMAT (14H C IS SINGULAR)
  GO TO 803
  ERASE SUMA,SG,SG1,NX,IN
  DO 1000 I=1,13,12
  IN=IN+1
  SUMA = 0.0
  DO 1001 J=2,J1
  SUMA=SUMA+A(I,J)*SJT(IN,J-1)
  IF(I-1)1003,1002,1003
  R(I)=(2.*ALFA/57.29578)-.636618*A(1)
  GOTO 1004
  R(I)=2.*(ALFA     /57.29578)*CTH(I) -.636618*STH(I)*(A(I)*CTH(I)
 1 /STH(I) +SUMA)
  SG=SG+R(I)*CTH(I)*SM(I )
  NX=NX+1
  GX(NX)=R(I)
  SG1=SG1+R(I)*STH(I)**2*CTH(I)*SM(I )
  CL=6.2832*SG*DX
  CM=-6.2832*SG1*DX
  CD=.079577*H*CL**2
  ERASE CM1,CM2
  ERASE F1,IE
  DO 2497 I=I1,I3,I2
  CXT(I)=G1(I)*CTH(I)
  F1=F1+G1(I)*CTH(I)*SM(I)*DX
  DO 2200 I=I1,I3,I2
  ERASE XSCD
  DO 2100 IP=I1,I3,I2
  AK=SQRTF(4./(H**2*(CT(I)-CT(IP))**2+4.))
  IF(AK-1.)3111,2100,3111
  IF(AK-.99)3108,3109,3109
  CALL ELLIP(X1,AK,X3,X4,BF,BS)
  GO TO 3107
  AK2=AK**2
  CALL YSELL(AK2,BS,BF)
  XSCD=XSCD+(R(IP)*CTH(IP)*H*(CT(I)-CT(IP))/AK)*(BF-BS)*SM(IP)*DX
  CONTINUE
  SCD(I)=XSCD
  ERASE CM1
  DO 2300 I=I1,I3,I2
  CM1=CM1+CXT(I)*SCD(I)*SM(I)*DX
  CM1=+.25*CL*F1+CM1
  CM2=CM+CM1
  NN=2*NX-2
  KX=NX-2
  DO 2301 KK=1,KX
  NX1=NX+KK
  NX2=NX-KK
  GX(NX1)=-GX(NX2)
  CALL GMHAS(NN,NH,GX,RY(200))
  AO=RY(200)
  DO 5000 J=1,NH
  JFIX=200-J*5
  AX(J)=RY(JFIX)
```

```
5000 BX(J)=RV(JF1X-1)
     BO=RV(199)
5006 FORMAT(I10,2E15.6)
     DO 5093 I=I1,I3,I2
     ERASE Y1,Y2
     L=I-1
     DO 5003 K=1,NM
     TX=FLOATF(L*K)/57.29578
     Y1=Y1+AX(K)*COSF(TX)
5003 Y2=Y2+BX(K)*SINF(TX)
     Y3=AO+Y1+BO+Y2
5093 CONTINUE
     ERASE IN
     DO 7500 I=I1,I3,I2
     IN=IN+1
     E=FLOATF(I-1)/57.29578
     SLT=-CUBERTF(E)
     ULT=CUBERTF(3.1416-E,
     PR=GAUSS(SLT,ULT,NPP,DT)
     AK=SQRTF(4./(M**2*(CT(I)-COSF(DT**3+E))**2+4.0))
     IF(AK-1.0) 7502,7510,7510
7502 IF(AK-.99) 7508,7509,7509
7508 CALL ELLIP(X1,AK,X3,X4,BF,BS)
     GO TO 7507
7509 AK2=AK**2
     CALL YSELL(AK2,BS,BF)
     GO TO 7507
7510 ERASE BF,B3
7507 ERASE Y1,Y2
     DO 7503 K=1,NM
     ZK=FLOATF(K)*(DT**3+E)
     Y1=Y1+AX(K)*COSF(ZK)
7503 Y2=Y2+BX(K)*SINF(ZK)
     Y3=AO+Y1+BO+Y2
     PR=(DT**2*Y3/AK)*((4.-AK**2)*BS-(4.-3.*AK**2)*BF)*COSF(.5*(DT**3+E
    1)) *(DT**3+E)**2
     P(I)=(-
    X       3.*M/3.1416)*PR
     IF(I-1)8701,8700,8701
8700 PII(I)=.0
     POO(I)=.0
     GO TO 7500
8701 POO(I)=(P(I)-R(I)/STM(I))*COSDF(PHI)
     PII(I)=(P(I)+R(I)/STM(I))*COSDF(PHI)
7500 CONTINUE
2499 FORMAT(I10,7E15.6)
  50 FORMAT(9F8.6)
7555 ALFA=ALFAI
     RETURN
 803 CALL ENDJOB
     END
```

```
      FOR
      SUBROUTINE SUBWR
      DIMENSION SSM(181),SCM(181),CT(181),ST(181),CTH(181),STH(181),SJT(
     140,40),CJT(40,40),G(40,20),SM(182),APM(20,20),F(20),CB(40,20),B(40
     2,20),C(20,20),FF(181),A(20),GI(181),W(181),SU(181),VG(200),VQ(200)
     3, BVO(181),
     4FII(20), DIMM(20), FINM(20),AX(100),BX(100),RY(200),GX(200)
      COMMON SSM,SCM,CT,ST,CTH,STH,SJT,CJT,G,SM,APM,F,CB,B,C,FF,A,GI,W,S
     1U,VG,VQ,BVO,FII,DIMM,FINM,AX,BX,RY,GX,M,I1,I2,I3,DX,X1,X3,X4,NP,NM
      DIMENSION Y(181),S(181),TITLE(12),X(181),XX(181),XC(40,2),XT(40,2)
     1,XSC(40,2)
      COMMON Y,S,TITLE,X,XX,XC,XT,XSC
      DIMENSION AX1(40),BX1(40),AX2(40),BX2(40)
      COMMON BF,BS,AK,AO1,AO2,ALFA,MP1
      DIMENSION GG(181),GP(181),SMZ(20),X1(20),T1(181),T2(181),Z1(20),Z
     12(20),WR2(20,40),WT2(20,40)
      COMMON GG,GP,SMZ,X1,T1,Z1,Z2,T2,WR2,WT2 ,WK     ,AT
      DIMENSION WR4(20,40),WT4(20,40),WR6(20)
      COMMON WR4,WT4,WR6,CDI

      DIMENSION POL(181),PIL(181),PORL(181),PIRL(181),POO(181),PII(181)
      COMMON POL,PIL,PORL,PIRL,POO,PII,CDI,CTD,ALFAR,CL,CD,CM,CM1,CM2,PH
     11
      DO 11801 I=I1,I3,I2
      ERASE BRG,BRQ
      DO 11807 IP=I1,I3,I2
      AK=SQRTF(4./(M**2*(CT(I)-CT(IP))**2+4.))
      IF(AK-1.)11802,11810,11810
11802 IF(AK-.99)11808,11809,11809
11808 CALL ELLIP(X1,AK,X3,X4,BF,BS)
      GO TO 11811
11809 AK2=AK**2
      CALL VSELL(AK2,BS,BF)
      GO TO 11811
11810 ERASE BRG,BRQ
11811 BRQ=BRQ-.318309*M*SU(IP)*(BF-BS)*SM(IP)*DX
11807 BRG=BRG+.079577*GI(IP)*AK*(M**2*(CT(I)-CT(IP)) **2*(BF-BS)-2.*BS)*
     1CTH(IP)*SM(IP)*DX
      VQ(I)=BRQ
11801 VG(I)=BRG
      ERASE IN
      DO 12006 I=I1,I3,I2
      IN=IN+1
      L=I-1
      XE=-(.5*(1.+CT(I)))+1.0
      W00=VQ(I)-2.*SU(I)
      W01=VQ(I)+2.*SU(I)
      W0=VG(I)+W00
      W1=VG(I)+W01
      POR=-((-1.+X(IN))**2-1.+W0**2)
      PORN=S(IN)*POR
      PIR=-((-1.+XX(IN))**2-1.+W1**2)
      PIRN=Y(IN)*PIR
      PORL(I)=POR
      PIRL(I)=PIR
12006 CONTINUE
 1753 FORMAT(55H CHORD DIAMETER RATIO
     1F9.4///55H LIFT COEFFICIENT PER DEGREE (EQ3.3-2)
     1F9.4///55H INDUCED DRAG COEFFICIENT (EQ3.3-5)
     1F9.4///55H MOMENT COEFFICIENT FROM VERTICAL FORCES (EQ3.3-7)
```

```
     1F9.4///55H MOMENT COEFFICIENT FROM HORIZONTAL FORCES (EQ3.3-8)
     1F9.4///55H TOTAL MOMENT COEFFICIENT ABOUT L. E. (EQ3.3-6)
     1F9.4///55H INDUCED DRAG DUE TO RADIAL INDUCED VELOCITY (EQ3.3-4)
     1F9.4)
      PRINT 1753,M,CL,CD,CM,CM1,CM2,CDI
      READ 26000,AXA
      NOA=AXA
      READ 20025,(AX2(IA),IA=1,NOA)
      READ 20025,(AX1(IA),IA=1,NOA)
      DO 8889 IA=1,NOA
 1755 FORMAT(55H1GEOMETRIC ANGLE OF ATTACK IN DEGREES
     1E13.4 /55H POSITION OF SECTION AT ANGLE (PA) IN DEGREES
     1E13.4/)
      PRINT 1755,AX2(IA),AX1(IA)
 1756 FORMAT(115H       T           X           GSTAR         NCO           NC
     1I            PO            PI            POP          PIP        )
       PRINT 1756
      AX1(IA)=COSDF(AX1(IA))
      ERASE IN
      DO 7777 I=I1,I3,I2
      IN=IN+1
      POT=(POL(I)+P00(I)*AX2(IA))*S(IN)
      PIT=(PIL(I)+PII(I)*AX2(IA))*Y(IN)
      PORT=(POL(I)+P00(I)*AX2(IA)*AX1(IA))*S(IN)
      PIRT=(PIL(I)+PII(I)*AX2(IA)*AX1(IA))*Y(IN)
      IX=I-1
      Z=-(.5*(1.+CT(I)))+1.
 7777 PRINT 20023,IX,Z,G1(I),S(IN),Y(IN),POT,PIT,PORT,PIRT
      PRINT 1757
 1757 FORMAT(55H T AND X=STATIONS ALONG CHORD WHERE X=.5(1-COS(T))
     1       /55H GSTAR =CIRCULATION DISTRIBUTION (EQ2.3-15)
     1       /55H NCO AND NCI=NONLINEAR CORRECTION OUTSIDE AND INSIDE
     1     55H DUCT RESPECTIVELY (EQ3.2-3)
     1       /55H PO AND PI=NONLINEAR PRESSURE DISTRIBUTION OUTSIDE AND
     1       55H INSIDE THE DUCT RESPECTIVELY FOR PA=0 DEGREES
     1       /55H POP AND PIP =NONLINEAR PRESSURE DISTRIBUTION OUTSIDE
     1      55H AND INSIDE THE DUCT RESPECTIVELY FOR PA=INPUT
     1)
      PRINT 103
 8889 CONTINUE

      DIMENSION AAT(50),XXT(50),ZZT(50)
      READ 26000,ANT
      IF(ANT)1801,1802,1801
 1801 READ 26000,ANX,ANZ
      NNX=ANX
      NNZ=ANZ
      NNT=1
      AAT(1)=1.0
      READ 26000,(XXT(I),I=1,NNX)
      READ 26000,(ZZT(I),I=1,NNZ)
26021 FORMAT(3I8)
      DO 26022 JA=1,NNT
      DO 26022 JX=1,NNX
      PRINT 1758,XXT(JX)
      DO 26024 JZ=1,NNZ
      ERASE VAG,VRG,VAQ,VRQ
      DO 26023 I=1,181,5
```

```
      B1=2.*(ZZT(JZ)-AAT(JA))-1.-CT(I)
      B2=H**2*B1**2+(XXT(JX)-1.)**2
      BS=H**2*B1**2+(XXT(JX)+1.)**2
      B3=SQRTF(XXT(JX))
      B4=B3**3
      AK=SQRTF(4.*XXT(JX)/BS)
      IF(AK-1.) 26032,26030,26030
26032 IF(AK-.99) 26030,26039,26039
26038 CALL ELLIP(X1,AK,X3,X4,BF, BS)
      GO TO 26037
26039 AK2=AK**2
      CALL YSELL(AK2,BS,BF)
      GO TO 26037
26030 BS=1.0
26037 VAG=VAG+(-H/(6.2832*B3))*G1(I)*AK*(BF-BS-2.*(XXT(JX)-1.)*BS/B2)*CT
     1H(I)*SM(I)*DX
      VRG=VRG+(H/(6.2832*B4))*G1(I)*AK*H*B1*(BF-BS-2.*XXT(JX)*BS/B2)*CTH
     1(I)*SM(I)*DX
      VAQ=VAQ+(-H/(3.1416*B3))*SU(I)*AK*2.*H*B1*BS*SM(I)*DX/B2
26023 VRQ=VRQ+(-H/(3.1416*B4))*SU(I)*AK*(BF-BS+2.*XXT(JX)*(XXT(JX)-1.)*B
     1S/B2)*SM(I)*DX
      VA=VAG+VAQ
      VR=VRG+VRQ
26024 PRINT 26009,ZZT(JZ),VA,VR
26022 CONTINUE
 1758 FORMAT(55H1 INDUCED VELOCITY INSIDE THE DUCT AT A DUCT RADIUS OF
     1E9.4///55H      Z                  VA                VR                  )
26000 FORMAT(9F8.6)
26009 FORMAT(7E15.6)
20024 FORMAT(9I8)
20025 FORMAT(9F8.6)
  801 FORMAT(1//8E15.6)
  103 FORMAT(1H1)
20023 FORMAT(I8,8E13.4)
 3802 CALL END JOB
      RETURN
      END
```

```
  FOR
SUBROUTINE  YSELL( EKS , ELE , ELK)

PKS = 1.0 - EKS
ALA = 1.38629 - (0.5 * LOGF(PKS))
ELK = ALA + ((ALA - 1.0) * 0.25 * PKS)
ELE = 1.0 + (0.5 * (ALA - 0.5)*PKS)
RETURN
END
```

ACKNOWLEDGMENTS

The authors wish to express their appreciation to personnel of the Aerodynamics Laboratory for conducting the wind-tunnel tests and to personnel of the Open Shop of the Applied Mathematics Laboratory for their assistance in programming this problem on the IBM-7090 high-speed computer.

Also, the authors wish to thank Mr. O. L. Stephans of the Bureau of Ships for his invaluable contributions in all aspects of this investigation.

REFERENCES

1. Dickmann, H.E., "Grundlagen zur Theorie ringförmiger Tragflügel (frei umströmte Düsen)," Ingenieur-Archiv, Vol. II (1940) pp. 36-52. (Translation, Polytechnic Institute of Brooklyn, Pibal Report 353.)

2. Stewart, H.J., "The Aerodynamics of a Ring Airfoil," Quarterly of Applied Mathematics, Vol. II, No. 2, pp. 136-141 (1944).

3. Kuchemann, D. and Weber, J., "Concerning the Flow about Ring-Shaped Cowlings, Part II – Annular Bodies of Infinite Length with Circulation for Smooth Entrance," (Translation) National Advisory Committee for Aeronautics TM (Nov 1951).

4. Kuchemann, D. and Weber, J., "Aerodynamics of Propulsion," McGraw-Hill Book Co., Inc., New York (1953).

5. Pivko, S., "Determination of Velocity and Pressure Distribution along the Surface of Annular Airfoils with Thick Symmetrical Sections," Journal of the Royal Aeronautical Society, Vol. 60 (May and Jul 1956).

6. Malavard, L.C., "Recent Developments in the Method of Rheoelectric Analogy Applied to Aerodynamics," Journal of the Aeronautical Sciences, Vol. 24, No. 5 (May 1957).

7. Hacques, G., "Calcul par analogie rheoelectrique de la courbure ou de l'epaisseur d'un profil d'aile annulaire satisfaisant a une distribution de pression imposee, lorsque l'ecoulement presente la symetrie axiale," Academi Des Sciences, Comptes Rendus, Tome 245, No. 20 pp. 1700-1703 (13 Nov 1957).

8. Ordway, D.E., Sluyter, M.M., and Sonnerup, B.O.U., "Three-Dimensional Theory of Ducted Propellers," Therm Advanced Research Report TAR-TR602, THERM Inc., Ithaca, New York (Aug 1960).

9. Morgan, W.B., "A Theory of the Ducted Propeller with a Finite Number of Blades," University of California, Institute of Engineering Research, Berkeley (May 1961).

10. Weissinger, J., "Zur Aerodynamik des Ringflüge -, I. Die Druckverteilung dunner, st drehsymmetrischer Flügel in Unterschallströmung," Deutsche Versuchsanstalt für iftfahrt, E. V. Bericht Nr. 2, Mulheim (Sep 1955). (Translation, David Taylor Model Basin, MB Aero Memo 899.)

11. Weissinger, J., "Einige Ergebnisse aus der Theorie des Ring flügels in Inkompres- bler Stromung," Advances in Aeronautical Sciences, Vol. 2. Pergamon Press, pp. 798-831 959).

12. Bagley, J.A., Kirby, N.B., and Marcer, P.J., "A Method of Calculating the Velocity stribution on Annular Aerofoils in Incompressible Flow," Royal Aircraft Establishment echnical Note No. Aero 251, Farnborough (Jun 1959).

13. Hough, G.R., "The Aerodynamic Loading on Streamlined Ducted Bodies," THERM, c., TAR-TR625 (Dec 1962).

14. Haskel, A.L., Ordway, D.E., Hough, G.R., and Ritter, A., "A Detailed Numerical aluation of Shroud Performance for Finite-Bladed Ducted Propellers," THERM, Inc., TAR-R639 (Dec 1963).

15. Morgan, W.B., "Theory of the Annular Airfoil and Ducted Propeller," Fourth Sympo- um on Naval Hydrodynamics, Office of Naval Research ACR-73, Vol. 1 (1962).

16. Muskhelishvili, N.I., "Singular Integral Equations," P. Noordhoff, N. V. Groningen, olland (1953).

17. Mikhlin, S.G., "Integral Equations," Pergamon Press, New York (1957).

18. Robinson, A. and Laurmann, J.A., "Wing Theory," Cambridge University Press, eat Britain (1956).

19. Ribner, H.S., "The Ring Airfoil in Nonaxial Flow," Journal of Aeronautical Sci- ces, Vol. 14, No. 9, pp. 529-530.(Sep 1947).

20. Good, S.E., "AML Open-Shop Compiler," David Taylor Model Basin Applied Mathe- atics Laboratory Report 134 (May 1961).

21. "Theoretical Investigation and Examination by Measuring Tests in What a Degree the conomy of Flying Vehicles is Influenced by Pre-Cambered Skeletons of Airfoils Closed in hemselves," Bureau Technique Zborowski Report under Army Contract DA-91-508-EVC393 ug 1959).

22. Chaplin, H.R., "A Method for Numerical Calculation of Slipstream Contraction of a rouded Impulse Disc in the Static Case with Application to Other Axisymmetric Potential ow Problems," The Catholic University of America, School of Engineering and Architec- re, Washington, D. C. (1964).

23. Eichelbrenner, E.A., Angioletti, S., Greilier, Y.M., and Hellerstrom, R.S., "Theoretical Investigation and Control by Measuring Tests on the Behavior of the Three-Dimensional Turbulent Boundary Layer in an Annular Wing at Various Incidences," Bureau Technique Zborowski Report under Contract ONR N62558-3514 (Sep 1963).

24. Fletcher, H.S., "Experimental Investigation of Lift, Drag, and Pitching Moment of Five Annular Airfoils," National Advisory Committee for Aeronautics TN 4117 (1957).

25. Granville, P.S., "The Calculation of the Viscous Drag of Bodies of Revolution," David Taylor Model Basin Report 849 (Jul 1953).

INIT DISTRIBUTION

Copies

13 CHBUSHIPS
- 3 Tech Lib (Code 210L)
- 1 Appl Res (Code 340)
- 1 Ship Silencing (Code 345)
- 1 Prelim Des (Code 420)
- 1 Mach Des (Code 430)
- 2 Mach Sci & Res (Code 436)
- 1 Hull Des (Code 440)
- 3 Prop Shafting & Bring (Code 644)

20 CDR, DDC

4 CHBUWEPS
- 1 Lib (DLI-3)
- 1 Aero and Hydro (Code RAAD-3)
- 1 Res & Components (RuSD-342)
- 1 HydroPropulsion Sec (RuTO-32)

4 CHONR
- 2 Fluid Dyn (Code 438)
- 1 Undersea Programs (Code 466)
- 1 Air Programs Br (Code 461)

2 CDR, USNOTS, Pasadena
- 1 Commander
- 1 Underwater Ordance Dept

1 CDR, USNOL

1 DIR, USNRL

1 CO & DIR, USNMEL

1 SUPT, USNAVPGSCOL

1 ADMIN, MARAD

1 SNAME

1 DIR, ORL

1 DIR, Ames Res Ctr, Moffett Field

1 DIR, Langley Res Ctr, Langley Field

1 CO, U.S. Army Transportation Res Command, Fort Eustis

1 CHIEF, European Res Off

1 Bell Aerospace Corp.

Copies

2 Boeing Co.
- 1 Wichita
- 1 Morton, Pa.

1 Collins Radio Co.

1 Curtiss-Wright Corp.

1 Dcak Aircraft Co.

1 Douglas Aircraft Co., Inc.

1 The Garrett Corp.

1 Gen Elec Co., West Lynn

1 Gen Dyn Corp., Convair Div., San Diego

1 Hiller Aircraft Corp., Palo Alto

1 Hydronautics Inc.

1 Itek Corp., Vidya Div., Palo Alto

1 Lanier Aircraft Corp., Marlton, N.J.

1 Therm, Inc., Ithaca

1 United Aircraft Corp., East Hartford

1 Vanguard Air & Marine Corp., Bala Cynwyd, Pa.

1 Miss State College, State College

1 Univ of Wichita, Wichita

2 MIT
- 1 Head, Dept NAME
- 1 Library

1 Hydro Lab, CIT

1 DIR, Iowa Inst of Hydraulic Res

1 DIR, St. Anthony Falls Hydraulic Lab

1 PIB, Dept of Aero Eng & Appl Mech

1 Aerojet-General Corp., Axusa, Calif.

1 DIR, Davidson Lab, SIT

1 DIR, Inst of Eng Res, Univ of Calif., Berkeley

Copies

1 HD, DEPT of NAME, Univ of Mich, Ann Arbor

1 ADMIN, INST NAVARCH, Webb

2 Univ of Calif., Berkeley
1 Librarian
1 Head, Dept NAVARCH

1 Elec Boat Div . Gen Dyn Corp., Groton

1 Lockheed, Sunnyvale

David Taylor Model Basin. Report 1830.
PREDICTION OF THE AERODYNAMIC CHARACTERISTICS OF ANNULAR AIRFOILS, by W.B. Morgan and E.B. Caster.
Jan 1965. vi, 86p. diagrs., graphs, tables, refs.
UNCLASSIFIED

A computer program is presented which calculates the aerodynamic characteristics of annular airfoils on an IBM-7090 high-speed computer. A brief review of the theory is also presented. Experimental and computer results indicate that the theory gives reasonable prediction of the lift, induced-drag, and moment coefficients and also of the pressure distribution except when separation is present on the annular airfoil. The computer program can also be used for the design of ducted propellers if an infinite number of blades is assumed.

1. Annular airfoils--Aerodynamic characteristics--Theory
2. Annular airfoils--Aerodynamic characteristics--Wind tunnel tests
3. Annular airfoils--Aerodynamic characteristics--Programming
I. Morgan, William B.
II. Caster, Edmond B.

David Taylor Model Basin. Report 1830.
PREDICTION OF THE AERODYNAMIC CHARACTERISTICS OF ANNULAR AIRFOILS, by W.B. Morgan and E.B. Caster.
Jan 1965. vi, 86p. diagrs., graphs, tables, refs.
UNCLASSIFIED

A computer program is presented which calculates the aerodynamic characteristics of annular airfoils on an IBM 7090 high-speed computer. A brief review of the theory is also presented. Experimental and computer results indicate that the theory gives reasonable prediction of the lift, induced-drag, and moment coefficients and also of the pressure distribution except when separation is present on the annular airfoil. The computer program can also be used for the design of ducted propellers if an infinite number of blades is assumed.

1. Annular airfoils--Aerodynamic characteristics--Theory
2. Annular airfoils--Aerodynamic characteristics--Wind tunnel tests
3. Annular airfoils--Aerodynamic characteristics--Programming
I. Morgan, William B.
II. Caster, Edmond B.

David Taylor Model Basin. Report 1830.
PREDICTION OF THE AERODYNAMIC CHARACTERISTICS OF ANNULAR AIRFOILS, by W.B. Morgan and E.B. Caster.
Jan 1965. vi, 86p. diagrs., graphs, tables, refs.
UNCLASSIFIED

A computer program is presented which calculates the aerodynamic characteristics of annular airfoils on an IBM-7090 high-speed computer. A brief review of the theory is also presented. Experimental and computer results indicate that the theory gives reasonable prediction of the lift, induced-drag, and moment coefficients and also of the pressure distribution except when separation is present on the annular airfoil. The computer program can also be used for the design of ducted propellers if an infinite number of blades is assumed.

1. Annular airfoils--Aerodynamic characteristics--Theory
2. Annular airfoils--Aerodynamic characteristics--Wind tunnel tests
3. Annular airfoils--Aerodynamic characteristics--Programming
I. Morgan, William B.
II. Caster, Edmond B.

David Taylor Model Basin. Report 1830.
PREDICTION OF THE AERODYNAMIC CHARACTERISTICS OF ANNULAR AIRFOILS, by W.B. Morgan and E.B. Caster.
Jan 1965. vi, 86p. diagrs., graphs, tables, refs.
UNCLASSIFIED

A computer program is presented which calculates the aerodynamic characteristics of annular airfoils on an IBM 7090 high-speed computer. A brief review of the theory is also presented. Experimental and computer results indicate that the theory gives reasonable prediction of the lift, induced-drag, and moment coefficients and also of the pressure distribution except when separation is present on the annular airfoil. The computer program can also be used for the design of ducted propellers if an infinite number of blades is assumed.

1. Annular airfoils--Aerodynamic characteristics--Theory
2. Annular airfoils--Aerodynamic characteristics--Wind tunnel tests
3. Annular airfoils--Aerodynamic characteristics--Programming
I. Morgan, William B.
II. Caster, Edmond B.